# Report on Twisted Nematic and Supertwisted Nematic Device Characterization Program

(NASA Cooperative Agreement #NCC 2-803)

## 1.0 Introduction

In this study we measured the optical characteristics of normally white twisted nematic (NWTN) and super twisted nematic (STN) cells. Though no dynamic computer model was available the static observations were compared with computer simulated behavior. The measurements were taken as a function of both viewing angle and applied voltage and included in the static case not only luminance but also contrast ratio and chromaticity . We employed the computer model Twist Cell Optics, developed at Kent State in conjunction with this study, and whose optical modeling foundation, like the ViDEOS program, is the 4 x 4 matrix method of Berreman.

In order to resolve discrepancies between the experimental and modeled data the optical parameters of the individual cell components where not known were determined using refractometry, profilometry, and various forms of ellipsometry. The resulting agreement between experiment and model is quite good due primarily to a better understanding of the structure and optics of dichroic sheet polarizers. A description of the model and test cells employed are given in section 2 below. Section 3 contains the experimental data gathered and section 4 gives examples of the fit between model and experiment. Also included with this report are a pair of papers which resulted from the research and which detail the polarizer properties and some of the cell characterization methods.

## 2.0 Test Cell/Model Description

The basic structure of the experimental and model liquid crystal cells used in this research is shown in figure 1. It consisted of sheet polarizers, retardation layers, glass plates, ITO electrodes, polyimide alignment layers, and of course the liquid crystal itself. The TN cell was constructed in house at the Liquid Crystal Institute while the STN cell was constructed by Standish Industries.

### 2.1 Liquid Crystal

The liquid crystal used in the TN cell was ZLI 4792 which is a fluorinated compound specifically designed for active matrix displays. After filling the cell gap was measured to be 5.2μm. The resistance was unusually low ~1.5kΩ probably due to some shorting of the cell. The cell gap for the STN was 5.0μm.

In the model the director orientation of the liquid crystal was determined by a one dimensional energy minimization of the Oseen-Frank energy assuming strong anchoring by the polyimide alignment layer. For modeling purposes the liquid crystal layer was divided into a number of sub-layers in which the orientation was assumed constant. The elastic and optical constants supplied by Merck and used for the two liquid crystals are shown in table 1.

### 2.2 Polyimide

Rubbed polyimide surface layers aligned the liquid crystal in each test cell. The induced pretilt of the TN cell was measured at approximately 3° while that of the STN cell was given at between 6° and 8° and measured at roughly 7°. In each case the layer was assumed thin, roughly 25nm, with an index well matched to the glass substrates.

**Table 1: Liquid Crystal Mechanical and Optical Properties**

| | TN (ZLI 4792) | STN |
|---|---|---|
| $K_{11}(x10^{-12}N)$ | 13.2 | 13.3 |
| $K_{22}(x10^{-12}N)$ | 6.55 | 6.6 |
| $K_{33}(x10^{-12}N)$ | 18.44 | 19.4 |
| $\varepsilon_{\parallel}$ | 8.3 | 9.4 |
| $\varepsilon_{\perp}$ | 3.2 | 3.8 |
| $n_{e\infty}$ | 1.55 | 1.6203 |
| $n_{o\infty}$ | 1.4621 | 1.4837 |
| Cauchy value for $n_{e\infty}(nm^2)$ | 0.009229 | 0.017006 |
| Cauchy value for $n_{o\infty}(nm^2)$ | 0.005966 | 0.007412 |
| d/p | 0.033 | 0.50 |
| | | |

## 2.3 ITO

Electrical contact was achieved using the usual transparent indium tin oxide (ITO) layers. That used in the TN cell was quoted at and confirmed using profilometry to be approximately 25nm thick, while the STN cell was supplied with thicker 160nm layers. The index of refraction of ITO has a rather strong dependence on wavelength over the visible region and as one would suspect from its conductivity contains an imaginary component as well. Reported values in the literature [Wollam et al., SID 93 Digest, pg. 558] as well as those supplied with the STN cell show a linearly falling real component, dropping from about 2.0 at 400nm to approximately 1.65 at 700nm. Ellipsometric measurements at the wavelengths 488nm and 632.8nm on the TN cell substrates were also consistent with these numbers. The reported imaginary components were small; <0.02 in magnitude. Those measured for the TN substrates were larger than this at ~0.05, but the extreme thinness of this ITO layer combined with the large size of the real component

makes this number, found ignoring surface roughness, highly suspect. Thus in general the lower magnitude imaginary components were used in modeling.

## 2.4 Glass Substrates

The TN cell used borosilicate glass substrates while the STN cell was as supplied. Since the variation with wavelength of glass' index of refraction is so small when compared to the ITO, liquid crystal, etc. this has been ignored in modeling. The glass was simply treated as a dielectric layer with constant index. Further, to avoid the multiple interference fringes which plague theoretical treatments of idealized thick parallel layers, each interface of the glass plates were treated in the model as if they were semi-infinite in thickness.

## 2.5 Retarders

No separate retarders were used on the experimental cells, but as is described in section 2.6 a retardation layer was still needed in the model to produce a faithful simulation. In the model these layers were treated as biaxial dielectrics with no wavelength dependence and one principal axis along the layer normal.

## 2.6 Polarizers

Polarizers are optically rather complicated components which come in a great variety of styles. Those used in this study were the high efficiency sheet polarizers G1220 DU supplied by Nitto Denko. In the model the polarizer was treated as a uniaxial medium a few microns thick with complex indices of refraction. The optic axis was taken to be along the absorption direction and the imaginary components (extinction coefficient) of the ordinary and extraordinary indices set to match the transmission of light polarized parallel and perpendicular to the axis as a function of wavelength. The real components could not be measured so those supplied by the manufacturer at a wavelength of 589nm had to be used over the entire visible spectrum.

A real sheet polarizer, however, is slightly more complicated than this as exhibited in figure 2. It consists of a stretched poly vinyl alcohol (PVA) film protected by a sandwiching pair of tri-acetyl cellulose (TAC) layers. The polarizing effect comes from two thin (~3μm) layers of iodine absorbed into either side of the PVA. It is essentially only these two layers combined into one which were directly simulated in the model. For these high efficiency polarizers, simulations showed that ignoring the intervening birefringent PVA layer had little affect. Ellipsometric measurements on samples of the TAC layers however revealed that they exhibited an out of plane negative retardation which as will be shown does need to be considered. In the present model this was done by incorporating this retardation into the retardation layer. The ignoring of the wavelength dependence may, however, cause some problems particularly with coloration.

## 3.0 Experimental Data

All the luminance and contrast ratio measurements made on the test cells were performed using the following goniometer setup. This consisted of a goniometer capable of rotating the cell in the three orthogonal directions, a light source, and a detector. The light source was a Photo Research LRS 455 Light Reference Standard. This is in essence a tungsten-halogen lamp fit with an integrating sphere, and was typically run at a color temperature of 2856K in order to simulate the CIE illuminant A standard. The detector for the static measurements was a Photo Research SpectraScan 704 photoradiometer capable of measuring intensities at wavelengths from 380nm to 780nm at 2nm intervals. Software then calculated from these measurements the luminance, color coordinates, etc. For the dynamic observations data was collected using a photo diode specially fit by Photo Research with a matching photopic filter in order to match the spectral response of

the eye. During the measurements the light source and detector were fixed and the goniometer rotated the cell between the two.

### 3.1 Twisted Nematic Cell

Figure 3 shows the relative luminance versus root mean squared voltage (V) for the NWTN cell for on axis viewing. From this data 5 voltages (2.05V, 2.55V, 2.81V, 3.18V, 5.15V) approximately equally spaced in luminance along with 0.0V were chosen for more detailed study. These corresponded to on axis transmissions (compared to that at 0.0V) of 99%, 72%, 50%, 26%, and 1% respectively. Viewing angle luminance measurements were then made every 10° in the polar direction and 5° azimuthally. Figures 4 to 9 show conoscopic plots of these measurements for each voltage. In these contour plots the radial axis corresponds to the polar viewing direction with the origin being for on axis viewing and the perimeter being at a polar viewing angle of 60° (the maximum achievable with our goniometer setup). The azimuthal direction corresponds to the azimuthal viewing angle. For this cell the rear (towards the light source) polarizer and rub are at 90° while the front (toward the detector) are along the 0° line. The roughly 5° to 10° period waviness in the contour lines is an artifact of the contour generating software and the density of data points. The data is also graphed in the form of contrast ratio plots in figures 10 through 14, where the ratio is between the luminance at the indicated voltage and 0.0V. Spectral data was also taken at these voltages at selected viewing angles some examples of which are shown in figures 15 through 28. The oscillations in these curves are a real effect due to interference occurring between the two ITO coated glass plates. Plots of the dynamic switching of the TN cell are shown in figures 29 through 35. Here a 100ms voltage pulse is applied to the cell starting at time 0 and the luminance is in arbitrarty units.

## 3.2 Super Twisted Nematic

A luminance versus voltage curve for the STN cell, setup in the yellow mode, is shown in figures 36 and 37. The coordinate system being employed and its relation to the rubbing and polarizing directions is probably best described by figure 38. Once again we attempted to select a series of voltages roughly equally spaced in luminance for further measurement. Those chosen were 0.00V, 2.25V, 2.36V, 2.38V, 2.39V, and 2.45V corresponding to luminances, compared to 2.25V, of 105%, 100%, 77%, 46%, 21%, and 4%. The significance of these gray levels and their exact voltages, however, is arguable due to the presence of apparent rubbing inhomogenaities in the cell. These exhibited themselves as linear features parallel to the rubbing directions where the cell appeared to switch at slightly higher or lower voltages than neighboring areas. The density of these lines, indeed one could argue that the entire switching area consisted of them, made picking a visually uniform region impossible. Figures 39 through 44 are again conoscopic plots of the luminance as a function of viewing angle. As before the oscillations in the contour plots are artifacts due to the software. This data is also presented in the form of contrast plots in figures 45 through 48. The contrast ratios are taken between the luminances at 2.25V and the other indicated excitation voltage. In the STN even more important than shifts in luminance are shifts in color. Figures 49 to 65 show examples of the changes in the transmission spectra at various viewing angles while 66 to 73 show some of the corresponding color changes.

## 4.0 Model Fits

In order to determine the adequacy of the optical representation and characterization of the individual liquid crystal cell components, the above data was compared to that generated by the Twist Cell Optics program. In this work the primary focus was obtaining a good match

between model and experiment, but not necessarily the simplest match. Thus no detailed study of the relative importance of the various parameters used in the model and described earlier was undertaken. Overall the correspondence between model and experiment was quite good.

## 4.1 Twisted Nematic

A comparison of the model to the experimentally determined luminance versus voltage curve for the twisted nematic cell is shown by the indicated line in figure 74. As can be seen there is a sizable discrepancy. As mentioned before, however, the resistance of the TN cell was unusually low and this may have much to do with the difference. For instance the fit obtained by changing the model voltages by a shielding factor of 0.9 is also shown and gives a much better fit. Also figure 75 compares the model to an experimentally determined luminance versus voltage curve of another cell (with the same liquid crystal material, ZLI 4792, but a much higher resistance, > 1MΩ). Here the agreement is much better.

Taking into account the difference in model and experimental voltage by always matching the head on luminances and/or contrast ratios one can then do a good job of matching model with experiment at the other viewing angles as exhibited in figures 76, 77, and 78. Figure 76 is an iso-contrast plot comparing experiment to model, ignoring the negative retardation associated with the polarizers at an on axis contrast ratio of 3. In order to reduce the errors from the plotting software the data here was taken, and the model points calculated, at 5° instead of 10° increments in both polar and azimuthal directions. Figure 77 is the same as the previous one except an out of plane negative retardation of 55nm coming from the TAC on the polarizers has been included in the model. A significant improvement is seen especially in some of the high polar viewing angle positions. Figure 78 shows some examples comparing the spectra taken at a variety

of voltages and viewing angles with those calculated via the model both with and without the negatively birefringent TAC layer. Once again the significance of this birefringent layer is evident.

## 4.2 Super Twisted Nematic

The fit of model and experimental luminance curves for the STN cell at medium voltage resolution is quite good, figure 79. However, expanding the voltage scale about the threshold as in figure 80 reveals some significant differences at the ~0.05V level. Primarily the onset in the model is much more abrupt and the curve is much steeper. Again much of this may be due to limitations not with the model but with the cell quality. As noted before as the STN cell switched on, rubbing lines were readily apparent. Evidently the rubbing process resulted in variations in the surface pretilt angle or cell thickness which resulted in variations in the switch on voltage through the cell. It is also conceivable, however, that in this case the model for the director configuration may be inadequate. Namely we know that at low pretilts an STN cell can exhibit a striped domain. The model being one dimensional can not reproduce this behavior. It is thus possible that at higher pretilts, while the stripped domain disappears some vestige of the 2 and 3 dimensional dependence remains which is ignored in the present model.

In any case the near infinite slope in the model curve makes it difficult to compare on a point by point basis with experiment. Figures 81, 82, and 83 do show relatively good agreement in the transmission spectra at the end points of the curve at various angles, if the apparent difference of voltage shown by the on axis luminance is corrected for. Also figures 84 through 88 show that the model reproduces relatively well the path followed by the color coordinates through the switching. The model curves were generated by simply drawing a straight line between the color coordinates of 4 intermediate model points with the endpoints at the same voltages (0.0V

and 2.45V) as the experimental data. This coarseness accounts for the 'jerkiness' and in fact some of the error in these curves. The X on each diagram marks the endpoint of the model curve when the voltages have been adjusted to match on axis luminances, and in general better matches the endpoints of the experimental curve.

## 5.0 Conclusion

Table 2 summarizes the basic parameters found necessary to adequately model the TN and STN test cells used in this study. The faithful simulation of at least the static optics of a liquid crystal device both as a function of voltage and viewing angle is straight forward if not simply attainable. It depends on the optical properties, e.g. the indices of refraction as a function of wavelength, of each layer making up the display along with the electro-optic properties of the liquid crystal material. Perhaps the most subtle aspect to determining these parameters is to first

Table 2: Optical Parameters of Model Pixel Layers

| Layer | Parameters | Comments |
|---|---|---|
| Liquid Crystal | $K_{11}$, $K_{22}$, $K_{33}$, $\varepsilon_{\parallel}$, $\varepsilon_{\perp}$, p, $V_{rms}$ | Director: from elastic (K) and dielectric ($\varepsilon$) constants with pitch (p) and applied voltage (V) (polyimide $\theta_s$, $\theta_r$ also needed) |
| | $n_e(\lambda), n_o(\lambda), d_{LC}$ | indices typically follow Cauchy relation |
| Polyimide | $d_{PI}$, $n_{PI}$, $\theta_s$, $\theta_r$ | critical parameters surface pretilt $\theta_s$, rub directions $\theta_r$ |
| ITO | $d_{ITO}$, $N_{ITO}=n_{ITO}(\lambda)+i\kappa_{ITO}$ | $n_{ITO}(\lambda)$ typically linear e.g. $n_{ITO}(\lambda)\sim 2.47-1.17\lambda$ ($0.4\mu m<\lambda<0.7\mu m$) $\lvert\kappa_{ITO}\rvert$ typically small e.g. < 0.1 (*almost* ignorable) |
| Glass | $n_G$ | Modeled as semi-infinite to avoid multiple reflections. |
| Retardation Film | $n_x$, $n_y$, $n_z$, $d_R$ | Lack of $\lambda$ dependence may cause some coloration errors |
| Polarizers | $N_{\parallel}=n_{\parallel}+i\kappa_{\parallel}(\lambda)$ $N_{\perp}=n_{\perp}+i\kappa_{\perp}(\lambda)$ $d_P$, $\theta_P$ | $d_P$ non-critical (a few $\mu$m). $\kappa$'s set to match on axis transmissions. Retardation of protective coating must be included in with Retardation Film. Transmission directions ($\theta_P$) are of course critical. |
| | | |

identify the layers themselves. Thus, for example, while the dichroic sheet polarizers were initially treated as single layer components they actually consist of 4 distinct layers and must be modeled as at least a two layer device to be reasonably consistent with reality.

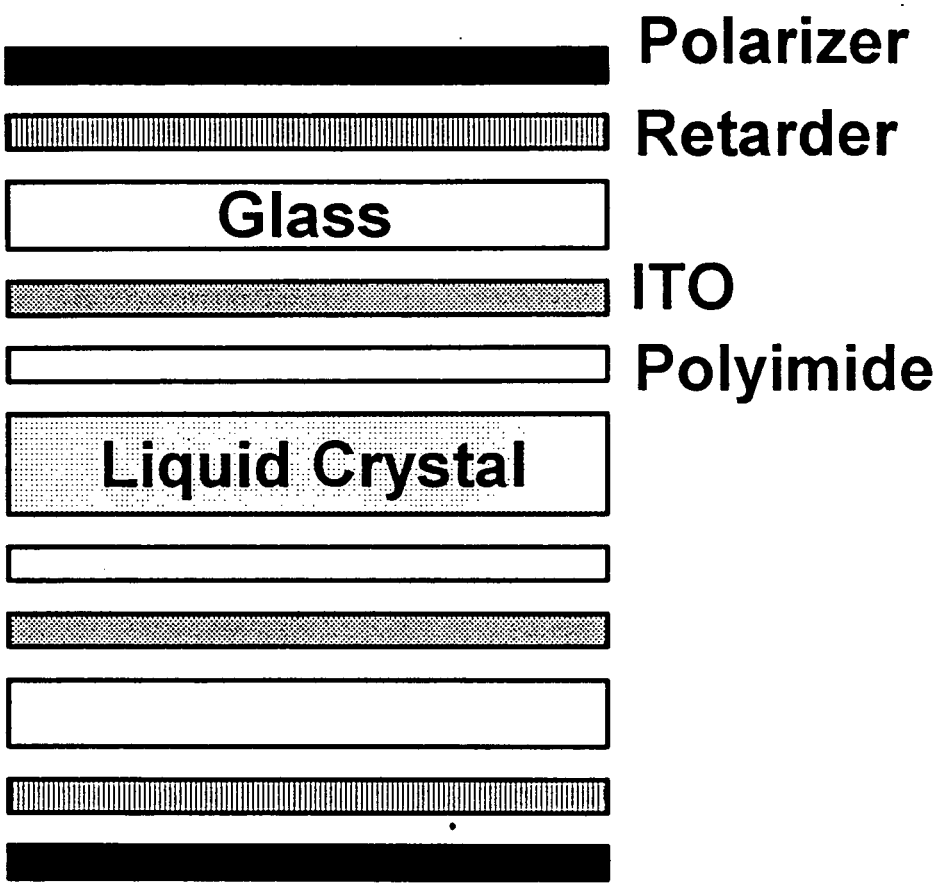


**Figure 1:** Basic structure of liquid crystal cells used in study.

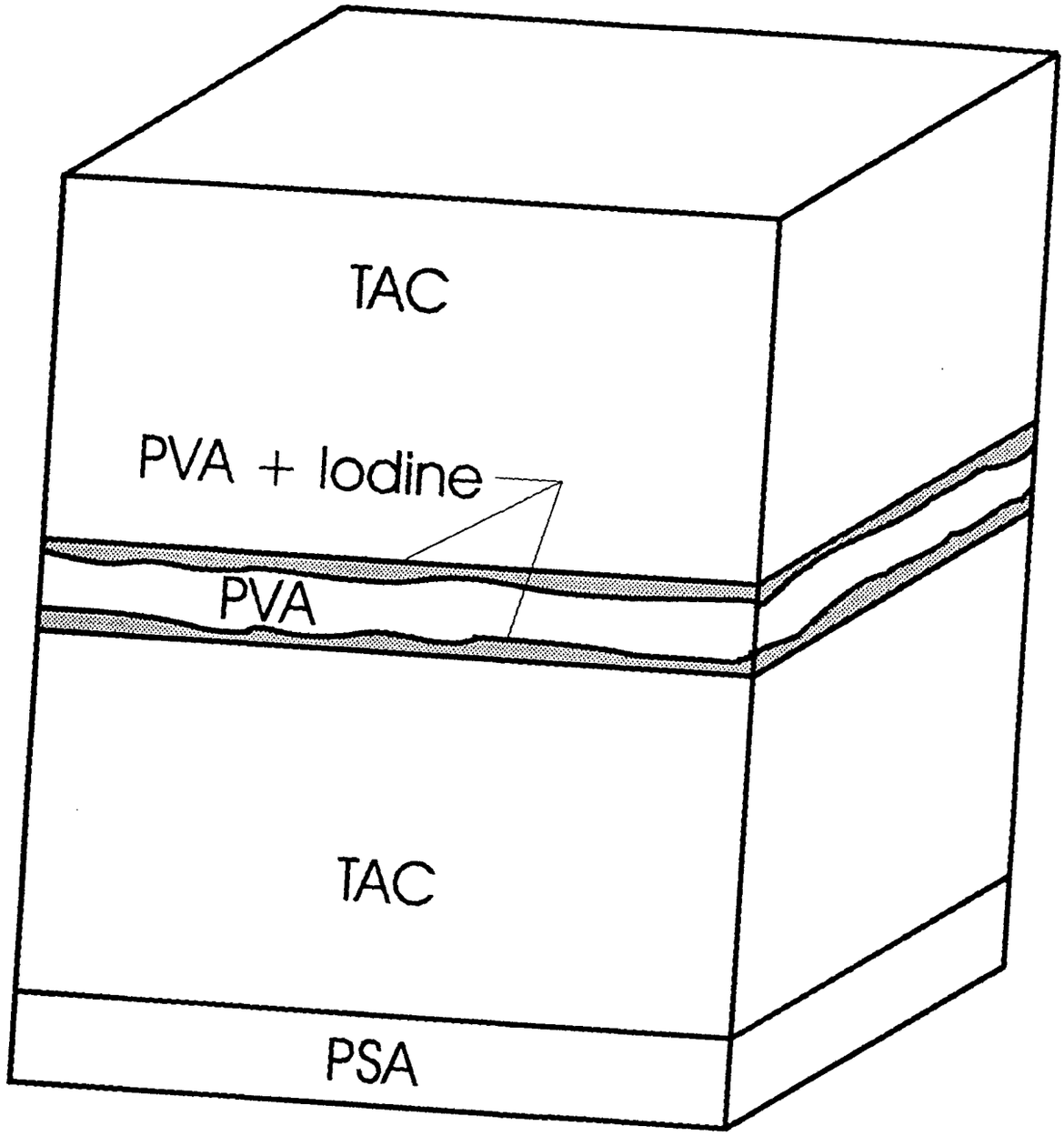


**Figure 2:** Structure of typical dichroic sheet polarizer.

# Experimental Luminance vs. Voltage for Normally White TN cell #1

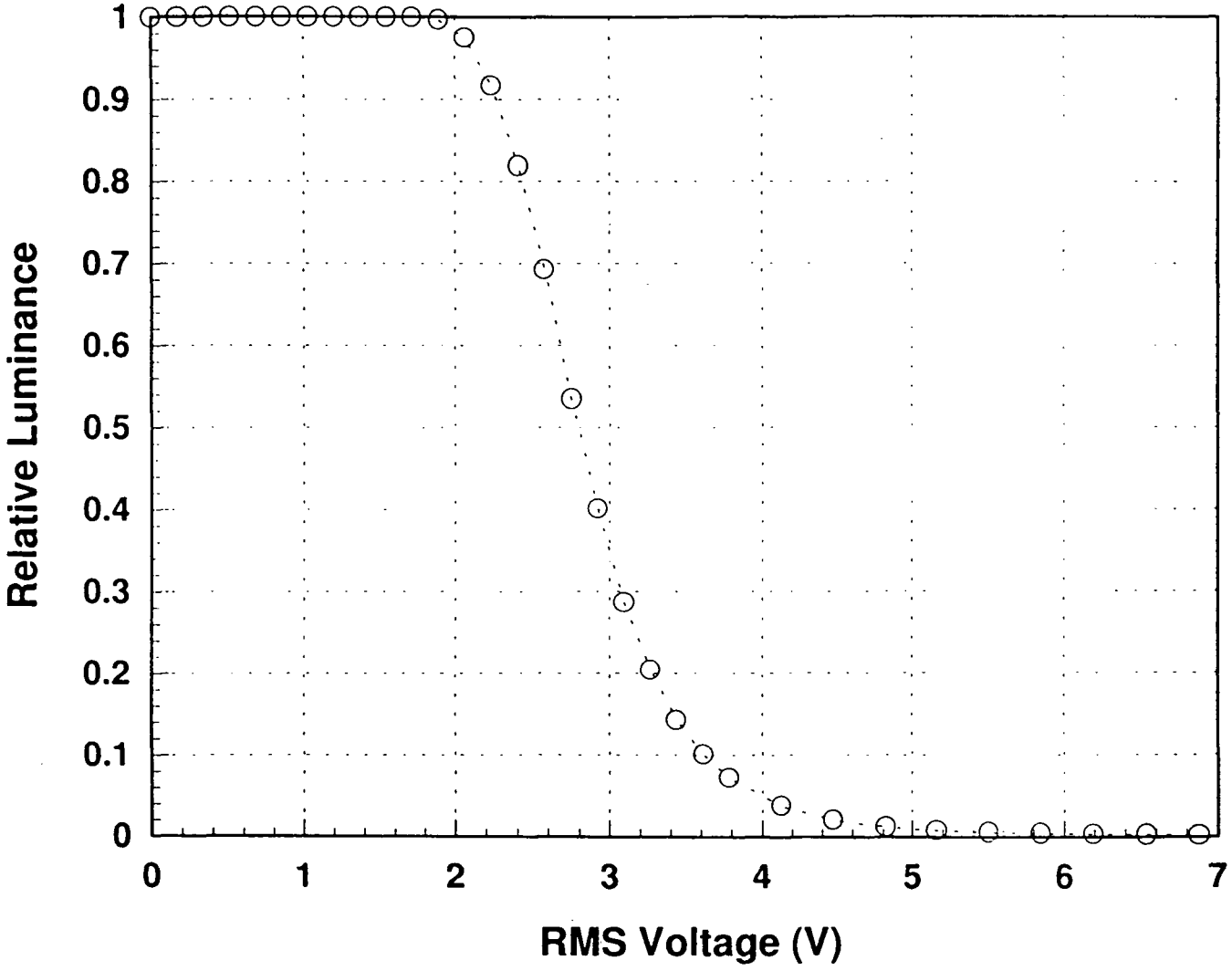


Figure 3

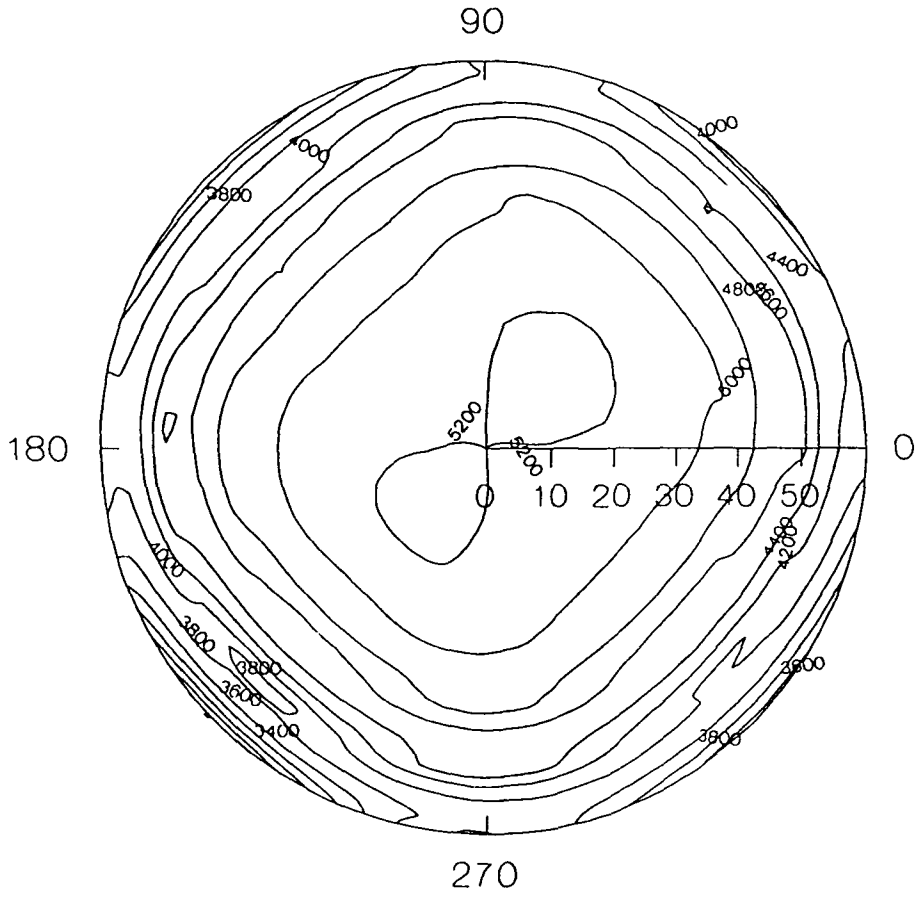


Source Luminance 14,750 fl
Data taken with Normally White TN Cell #1
Curves generated using Systat 5.03 with
smoothing set on NEXPO
grid on default setting (30 by 30)
Z ticks set at 20

**Figure 4**

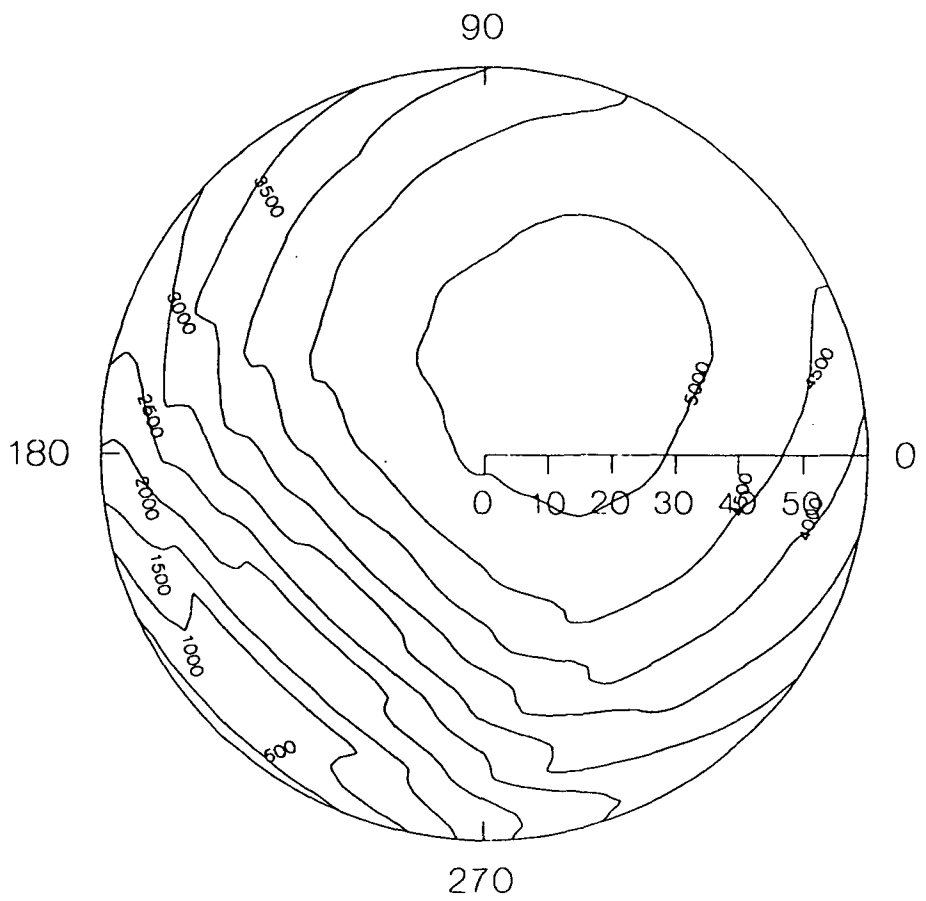


Source Luminance 14,750 fl
Data taken with Normally White TN Cell #1
Curves generated using Systat 5.03 with
smoothing set on NEXPO
grid on default setting (30 by 30)
Z ticks set at 20

**Figure 5**

Experimental Isoluminance curves at 2.55V

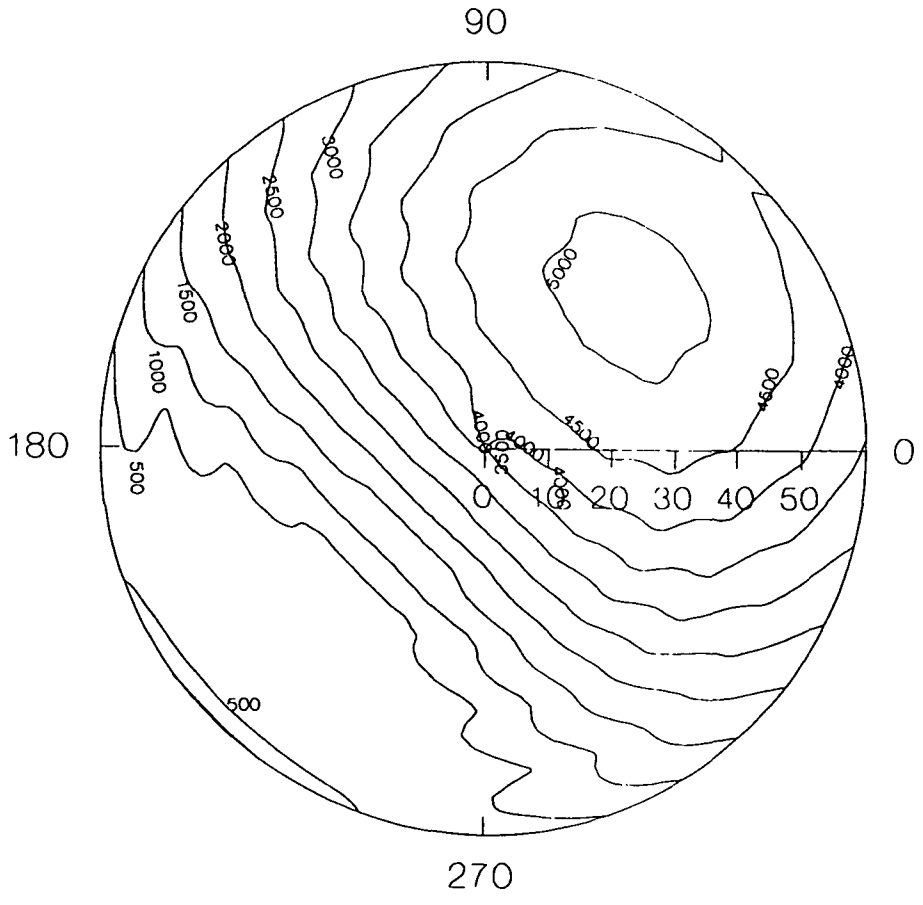


Source Luminance 14,750 fl
Data taken with Normally White TN Cell #1
Curves generated using Systat 5.03 with
smoothing set on NEXPO
grid on default setting (30 by 30)
Z ticks set on 20

**Figure 6**

Experimental Isoluminance curves at 2.81V

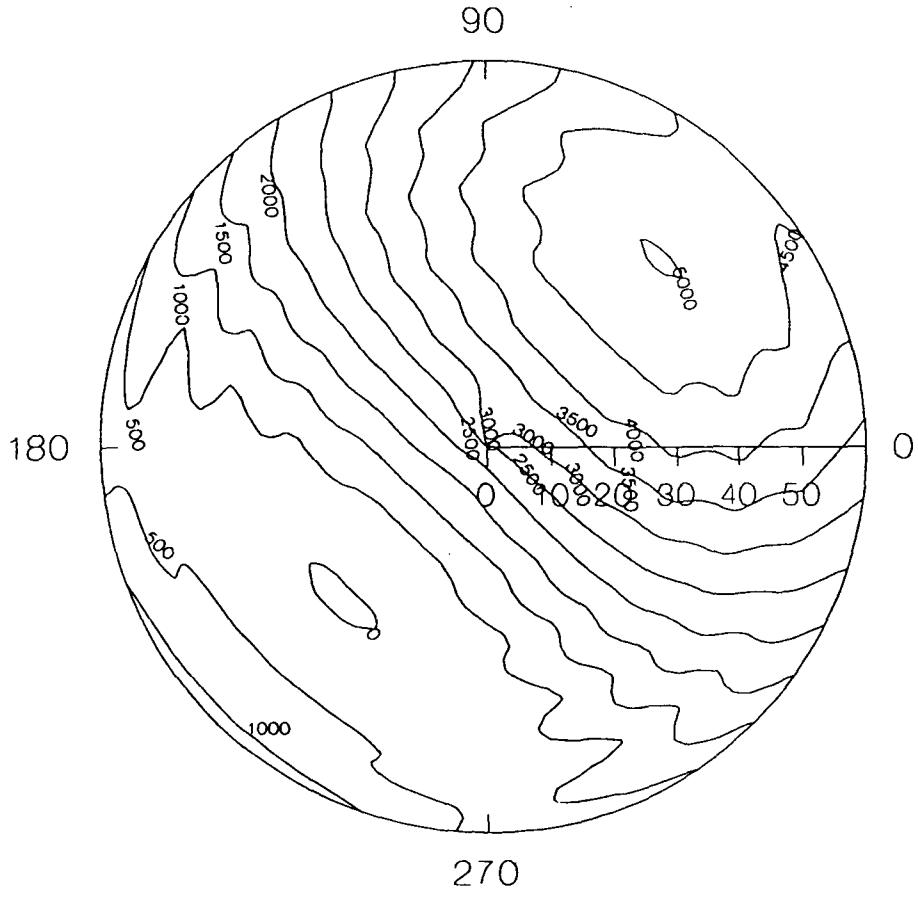


Source Luminance 14750 fl
Data taken with Normally White TN Cell #1
Curves generated using Systat 5.03 with
smoothing set on NEXPO
grid size on default (30 by 30)
Z ticks set at 20

**Figure 7**

# Experimental Isoluminance curves at 3.18V

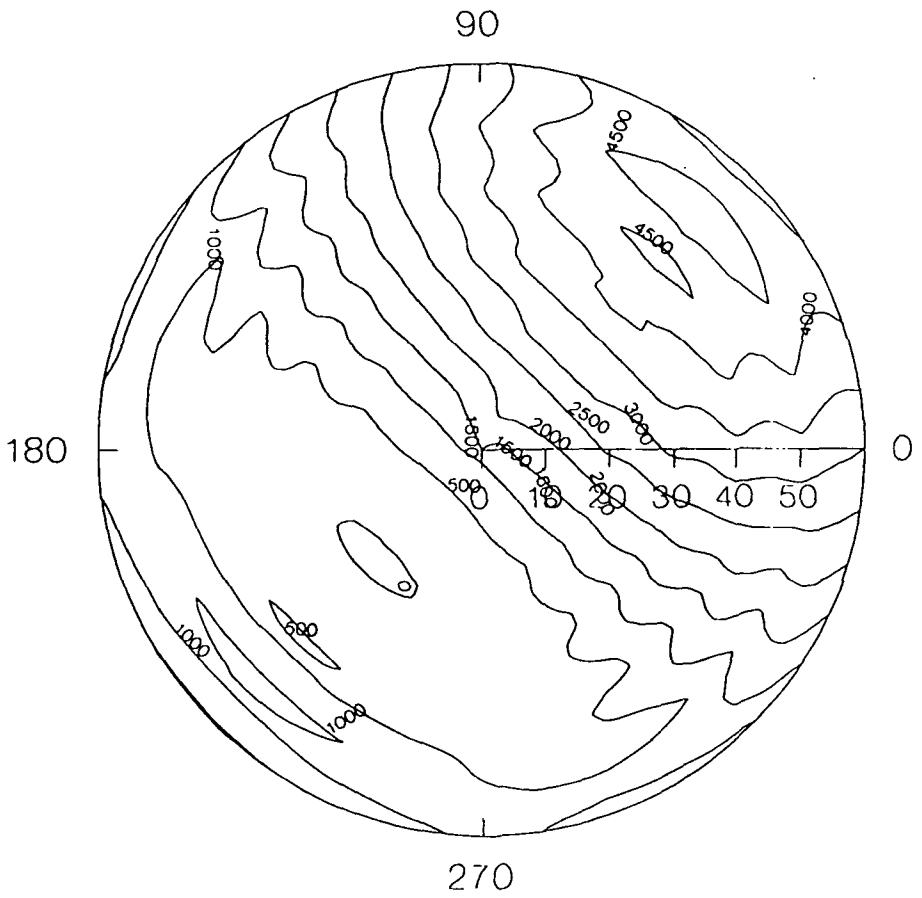


Source Luminance 14,750 fl
Data taken with Normally White TN Cell #1
Curves generated using Systat 5.03 with
smoothing set on NEXPO
grid size on default (30 by 30)
Z ticks set on 20

**Figure 8**

Experimental Isoluminance curves at 5.15V

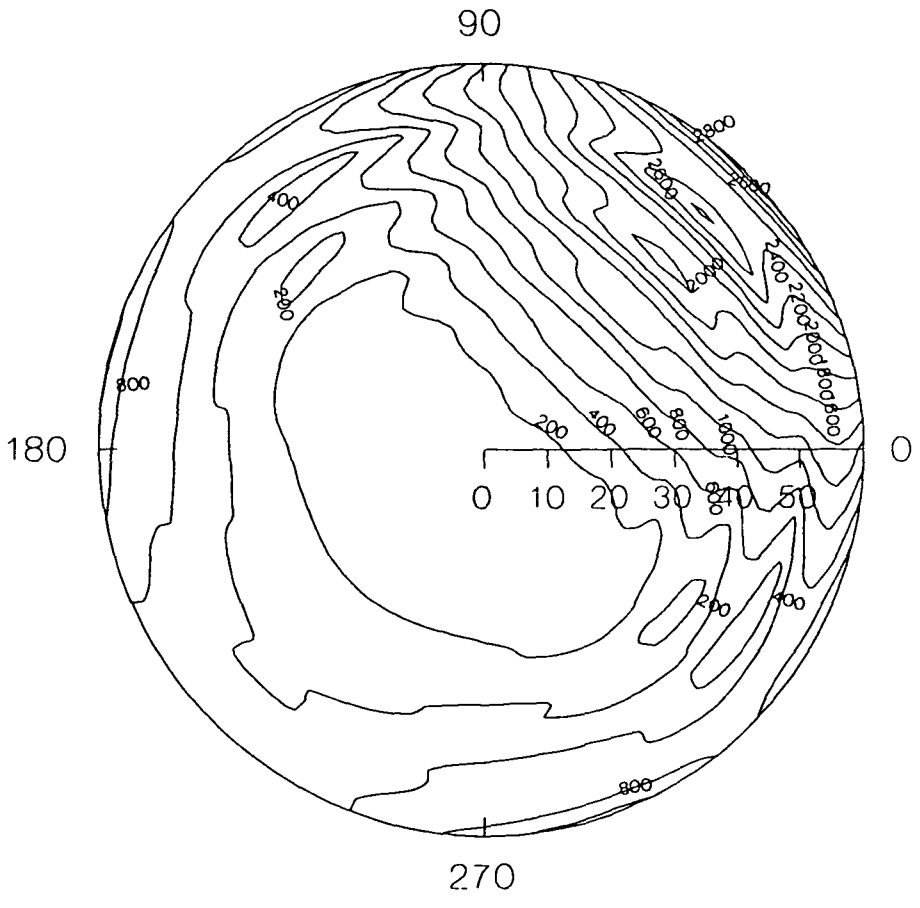


Source Luminance 14,750 fl
Data taken with Normally White TN Cell #1
Curves generated using Systat 5.03 with
smoothing set on NEXPO
grid size on default (30 by 30)
Z ticks set at 20

**Figure 9**

# Experimental Iso-contrast curves of Normally White TN cell #1 at 2.05V.

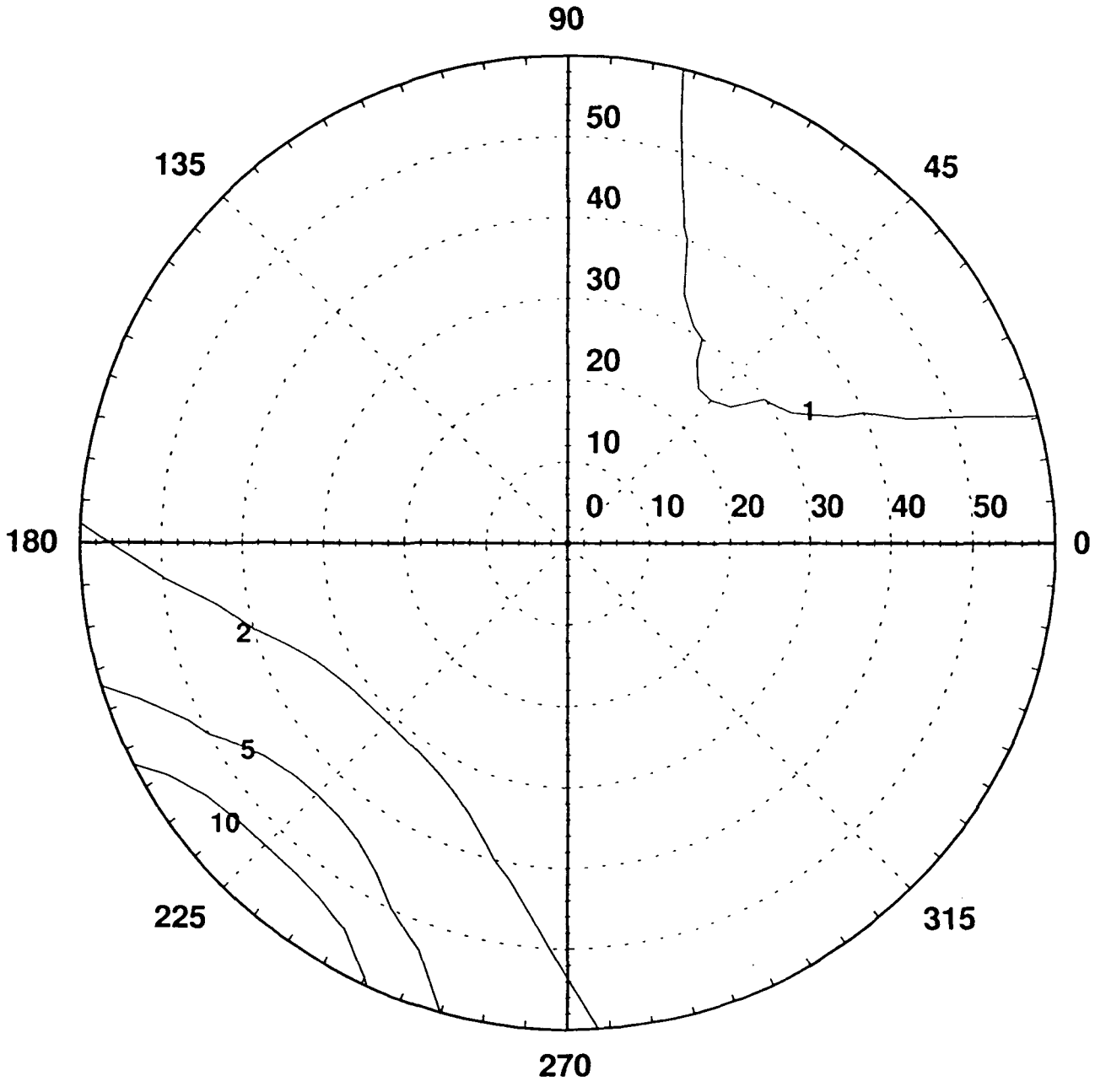


**Figure 10:** Iso-contrast curves are compared to luminance at 0.0V.

# Experimental Iso-contrast curve of Normally White TN cell #1 at 2.55V

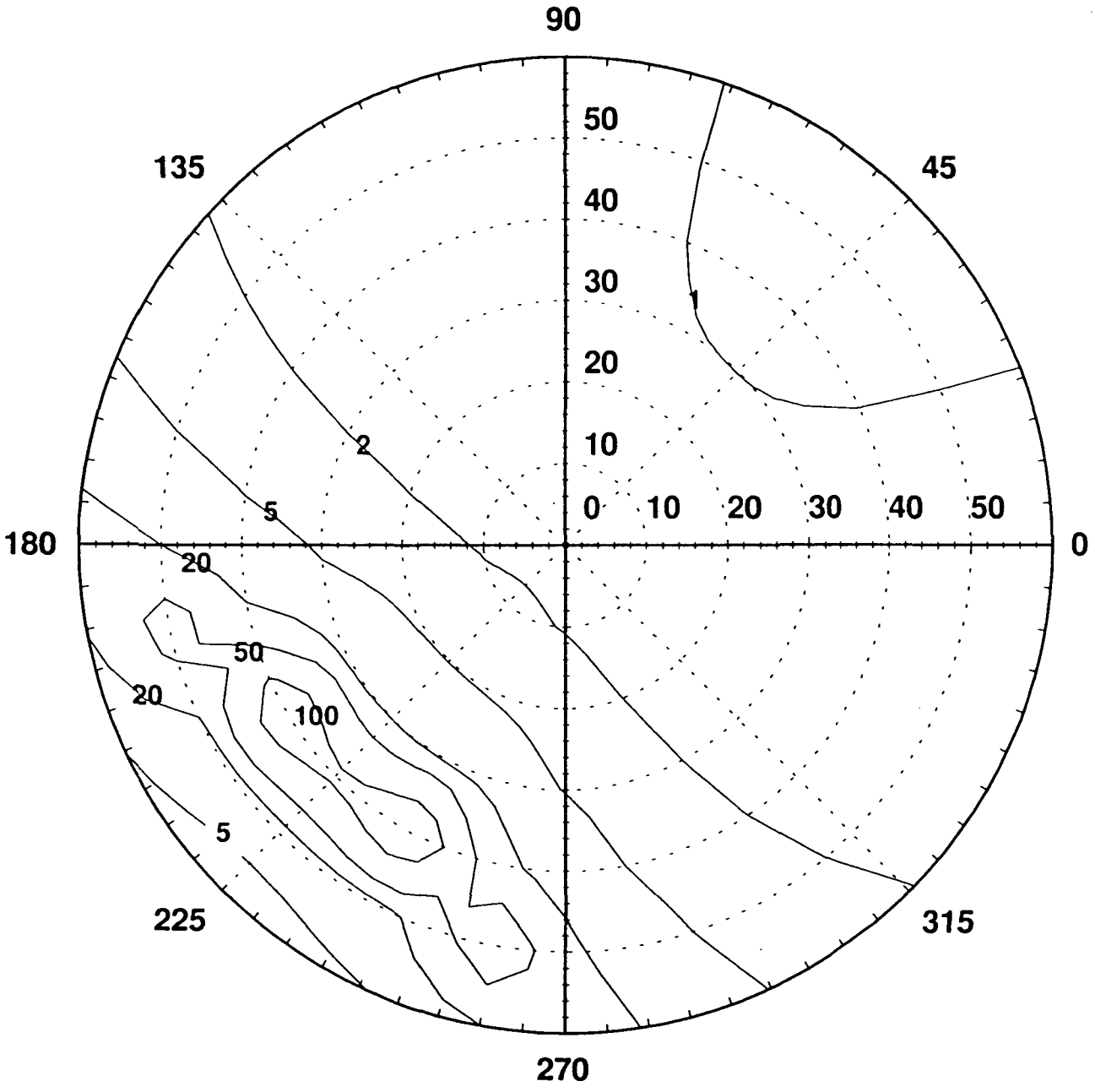


**Figure 11:** Iso-contrast curves are compared to luminance at 0.0V.

# Experimental Iso-contrast curve for Normally White TN cell #1 at 2.81V

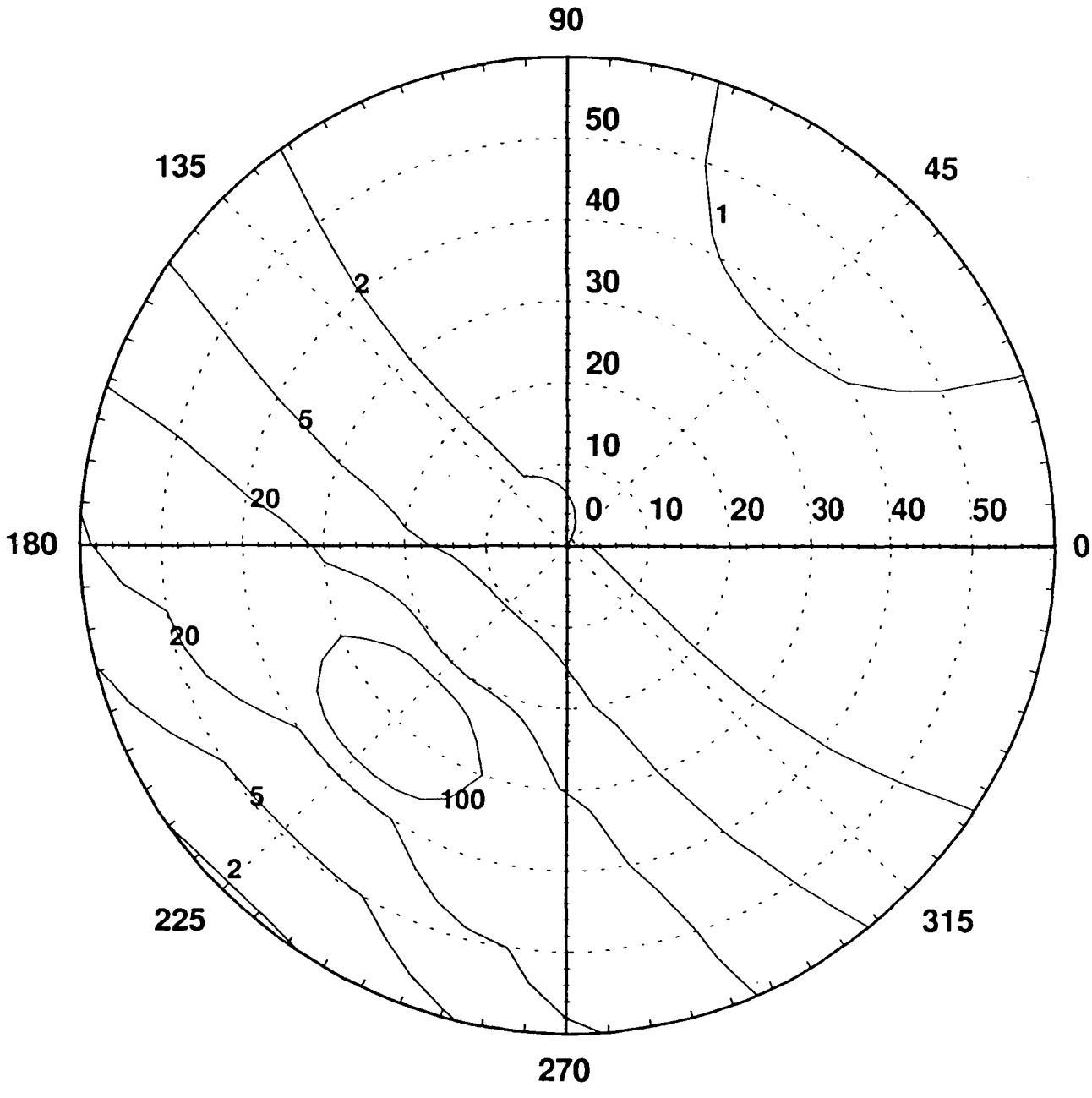


**Figure 12:** Iso-contrast curves are compared to luminance at 0.0V.

# Experimental Iso-contrast curve for Normally White TN cell #1 at 3.18V

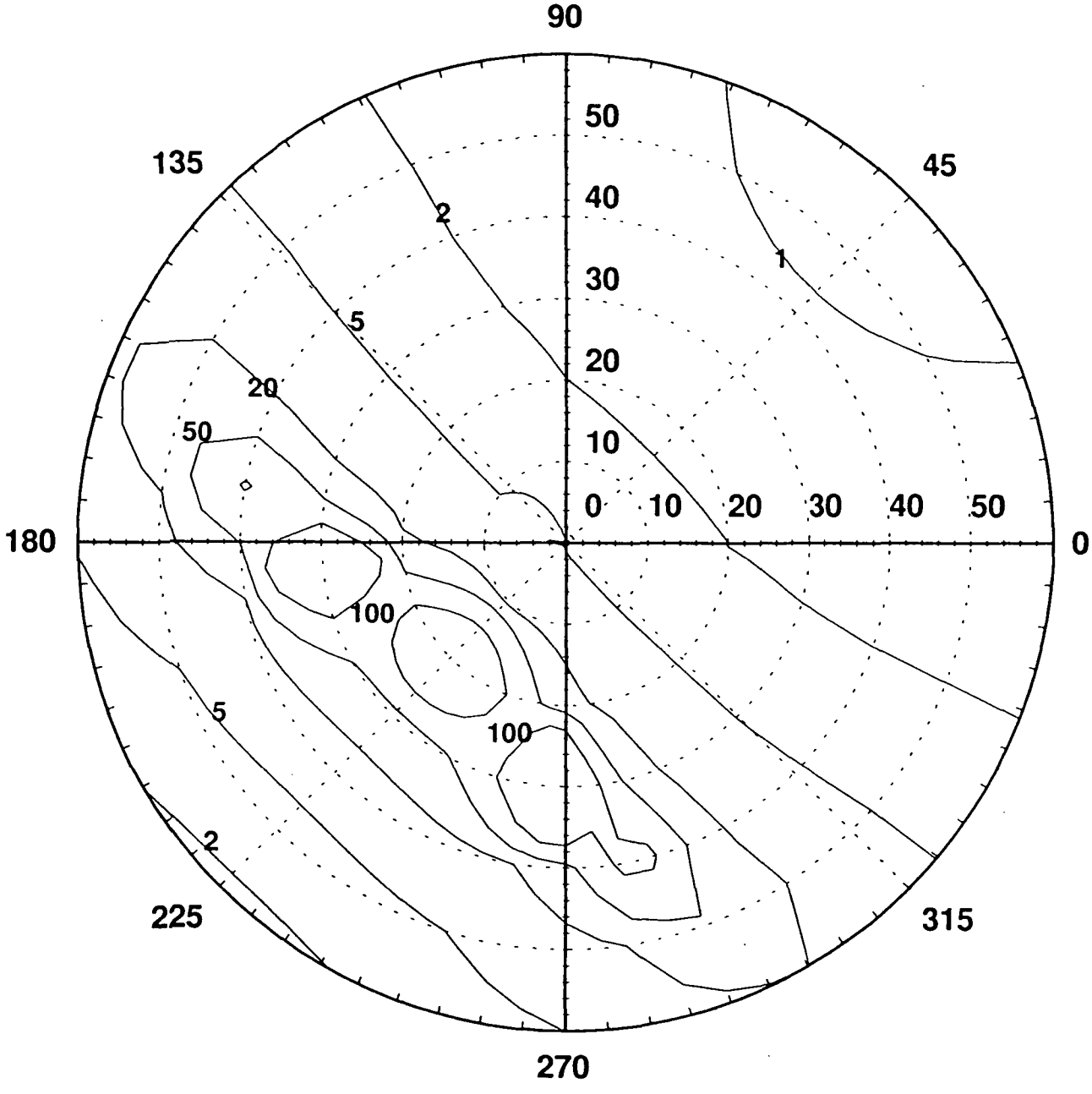


**Figure 13:** Iso-contrast curves are compared to luminance at 0.0V.

# Experimental Iso-contrast curve for Normally White TN cell #1 at 5.15V.

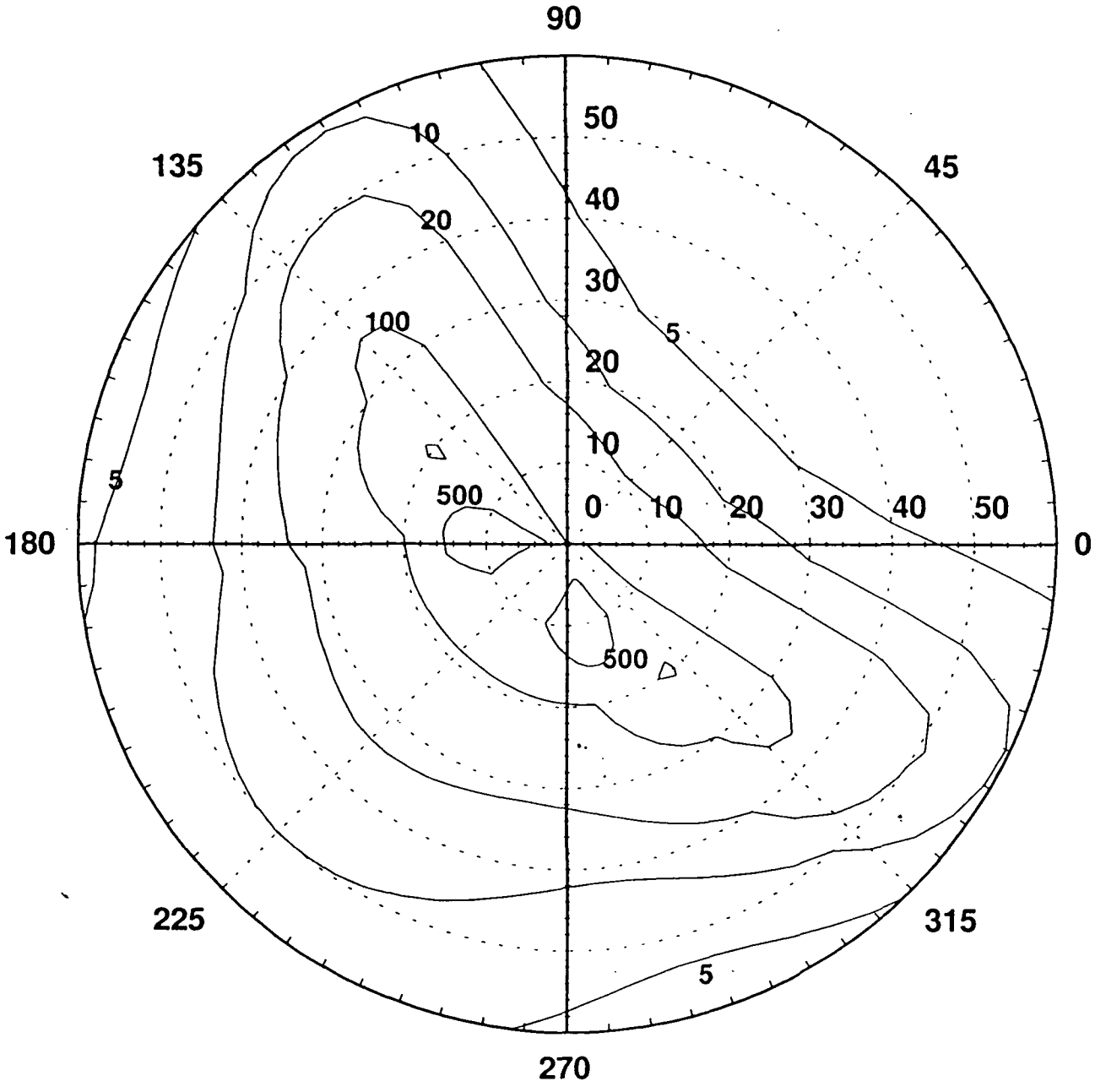


**Figure 14:** Iso-contrast curves are compared to luminance at 0.0V.

# Experimental Spectral Transmittance Normally White TN Cell (1) (ZLI-4792)

## $\Theta = 0.0$ degrees $\Phi = 0.0$ degrees

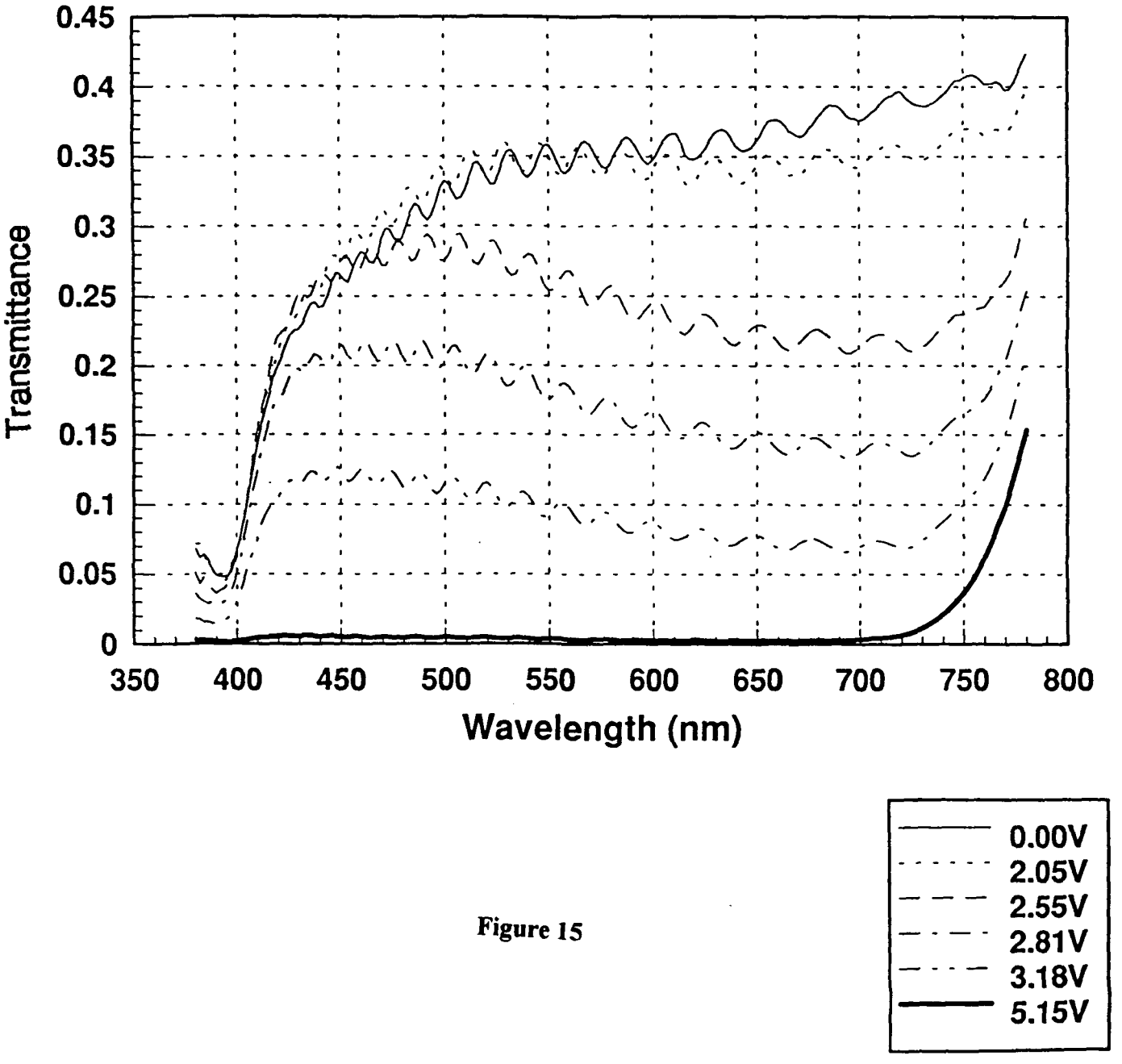


Figure 15

# Experimental Spectral Transmittance Normally White TN Cell (1) (ZLI-4792)

## $\Theta = 30$ degrees $\Phi = 45$ degrees

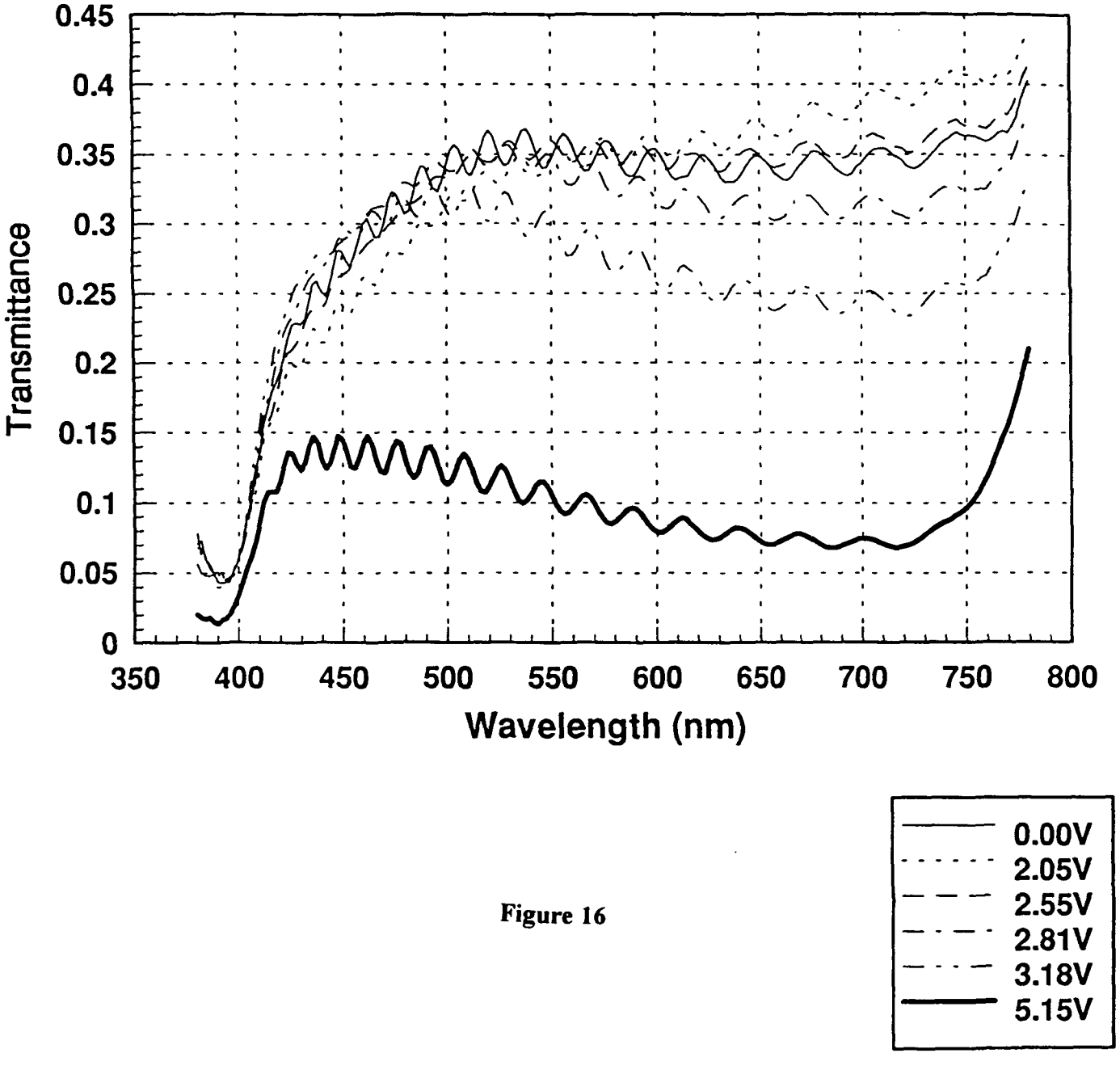


Figure 16

# Experimental Spectral Transmittance Normally White TN Cell (1) (ZLI-4792)

## Θ = 30 degrees  Φ = 90 degrees

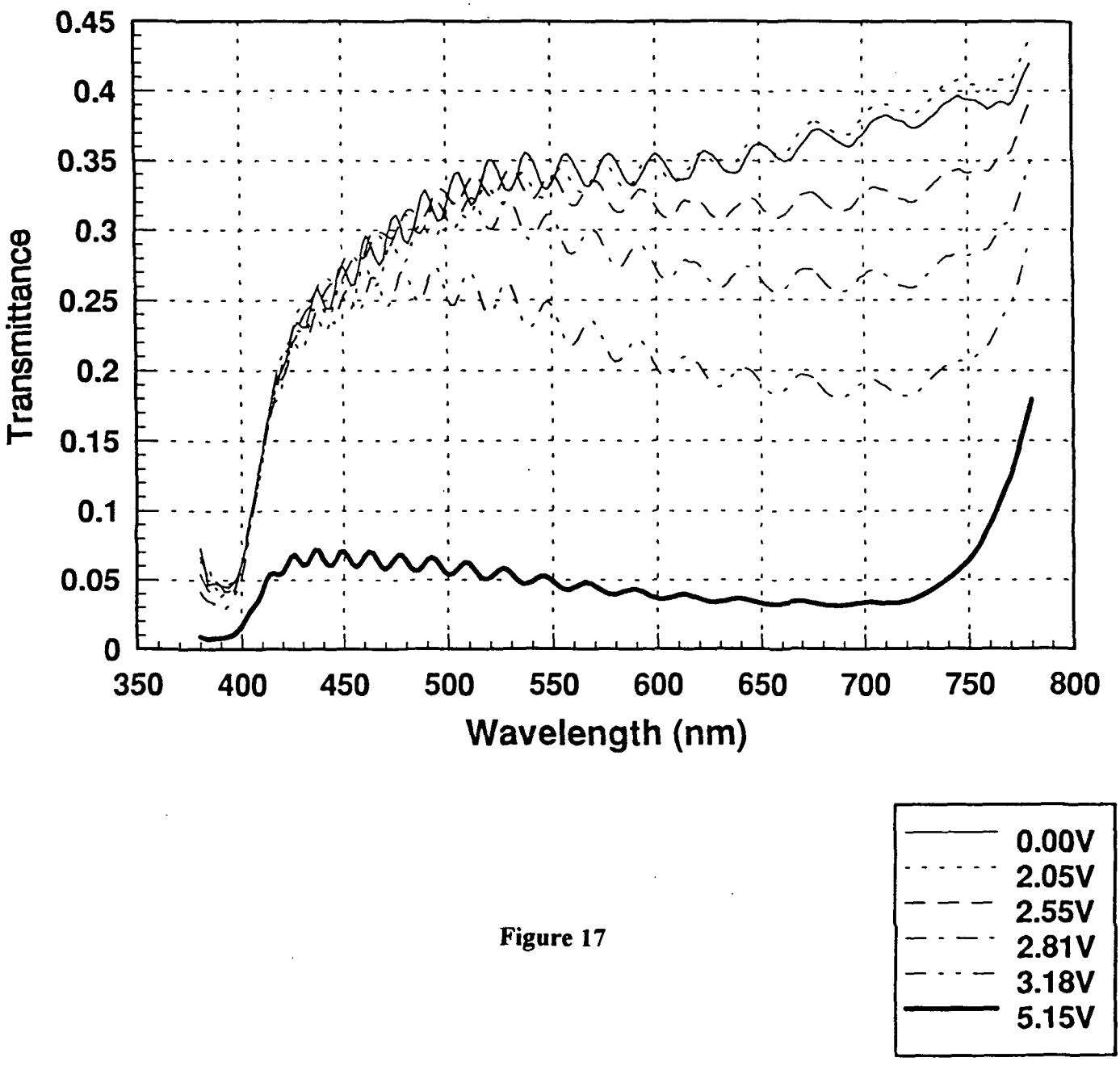


Figure 17

# Experimental Spectral Transmittance Normally White TN Cell (1) (ZLI-4792)

## $\Theta = 30$ degrees $\Phi = 0.0$ degrees

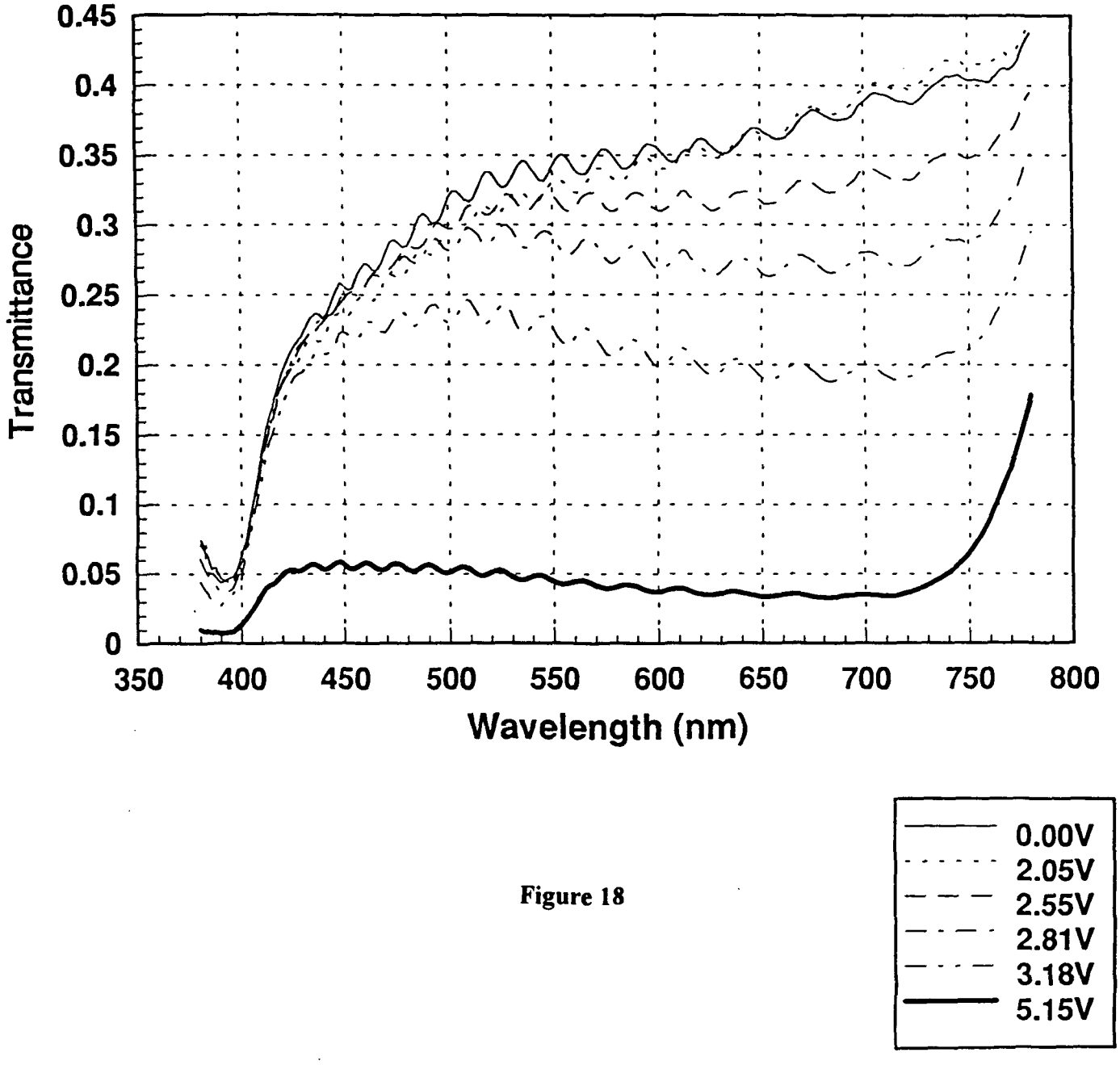


Figure 18

# Experimental Spectral Transmittance Normally White TN Cell (1) (ZLI-4792)

## $\Theta = 30$ degrees $\Phi = 135$ degrees

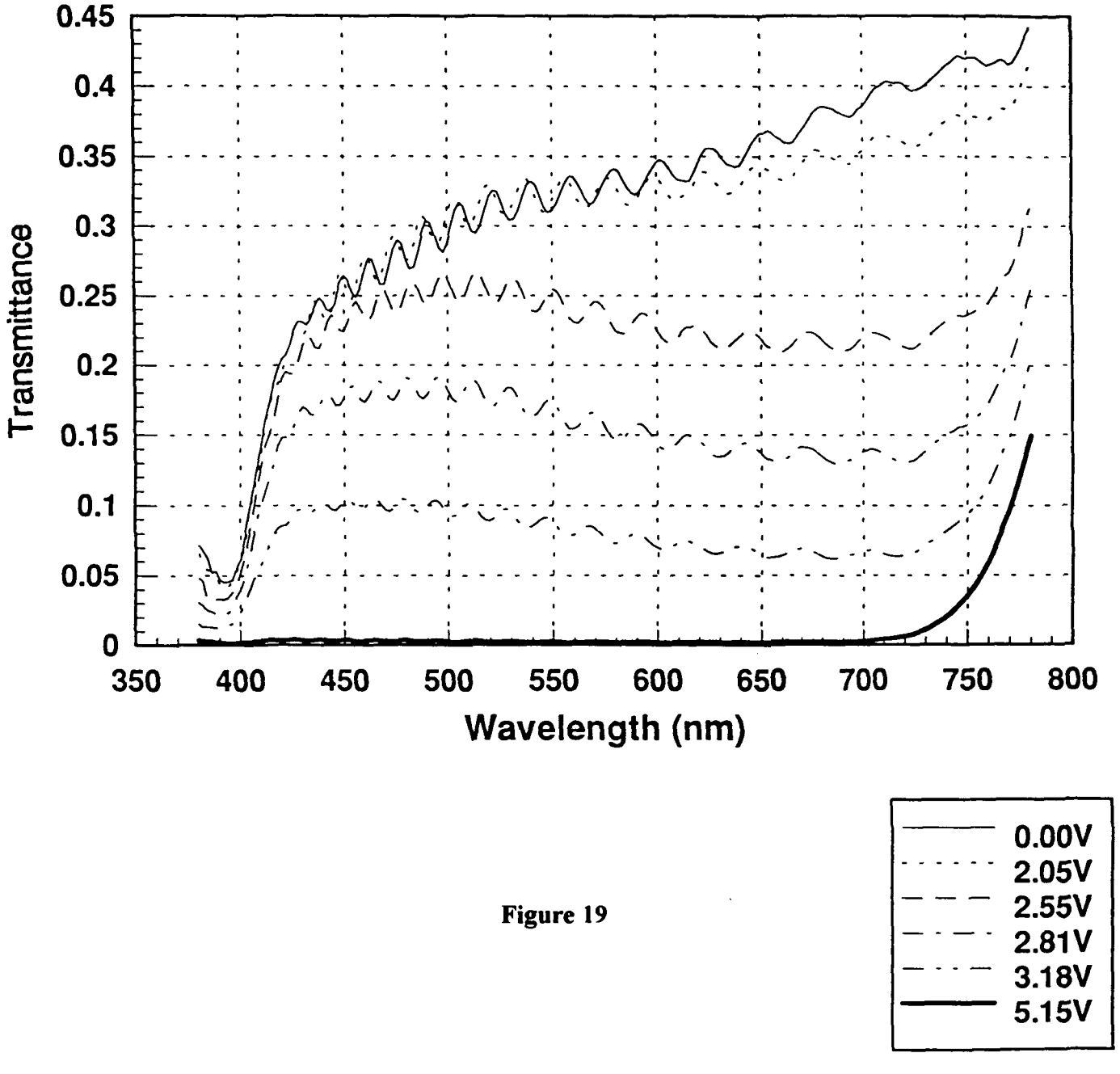


Figure 19

# Experimental Spectral Transmittance Normally White TN Cell (1) (ZLI-4792)

## $\Theta = 30$ degrees $\Phi = 315$ degrees

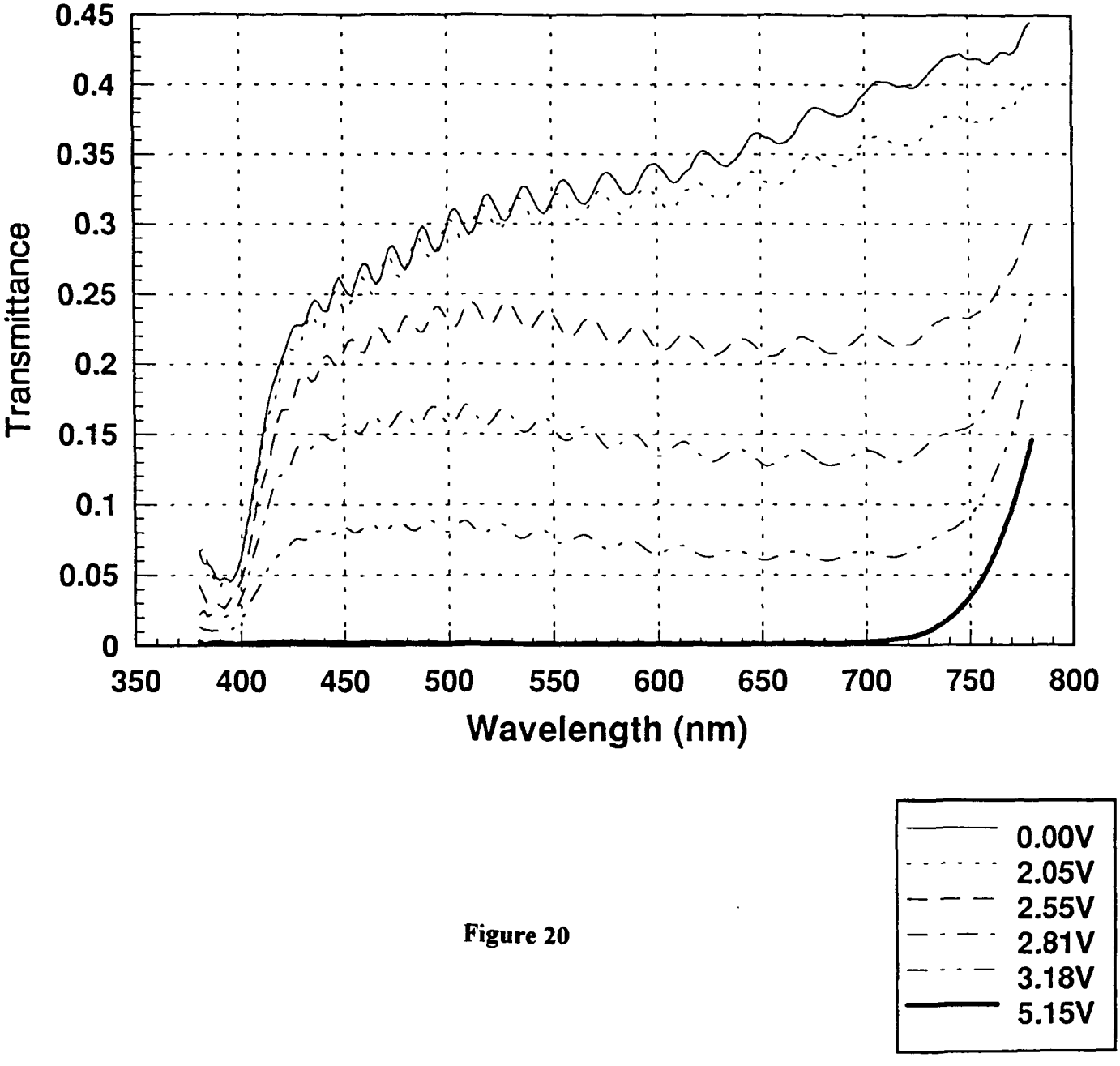


Figure 20

# Experimental Spectral Transmittance Normally White TN Cell (1) (ZLI-4792)

## $\Theta = 30$ degrees $\Phi = 180$ degrees

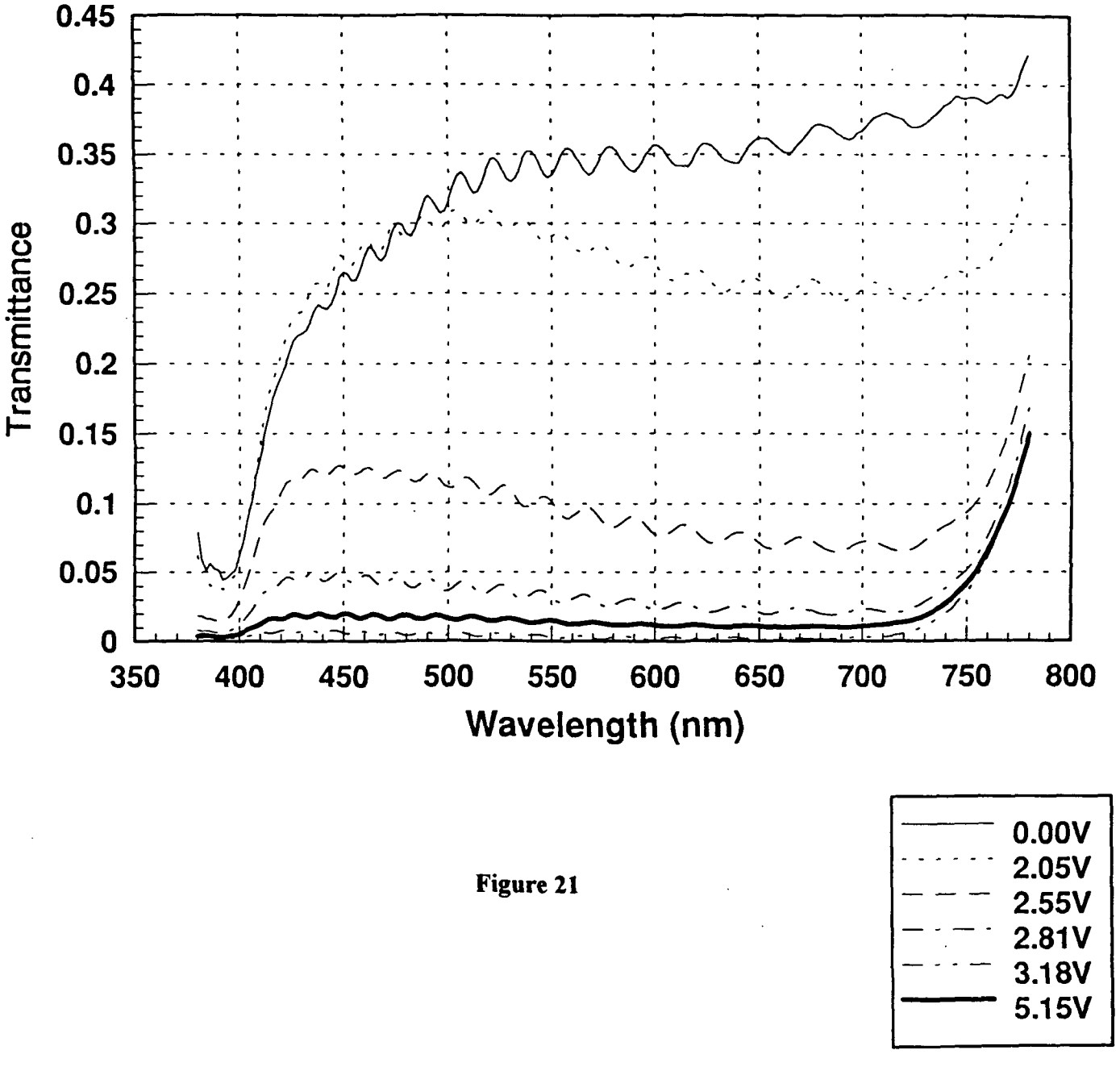


Figure 21

# Experimental Spectral Transmittance Normally White TN Cell (1) (ZLI-4792)

## $\Theta = 30$ degrees $\Phi = 270$ degrees

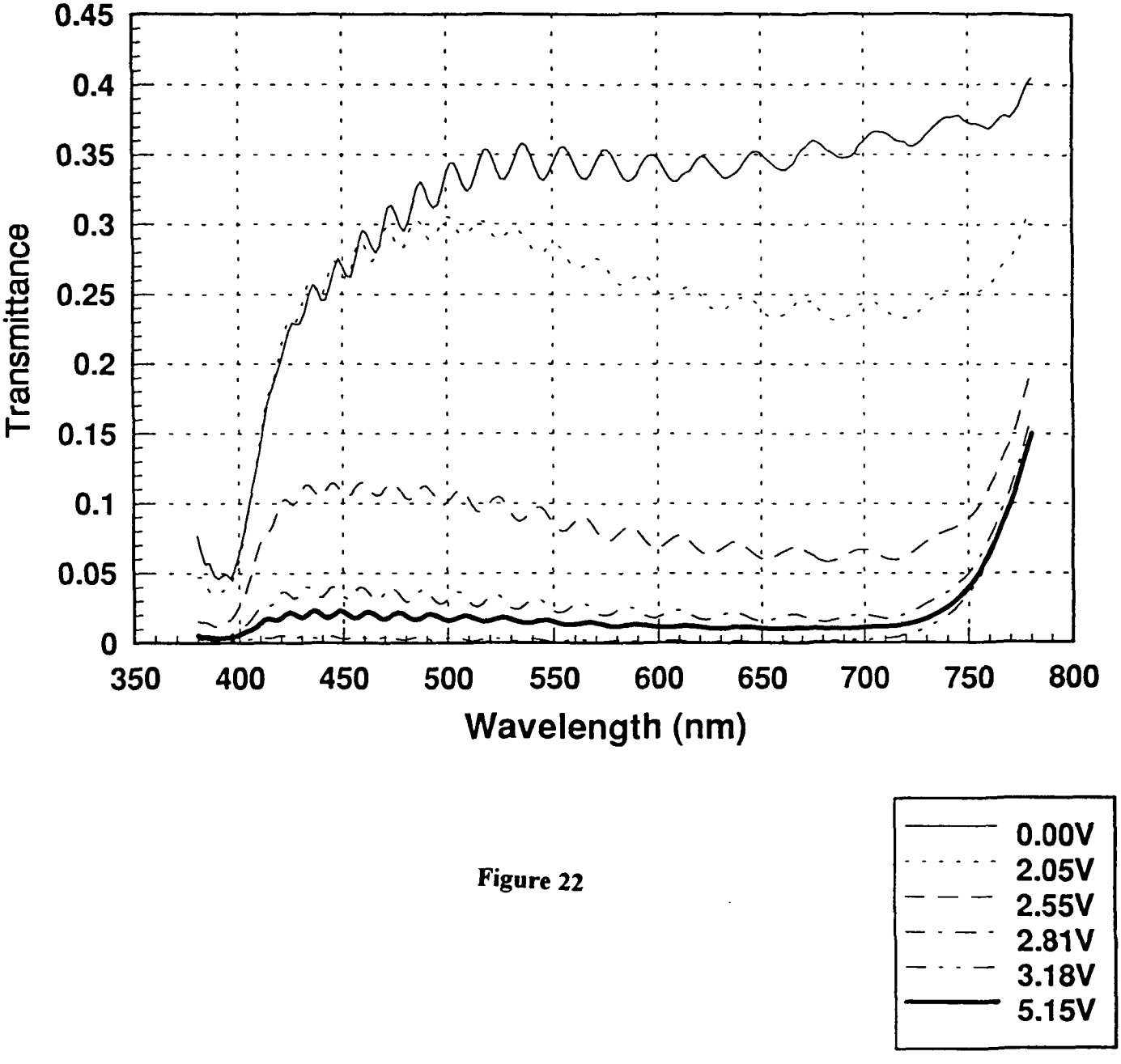


Figure 22

# Experimental Spectral Transmittance Normally White TN Cell (1) (ZLI-4792)

## $\Theta = 30$ degrees $\Phi = 225$ degrees

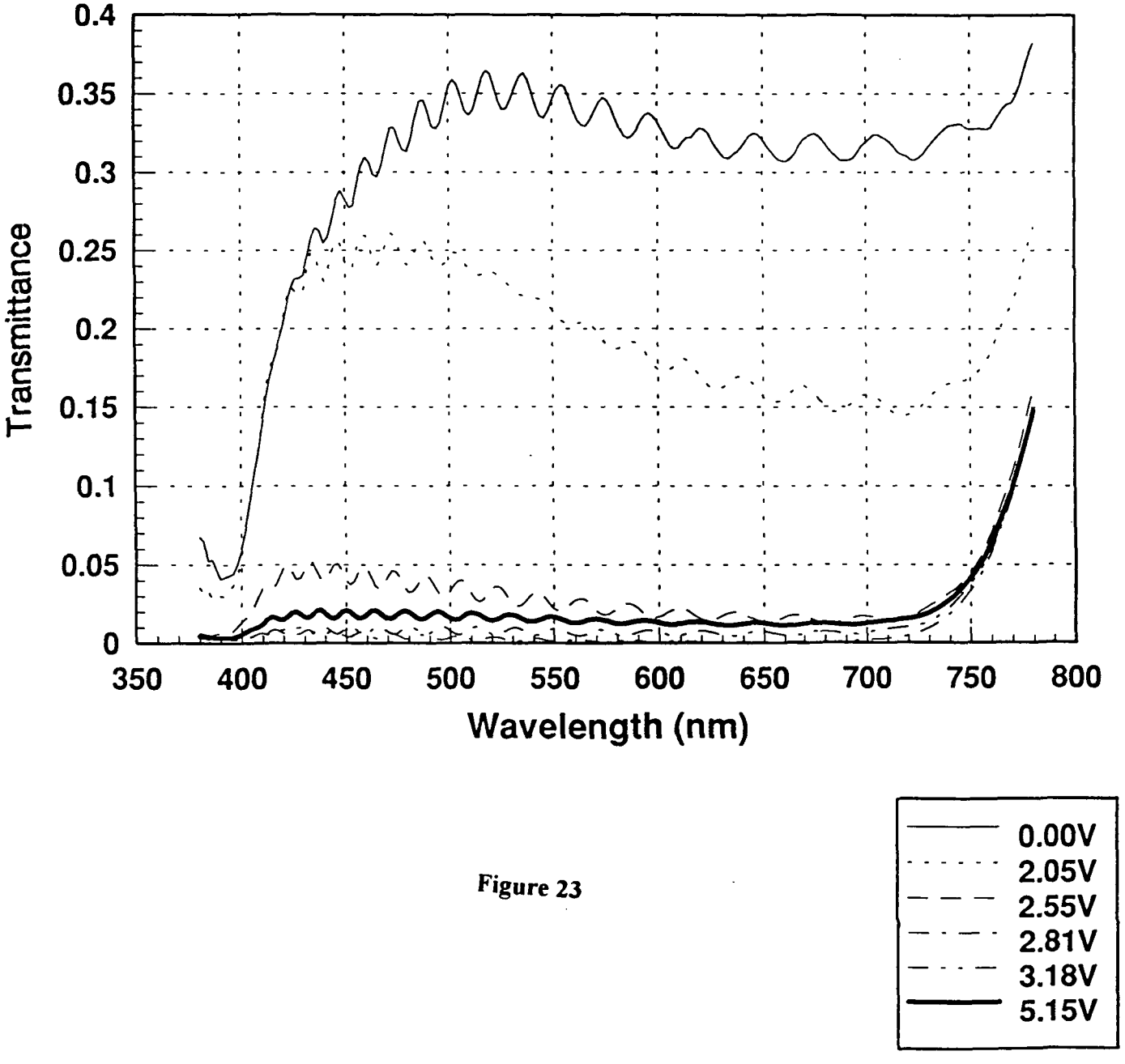


Figure 23

# Experimental Spectral Transmittance Normally White TN cell #1 (ZLI-4792)

## $\Theta$ = 50 degrees $\Phi$ = 45 degrees

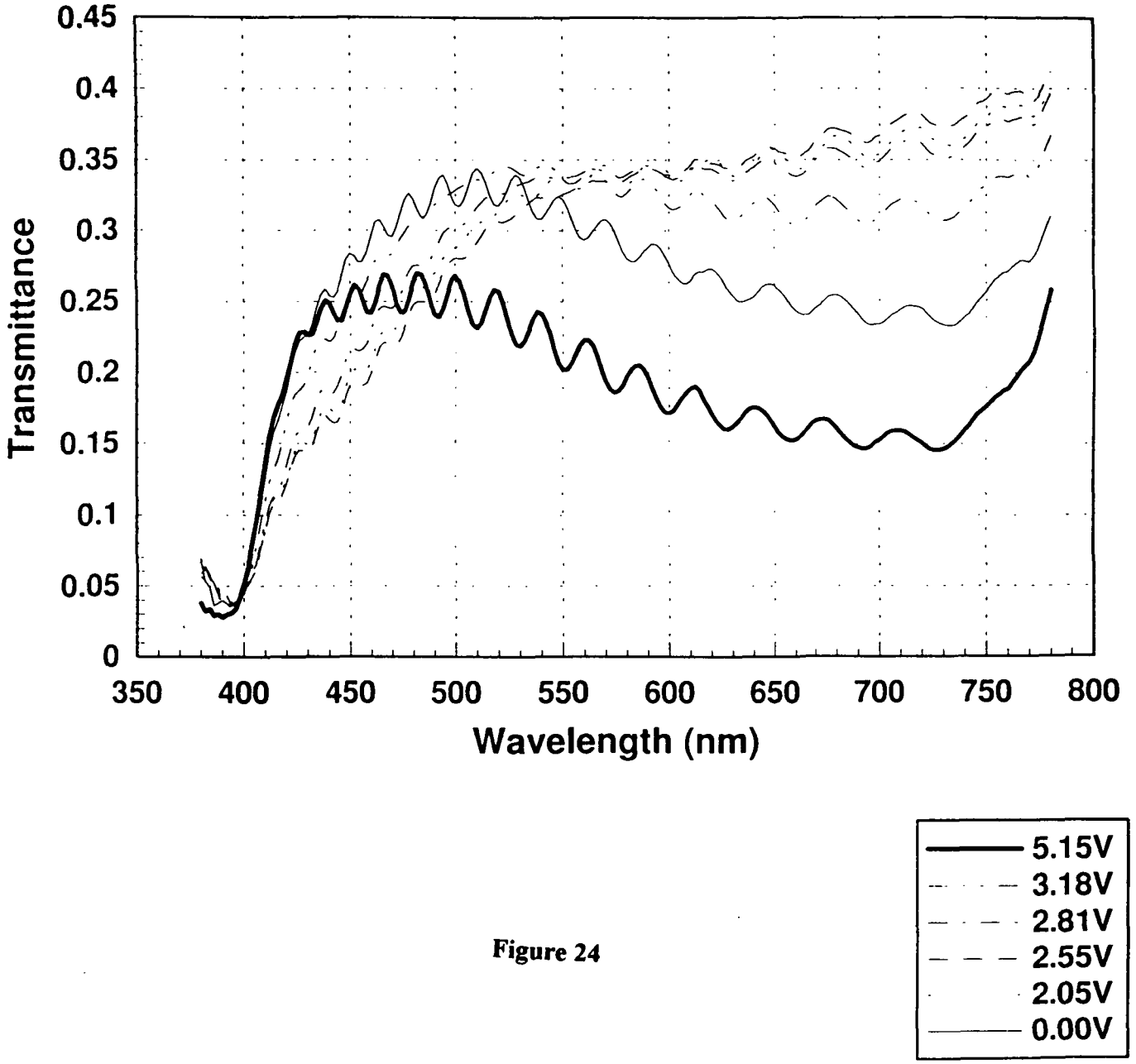


Figure 24

# Experimental Spectral Transmittance Normally White TN cell #1 (ZLI-4792)

## $\Theta$ = 50 degrees $\Phi$ = 90 degrees

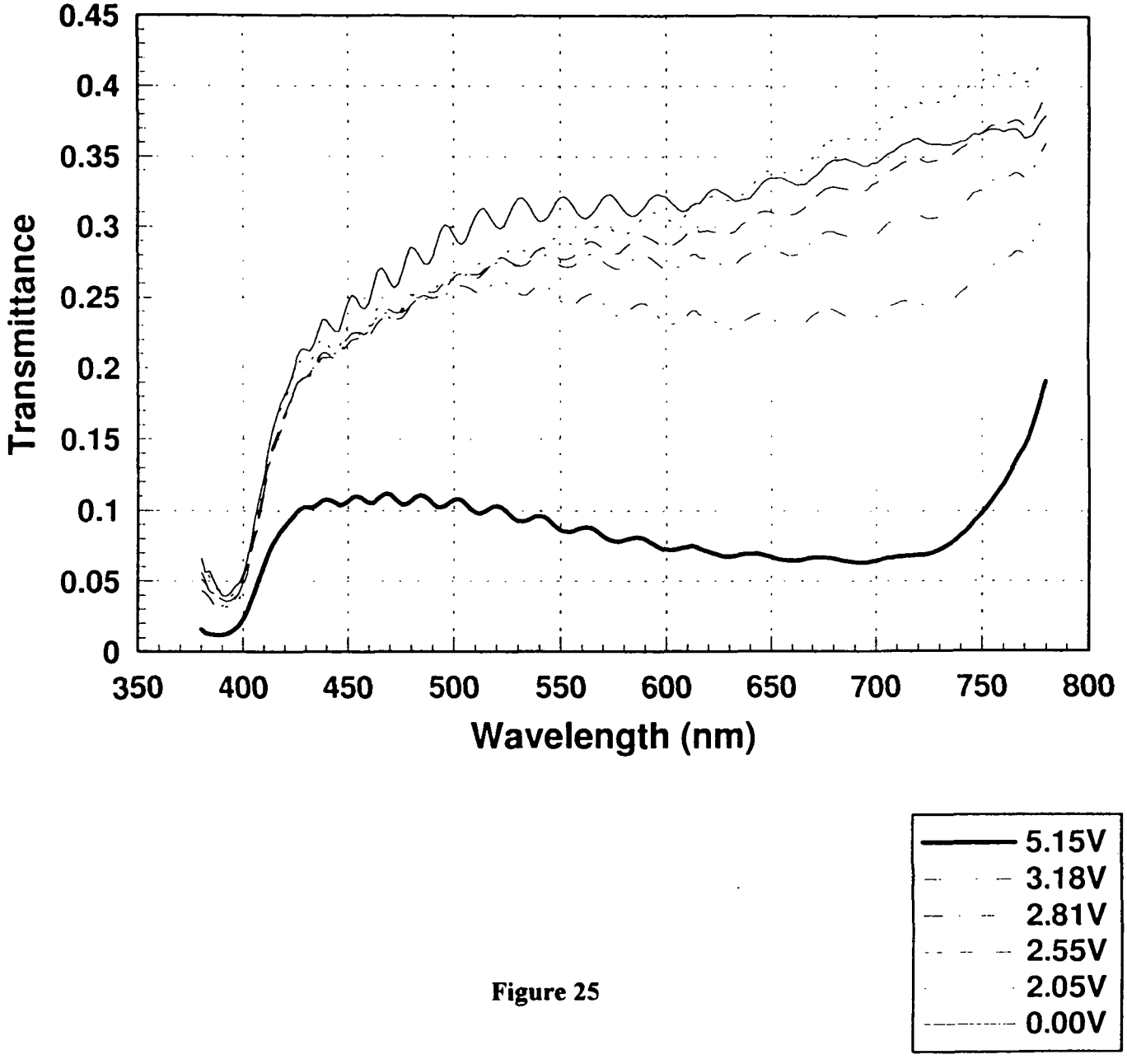


Figure 25

# Experimental Spectral Transmittance Normally White TN cell #1 (ZLI-4792)

## $\Theta$ = 50 degrees $\Phi$ = 135 degrees

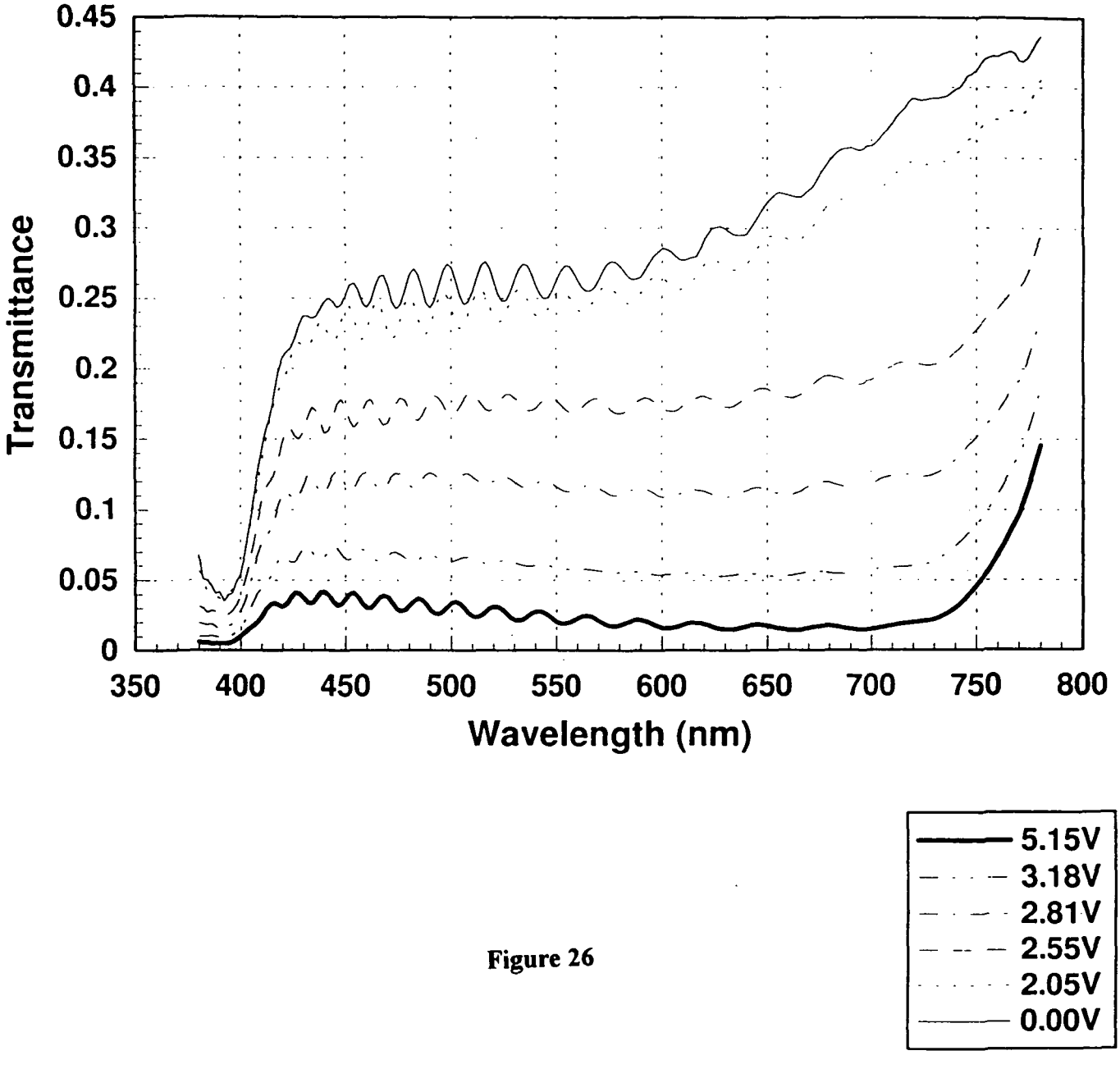


Figure 26

# Experimental Spectral Transmittance Normally White TN cell #1 (ZLI-4792)

## $\Theta$ = 50 degrees $\Phi$ = 180 degrees

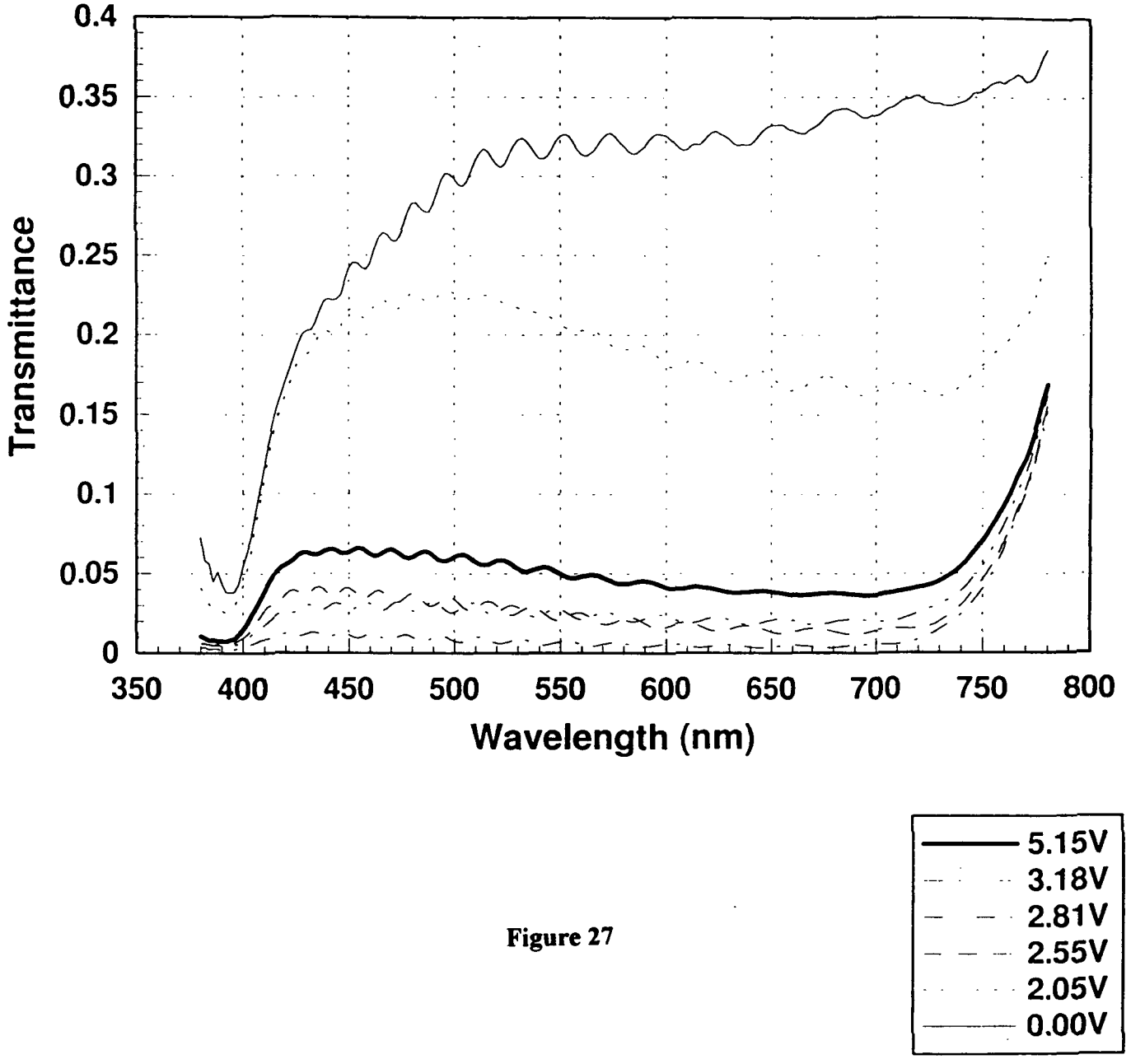


Figure 27

# Experimental Spectral Transmittance
# Normally White TN cell #1 (ZLI-4792)

## $\Theta$ = 50 degrees $\Phi$ = 225 degrees

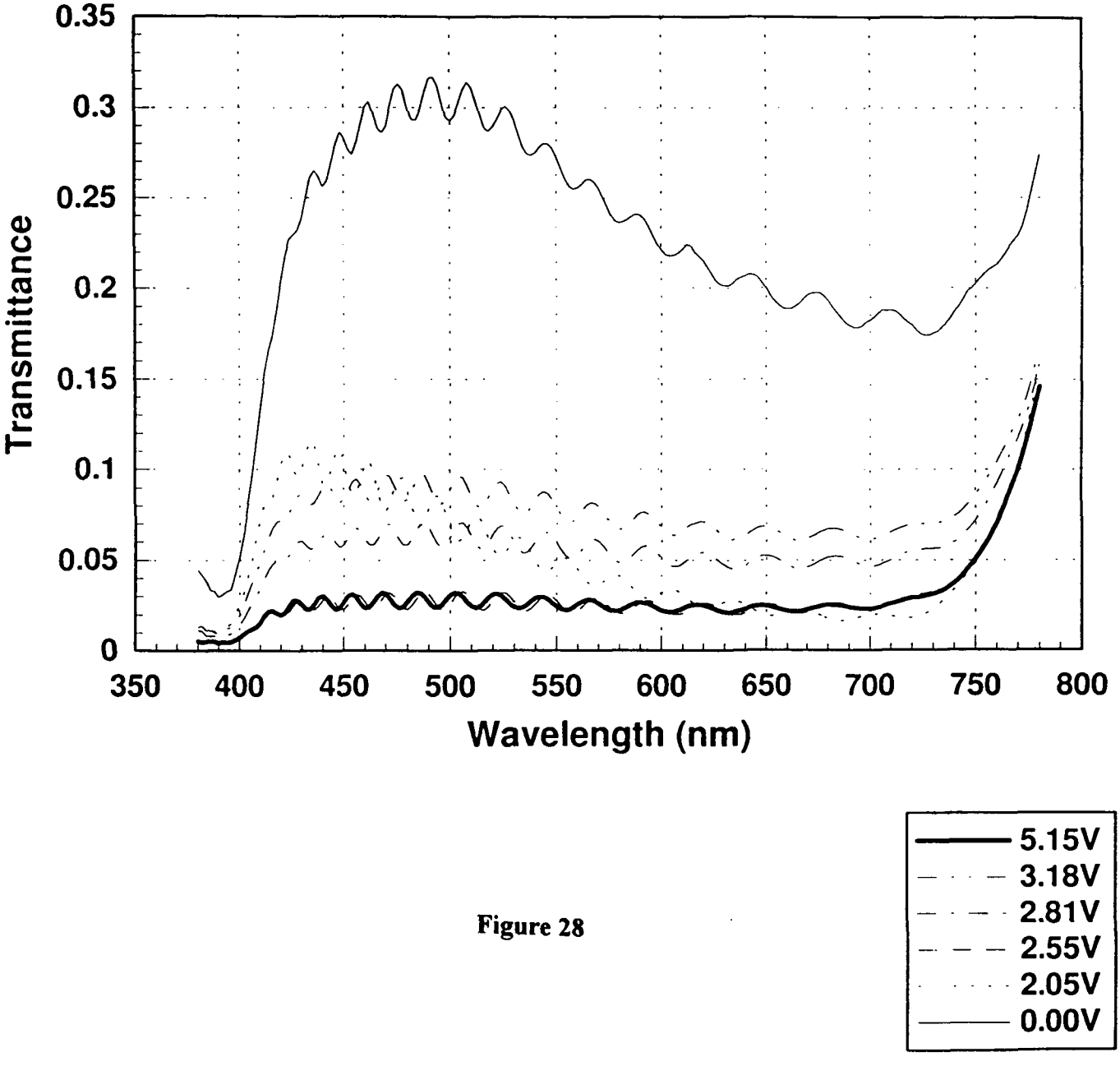


Figure 28

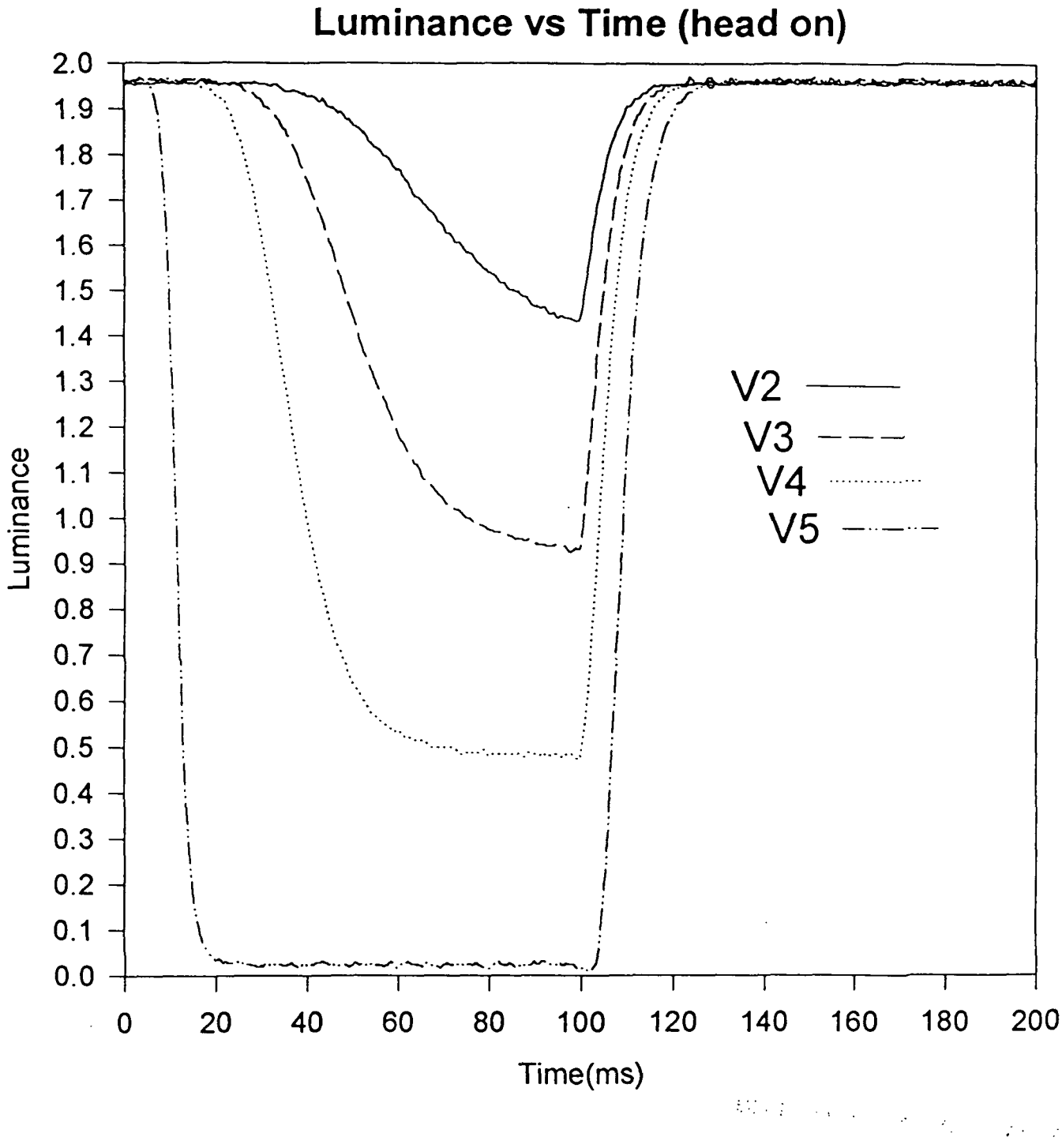


**Figure 29:** Dynamic switching behavior of NWTN cell #1, at voltages given in text and at $\theta = 0$, $\phi = 0$.

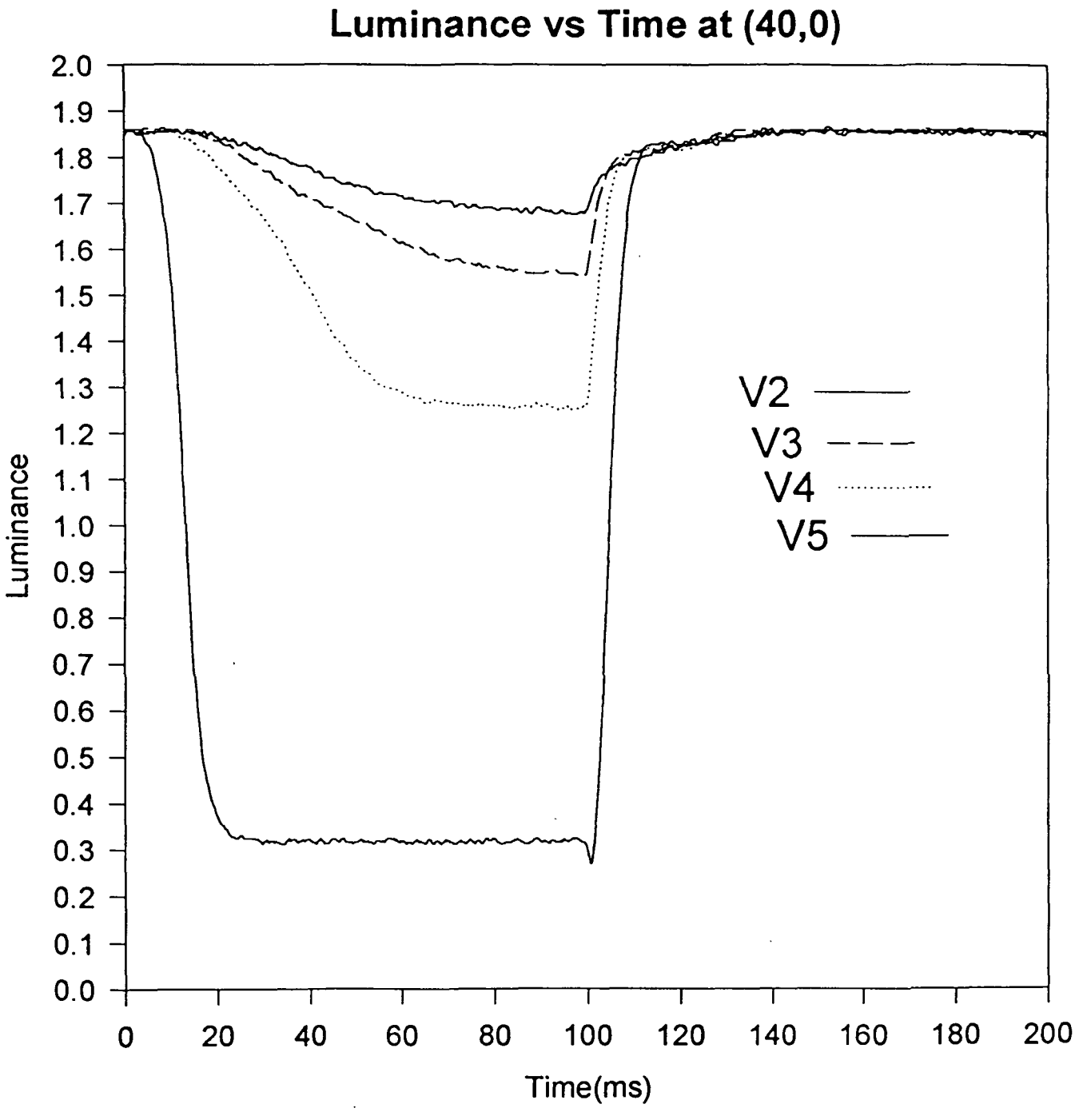


**Figure 30:** Dynamic switching behavior of NWTN cell #1, at voltages given in text and at $\theta = 40$, $\phi = 0$.

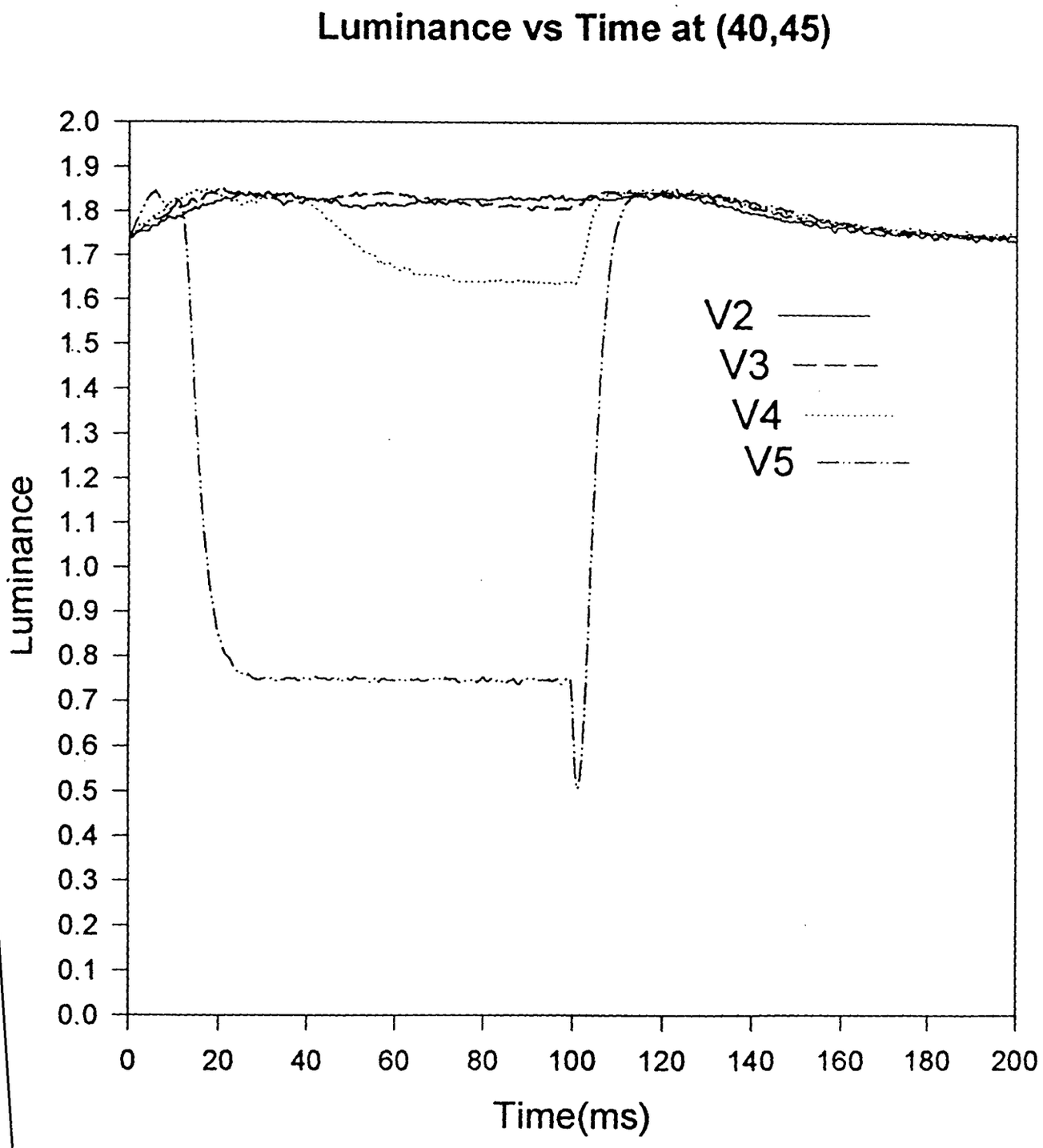


**Figure 31:** Dynamic switching behavior of NWTN cell #1, at voltages given in text and at $\theta$ =40, $\phi$ = 45.

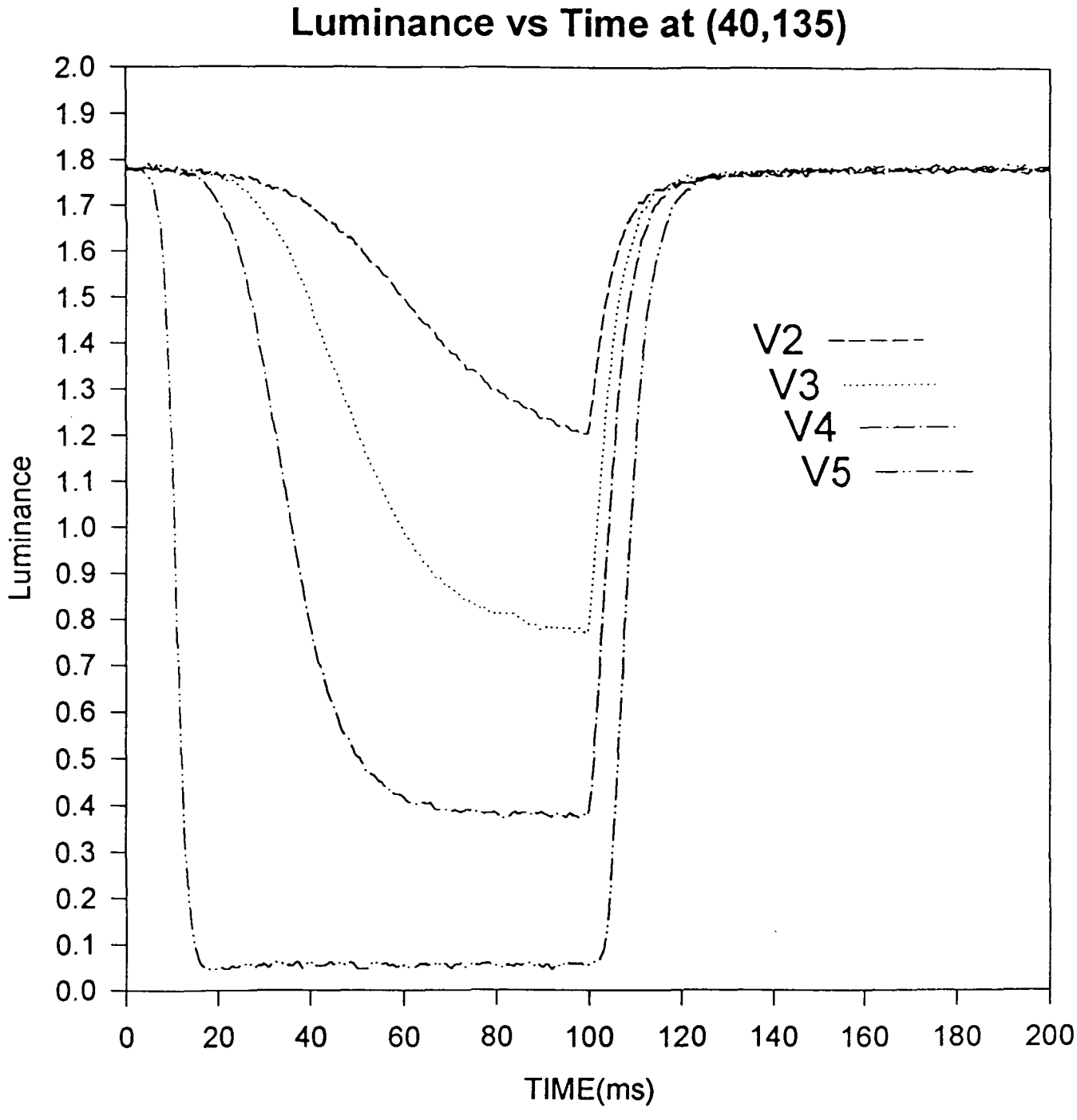


**Figure 32:** Dynamic switching behavior of NWTN cell #1, at voltages given in text and at $\theta$ =40, $\phi$ = 135.

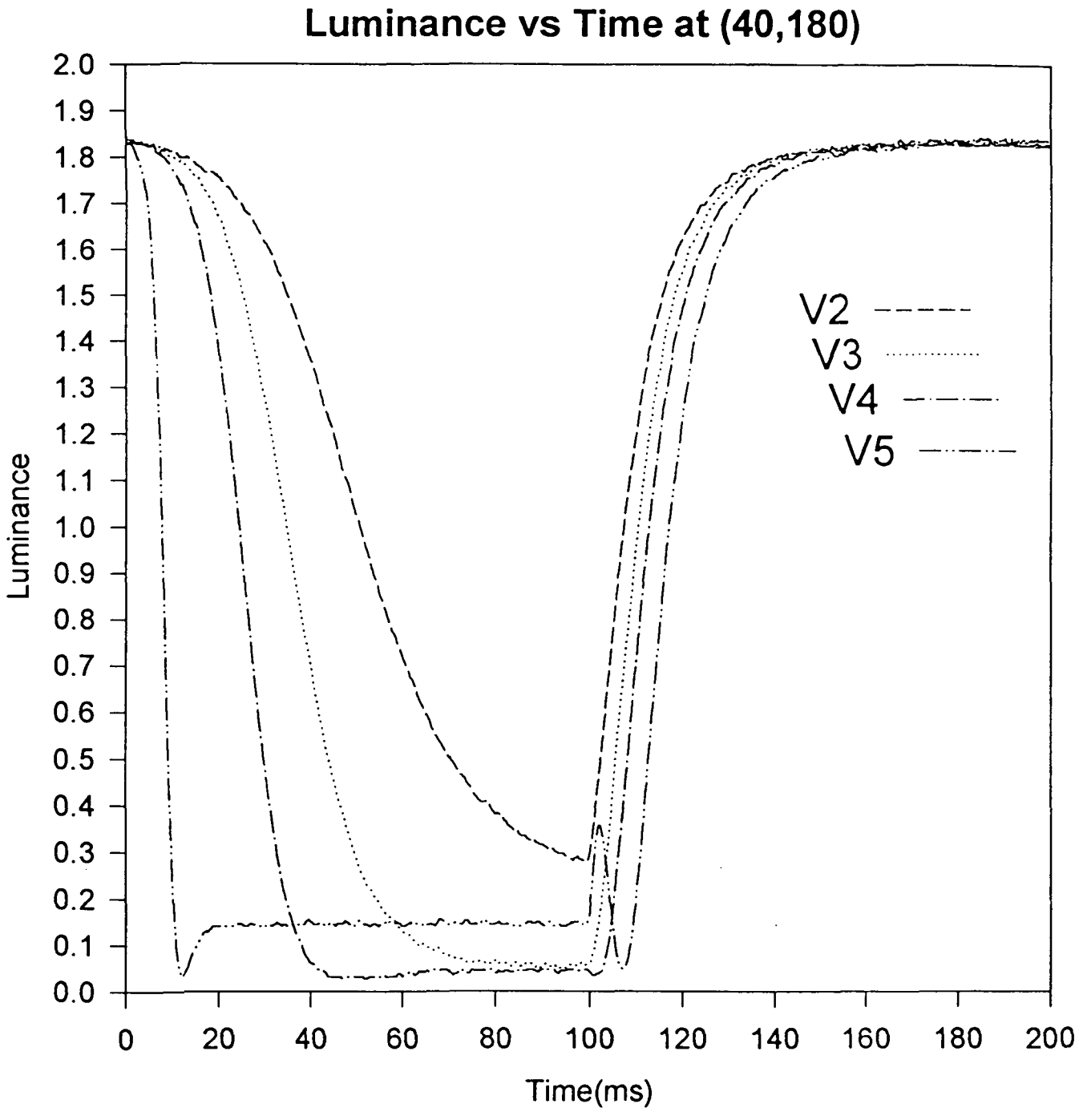


**Figure 33:** Dynamic switching behavior of NWTN cell #1, at voltages given in text and at $\theta$ =40, $\phi$ = 180.

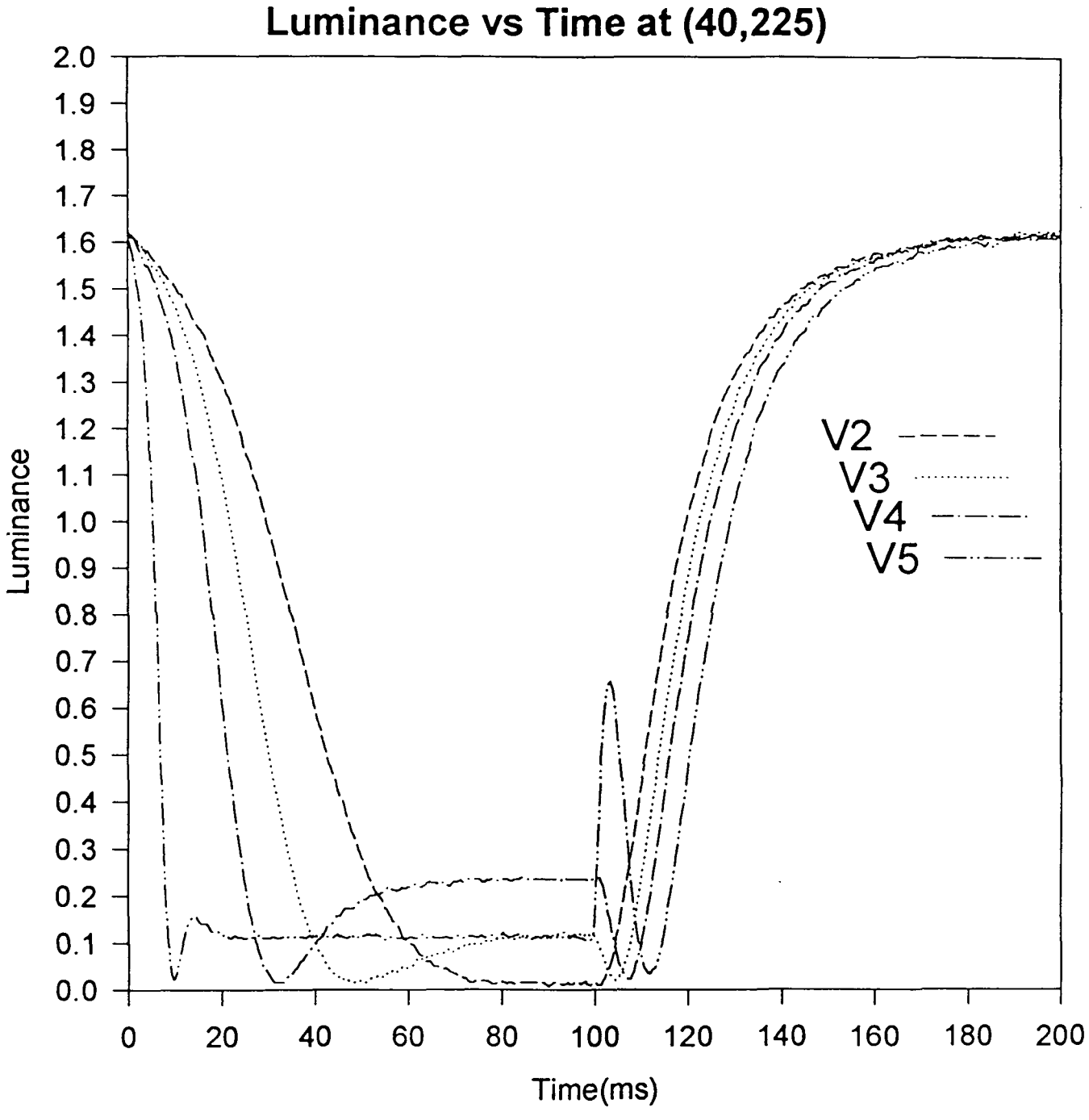


**Figure 34:** Dynamic switching behavior of NWTN cell #1, at voltages given in text and at $\theta$ =40, $\phi$ = 225.

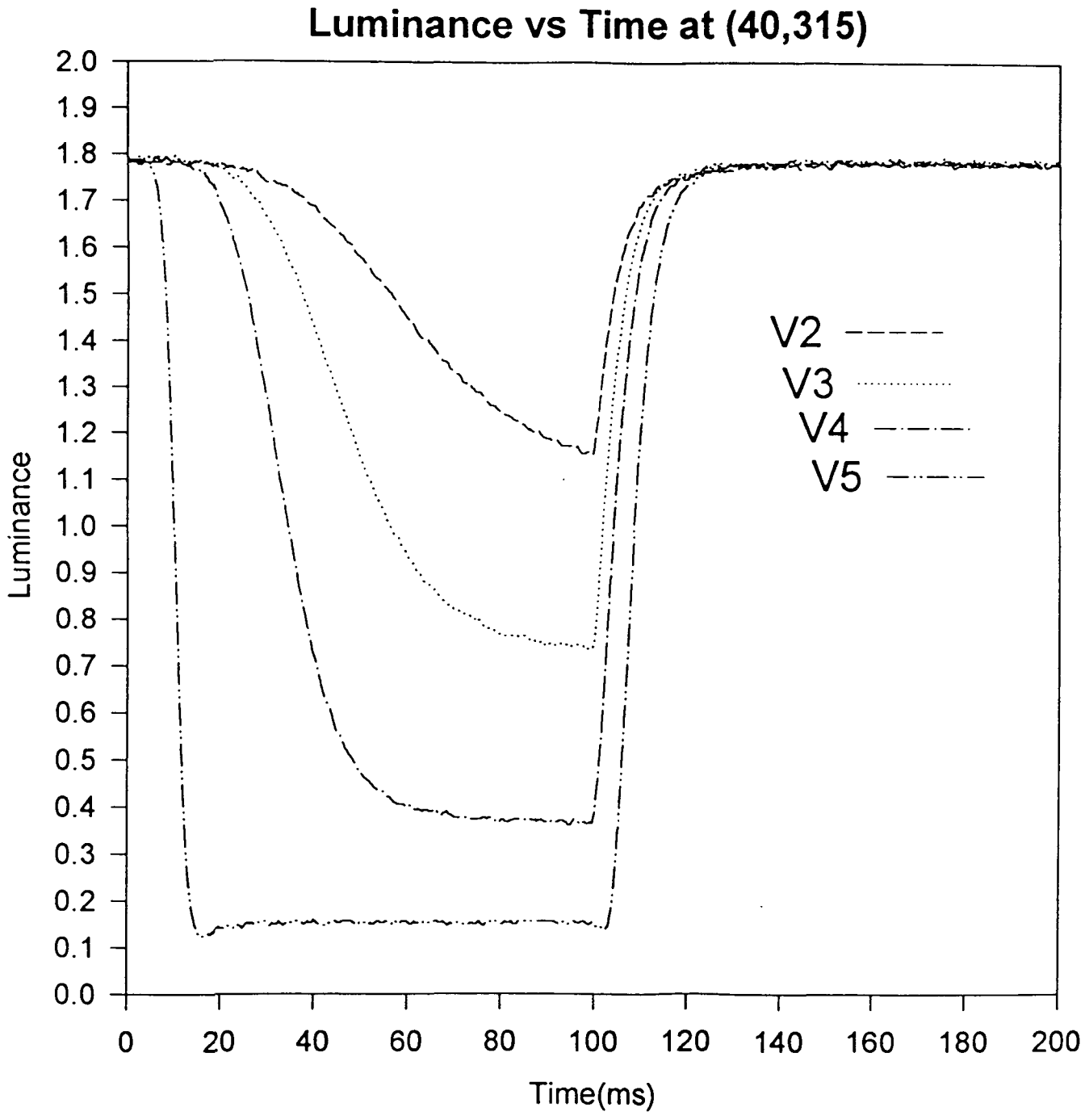


**Figure 35:** Dynamic switching behavior of NWTN cell #1, at voltages given in text and at $\theta$ =40, $\phi$ = 315.

# Luminance vs. Voltage for Standish STN 240 deg twist cell

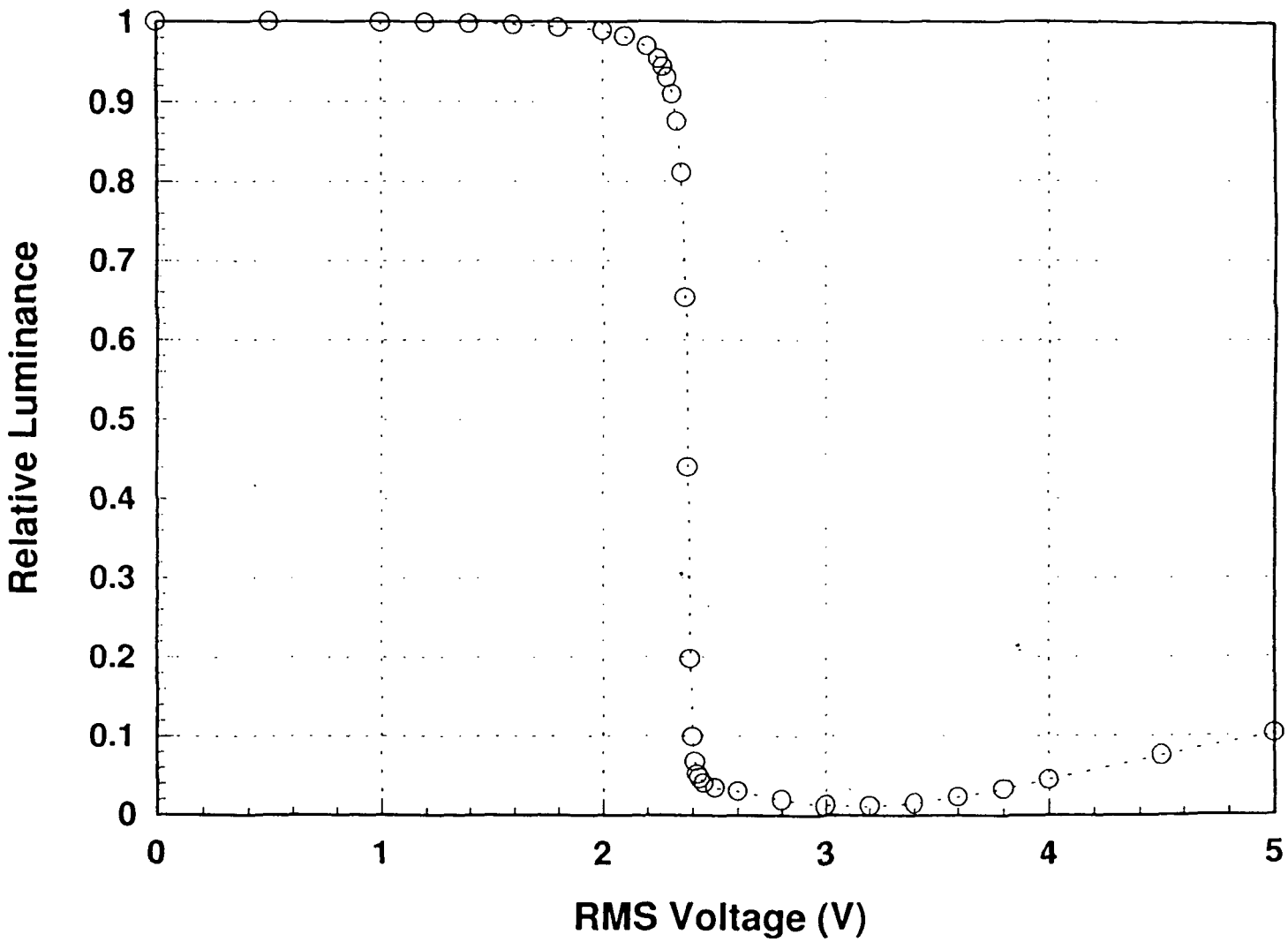


Figure 36

# Luminance vs. Voltage for Standish STN 240 deg twist cell

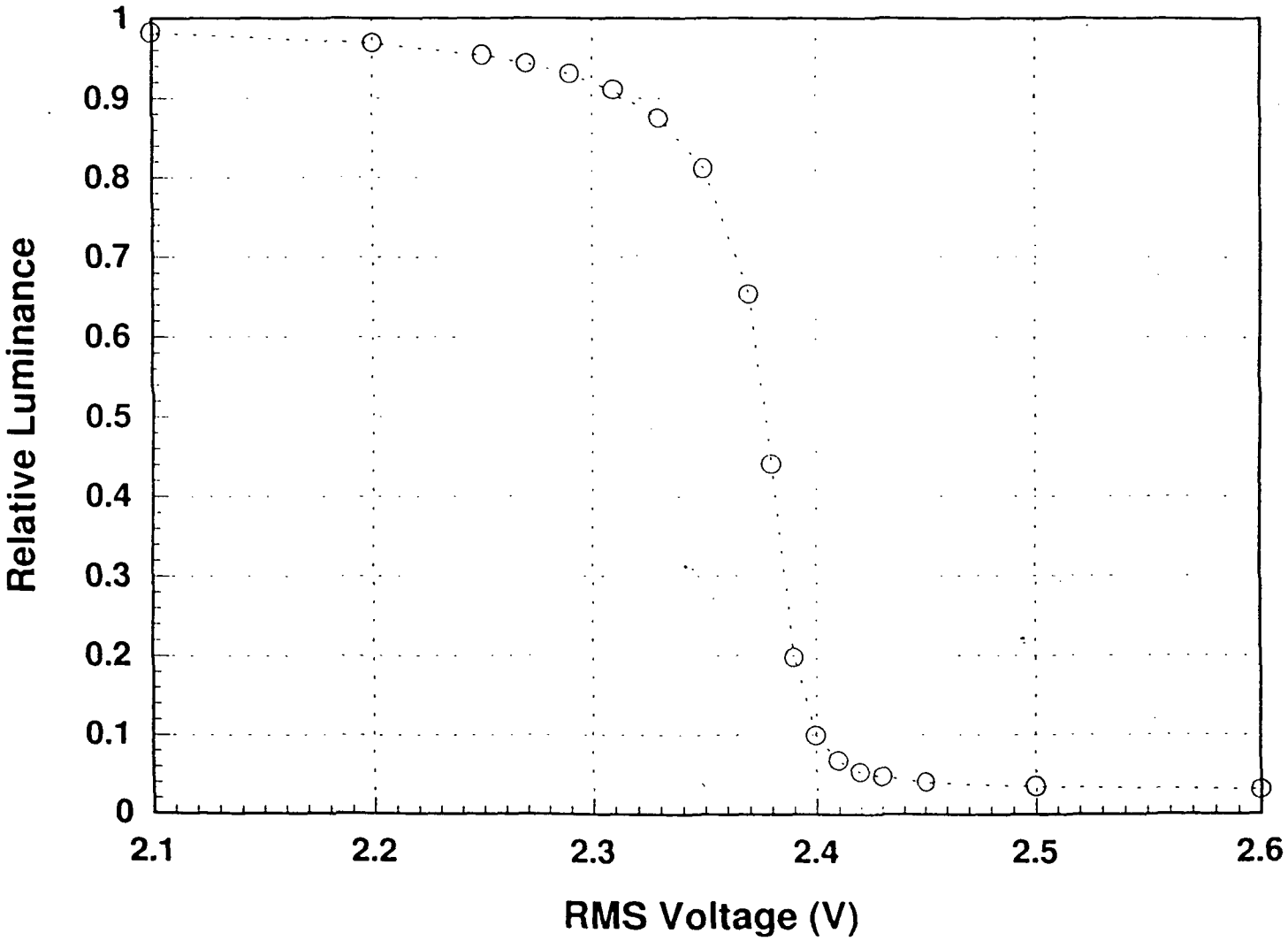


Figure 37

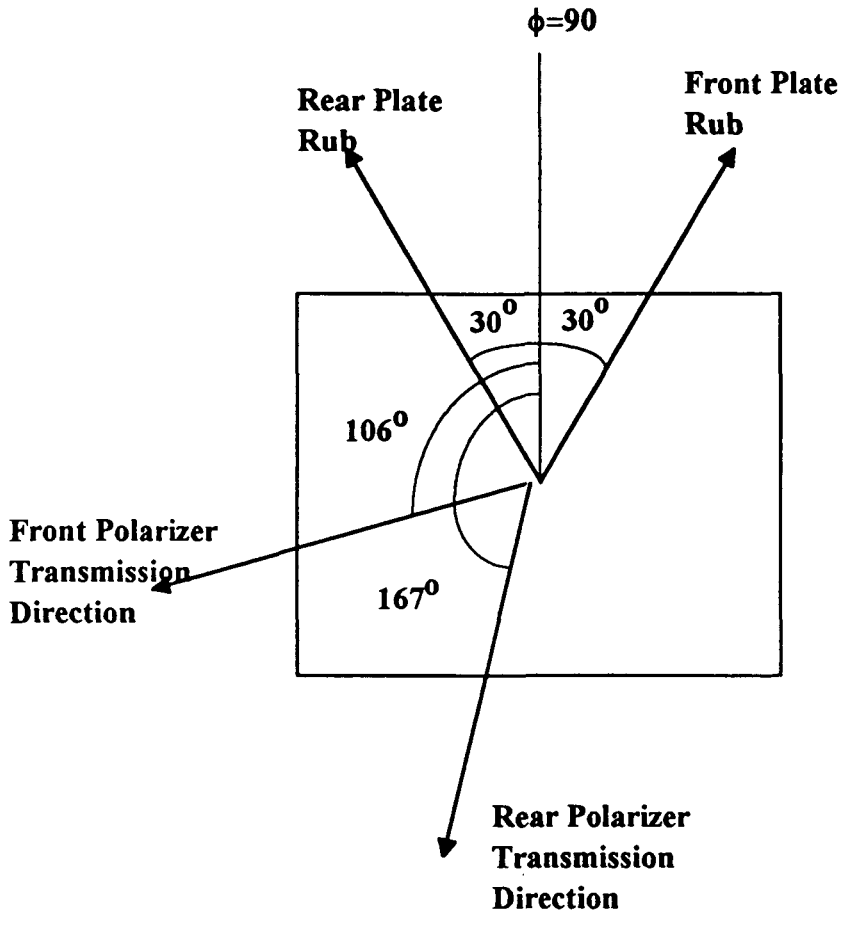


**Figure 38: STN Cell Geometry**

# Experimental Isoluminance curves at 0.0V

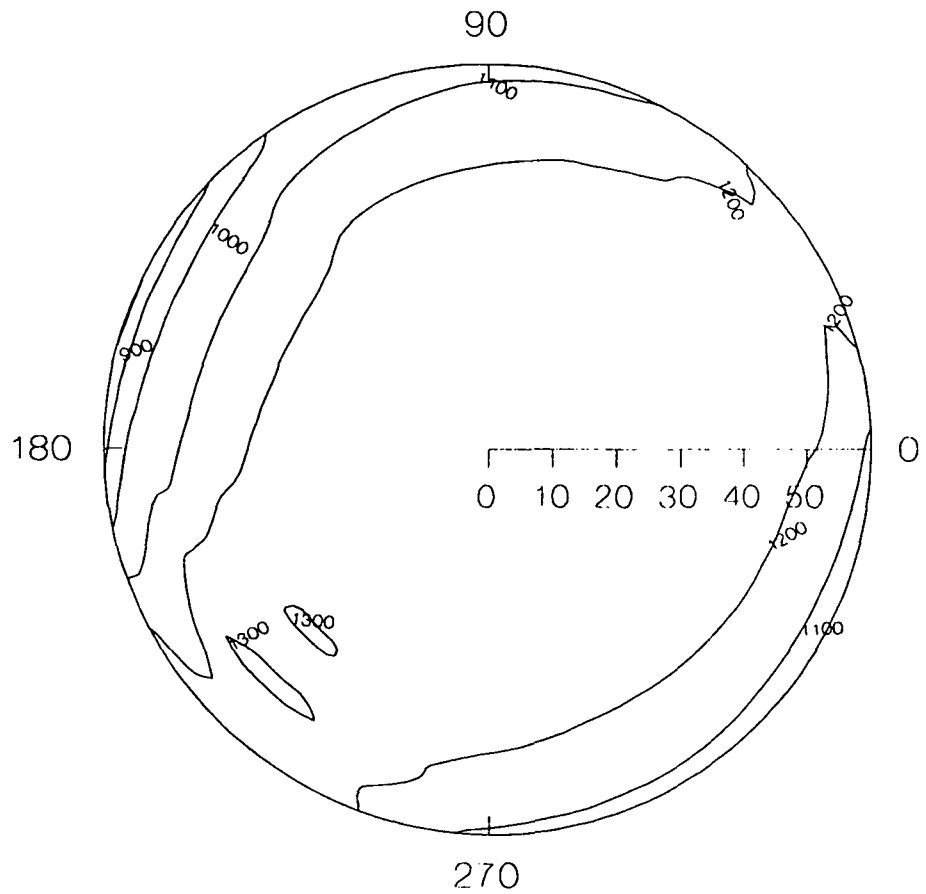


3990
Source Luminance ~~4368~~ fl
Data taken with Standish 240 deg STN cell
Curves generated using Systat 5.03 with
smoothing set on NEXPO
grid on default setting (30 by 30)
Z ticks set on 10

**Figure 39**

# Experimental Isoluminance curves at 2.25V

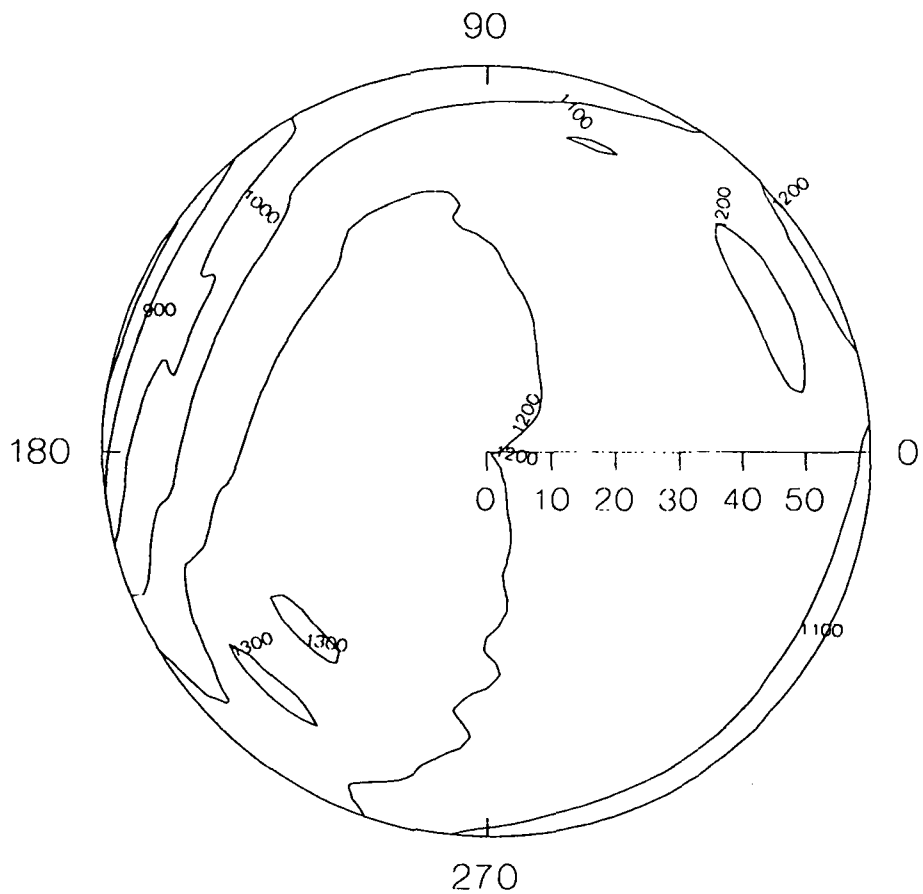


3990
Source Luminance ~~4368~~ fl
Data taken with Standish 240 deg STN cell
Curves generated using Systat 5.03 with
smoothing set on NEXPO
grid on default setting (30 by 30)
Z ticks set on 10

**Figure 40**

# Experimental Isoluminance curves at 2.36V

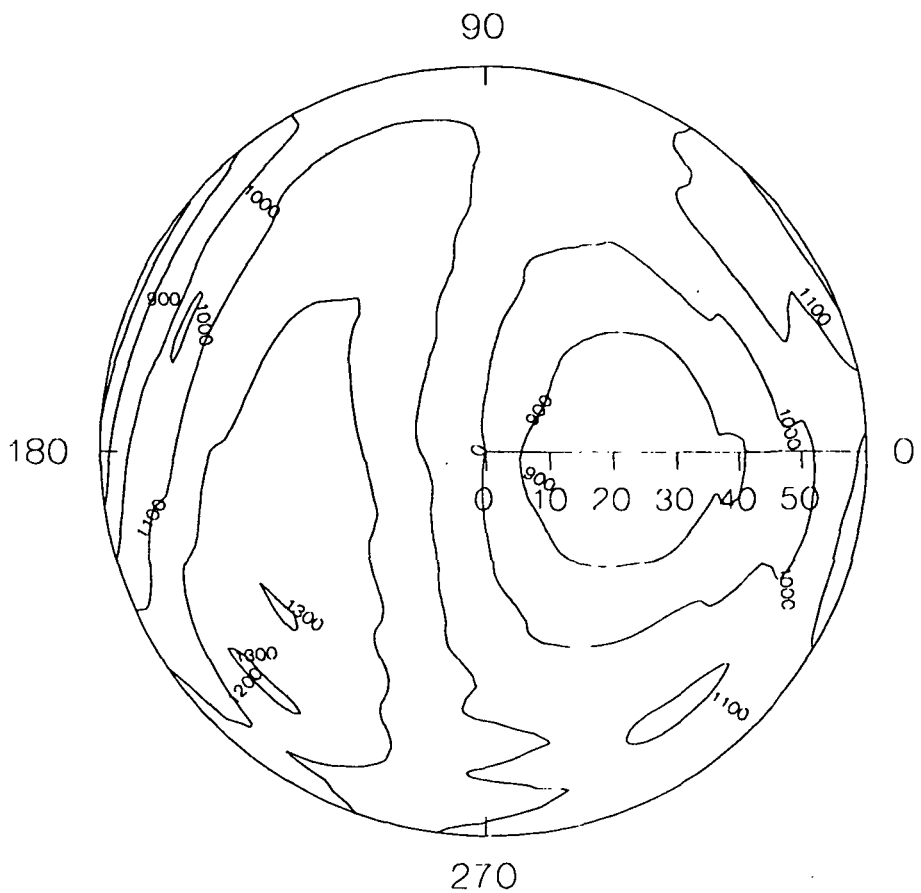


Source Luminance ~~4368~~ 3990 fl
Data taken with Standish 240 deg STN cell
Curves generated using Systat 5.03 with
smoothing set on NEXPO
grid on default setting (30 by 30)
2 ticks set on 10

**Figure 41**

# Experimental Isoluminance curves at 2.38V

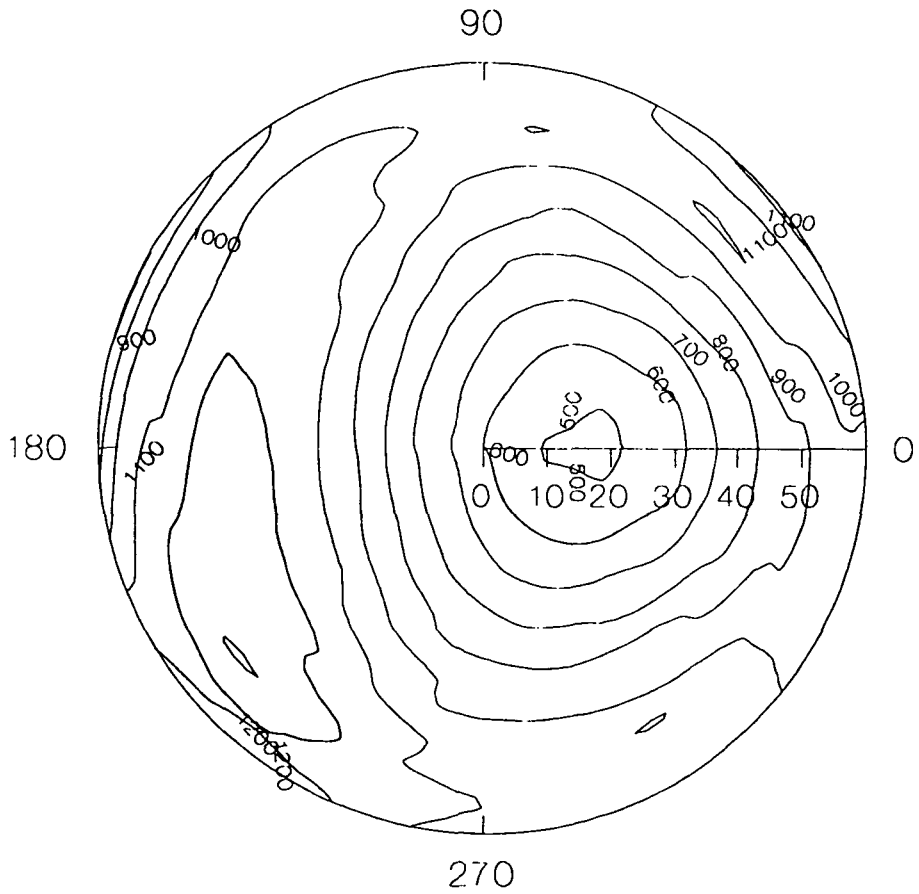


3490
~~4368~~ fl

Source Luminance ~~1387 fl~~
Data taken with Standish 240 deg STN cell
Curves generated using Systat 5.03 with
smoothing set on NEXPO
grid on default setting (30 by 30)
Z ticks set on 10

**Figure 42**

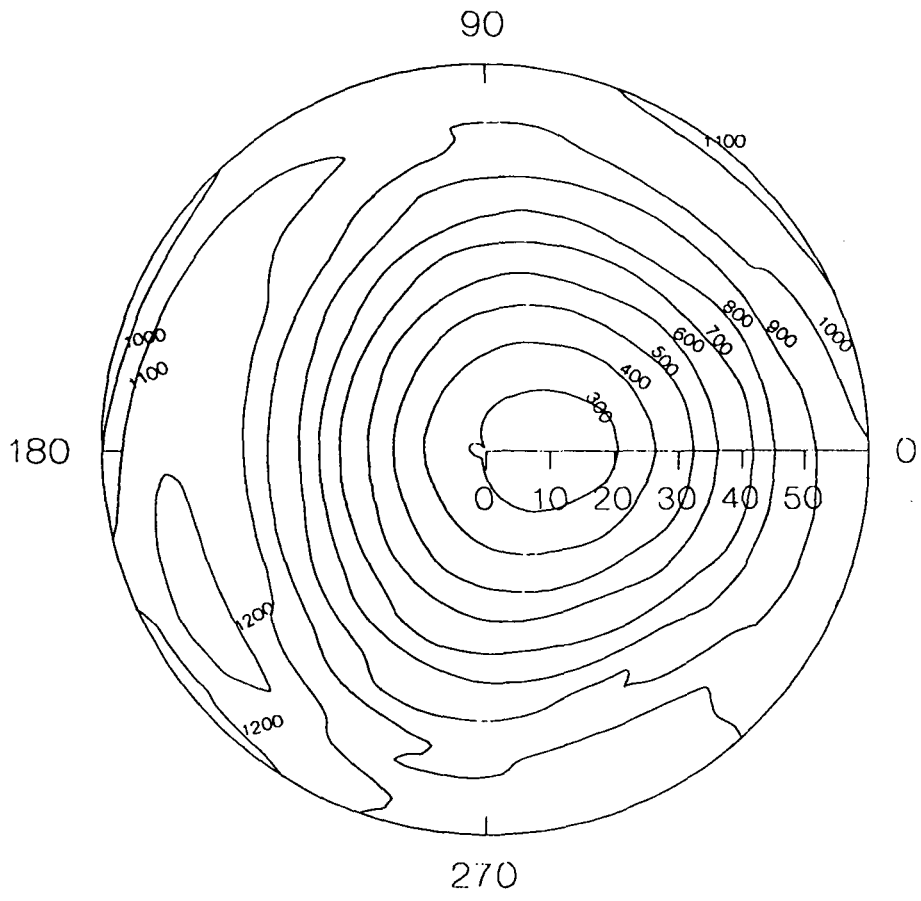


Source Luminance ~~4360~~ 3990 fl
Data taken with Standish 240 deg. STN cell
Curves generated using Systat 5.03 with
smoothing set on NEXPO
grid on default setting (30 by 30)
Z ticks set on 20

**Figure 43**

# Experimental Isoluminance curves at 2.45V

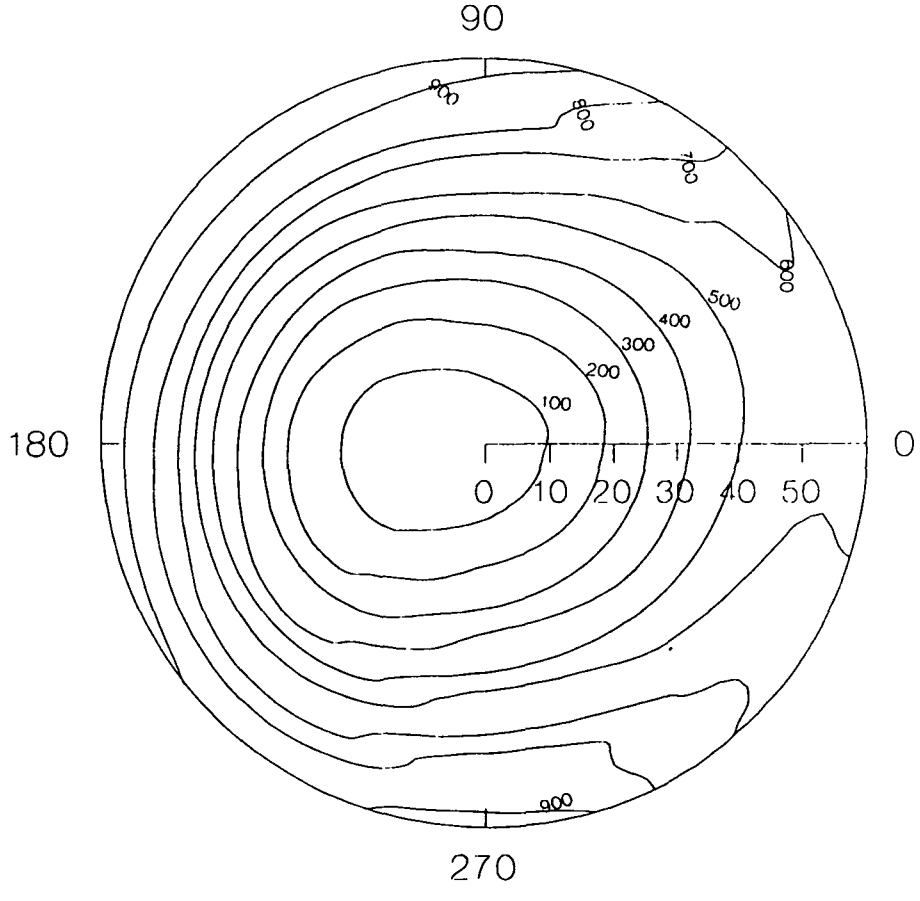


3990
Source Luminance ~~4360~~ fl
Data taken with Standish 240 deg. STN cell
Curves generated using Systat 5.03 with
smoothing set on NEXPO
grid on default setting (30 by 30)
Z ticks set on 20

**Figure 44**

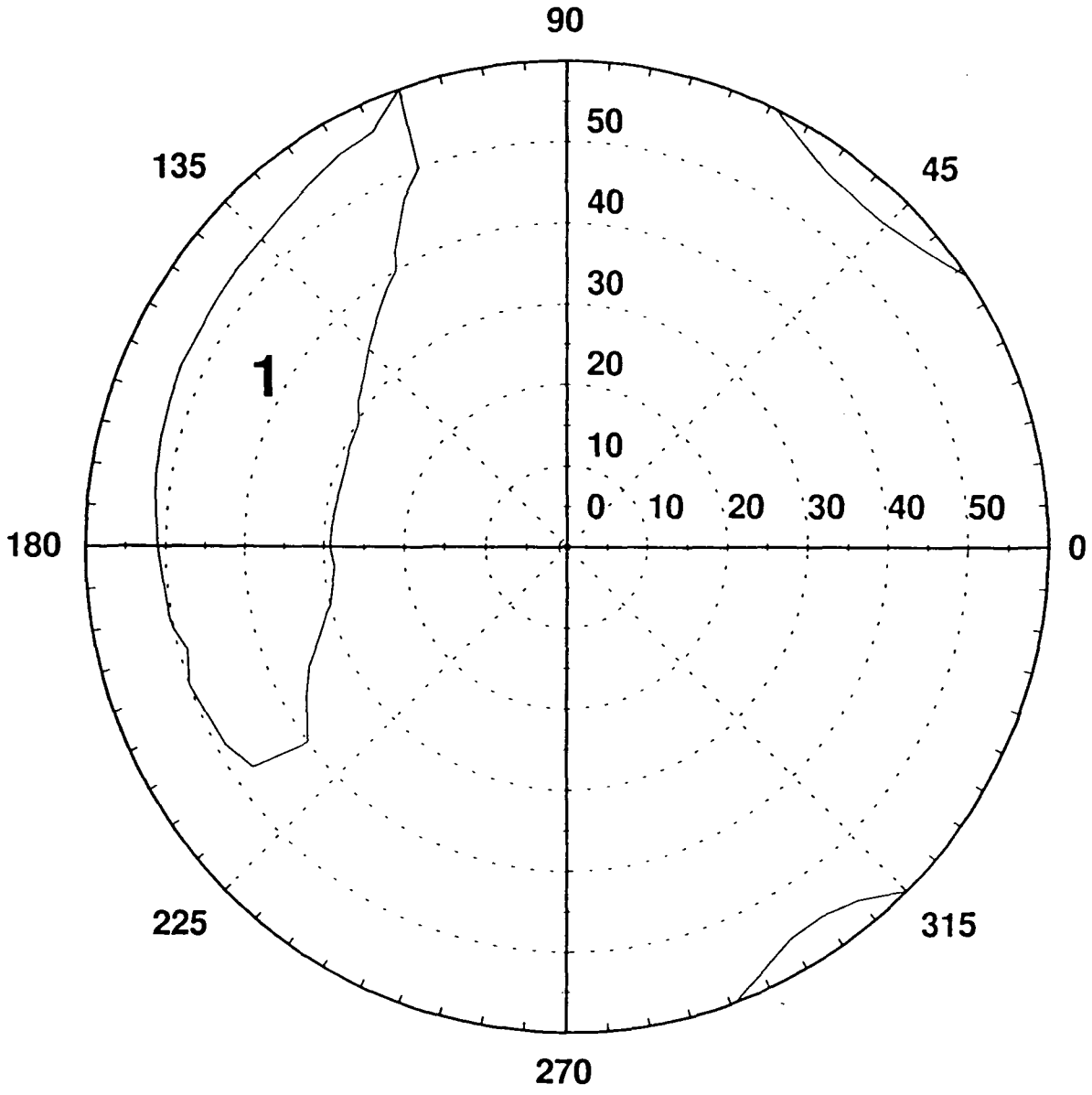
Iso-contrast for 240' STN(2.36/2.25)
90
135
45
180
0
225
315
270
50
40
30
20
10
0
10
20
30
40
50
1

Figure 45

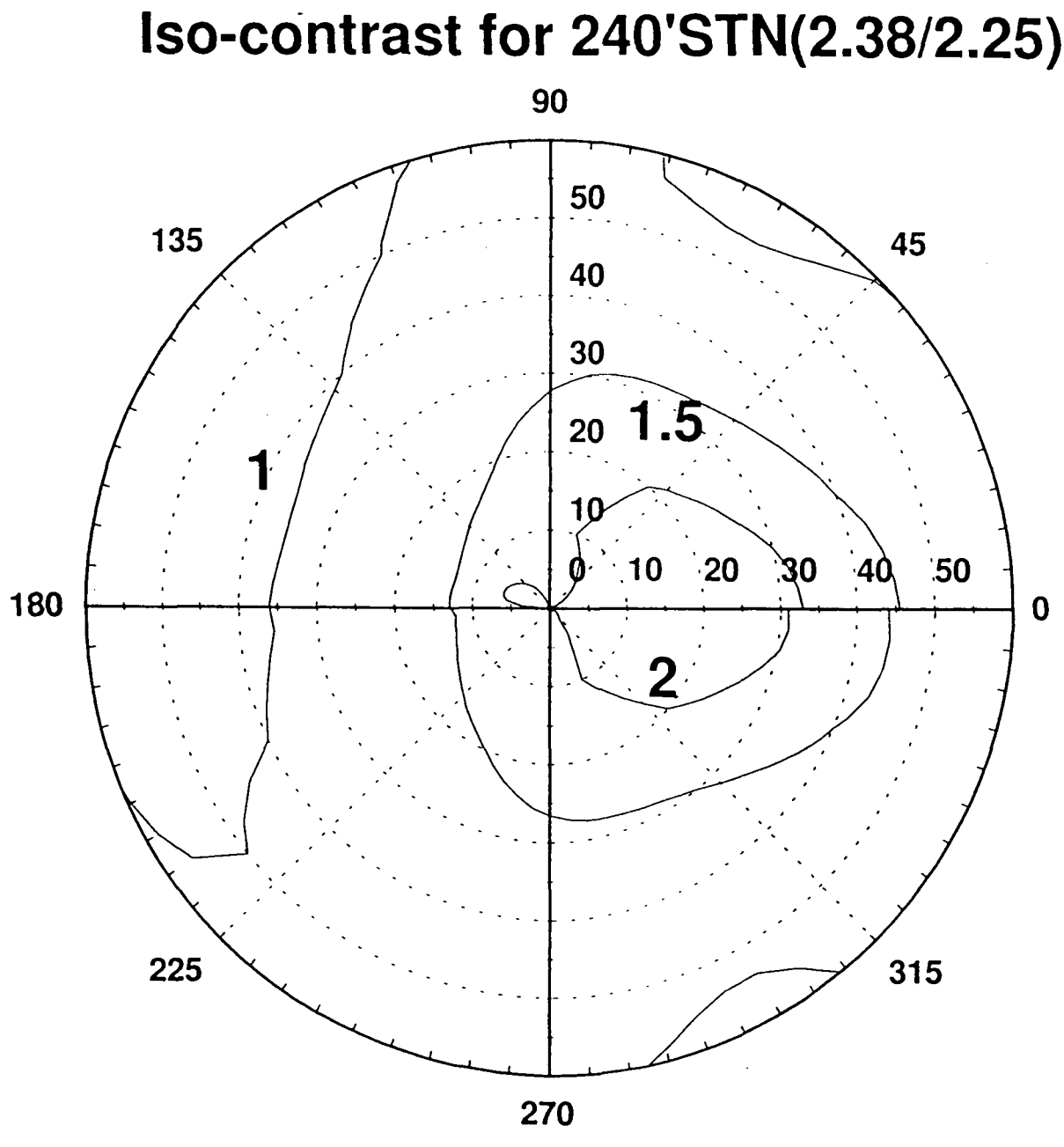
Iso-contrast for 240'STN(2.38/2.25)
90
135
45
180
0
225
315
270
50
40
30
20
10
0
10
20
30
40
50
1
1.5
2

Figure 46

# Iso-contrast for 240'STN(2.39/2.25)

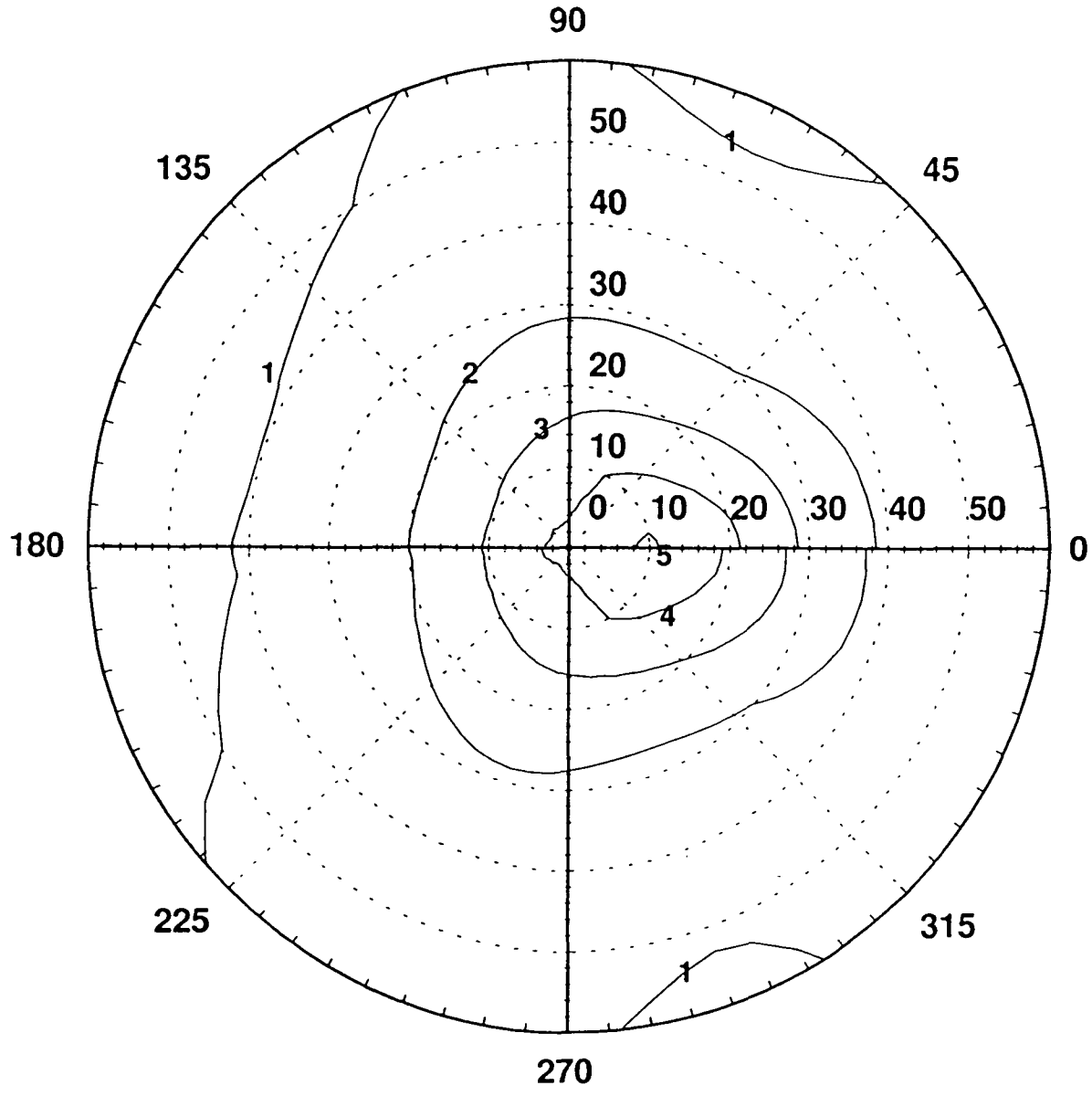


Figure 47

# Iso-contrast for 240'STN(2.45/2.25)

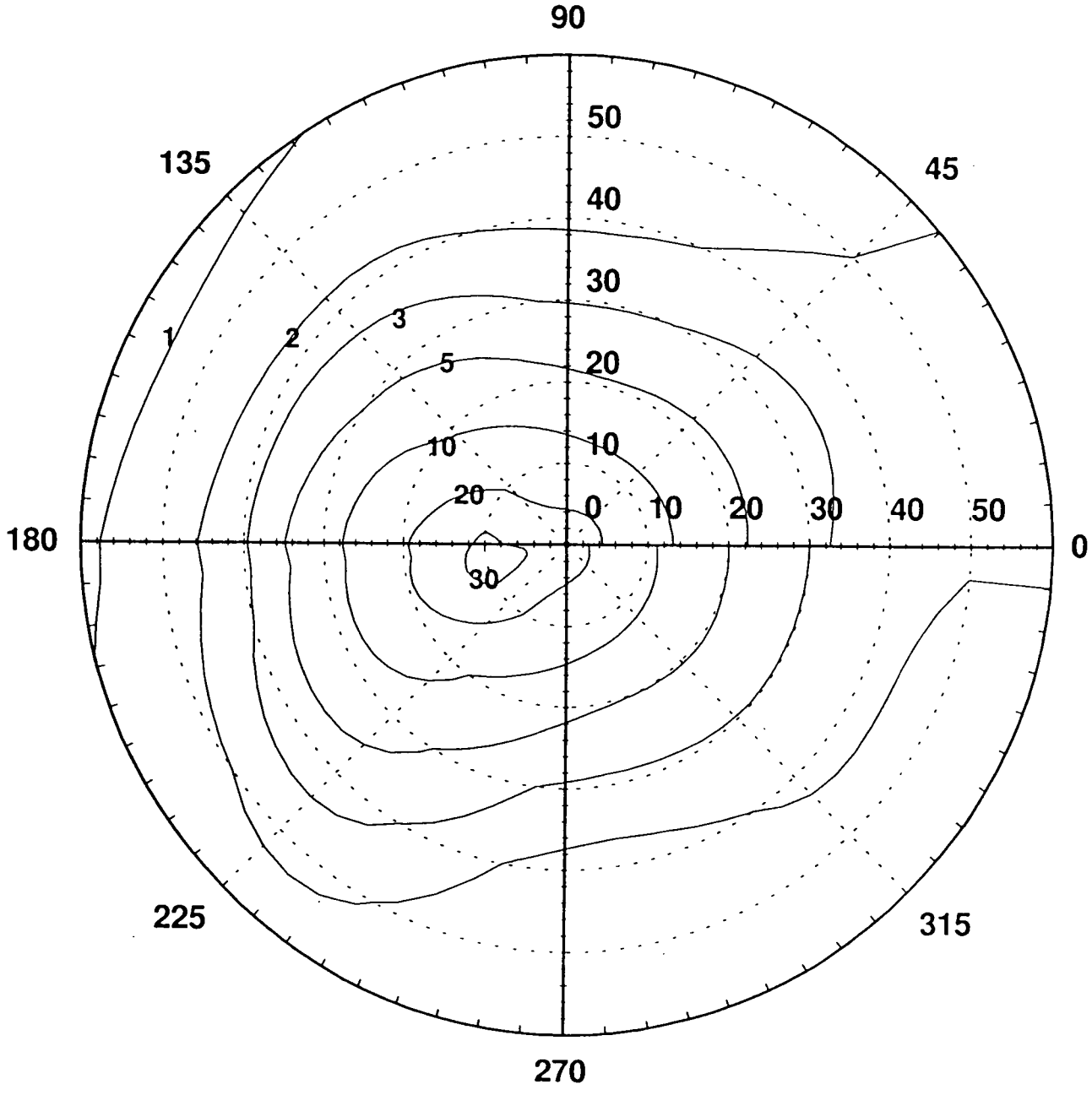


Figure 48

# Experimental Spectral Transmittance
# Standish STN Cell (1) (ZLI-4431)

## $\Theta = 0$ degrees $\Phi = 0$ degrees

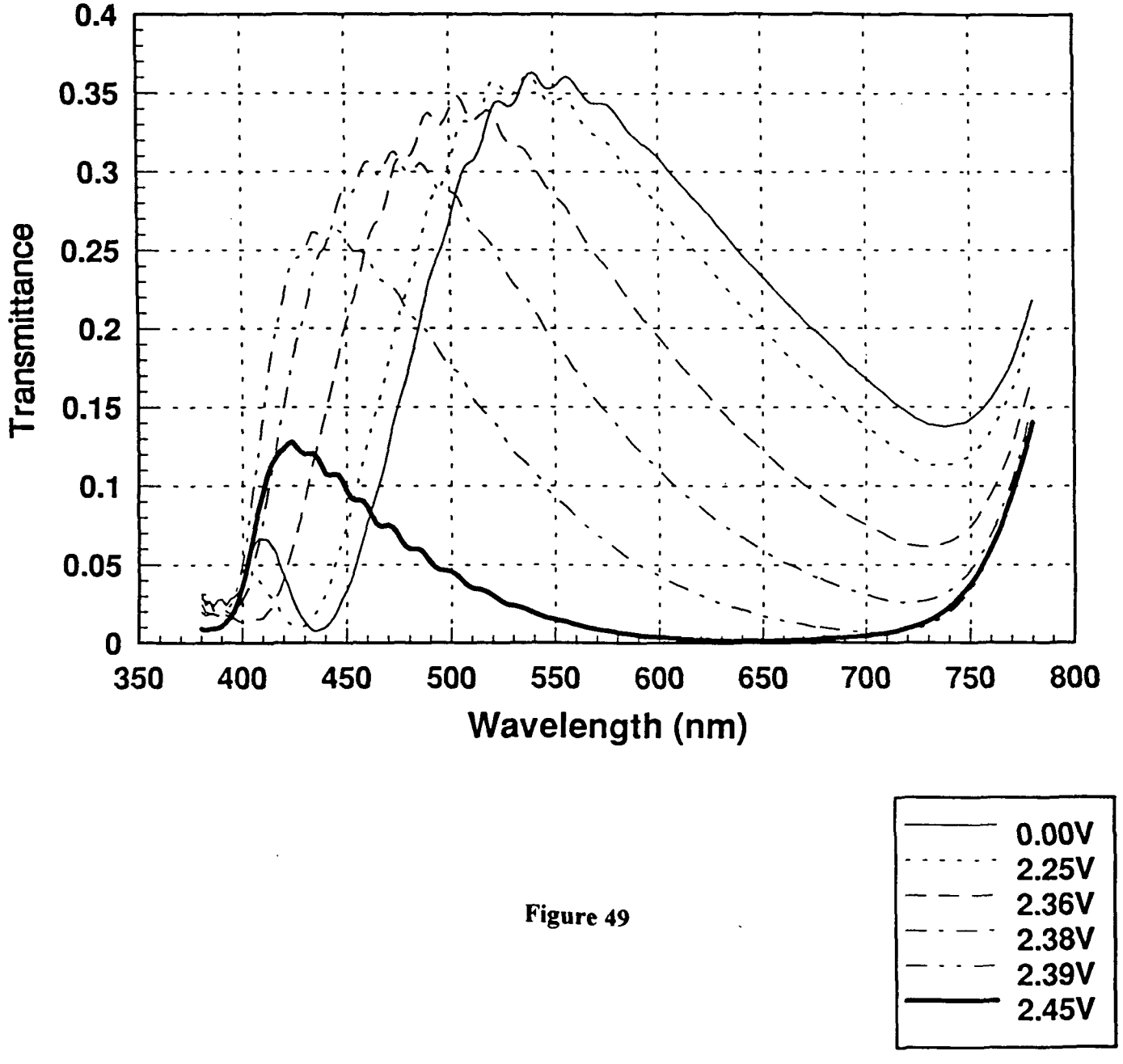


Figure 49

# Experimental Spectral Transmittance
# Standish STN Cell (1) (ZLI-4431)

## $\Theta = 30$ degrees $\Phi = 0$ degrees

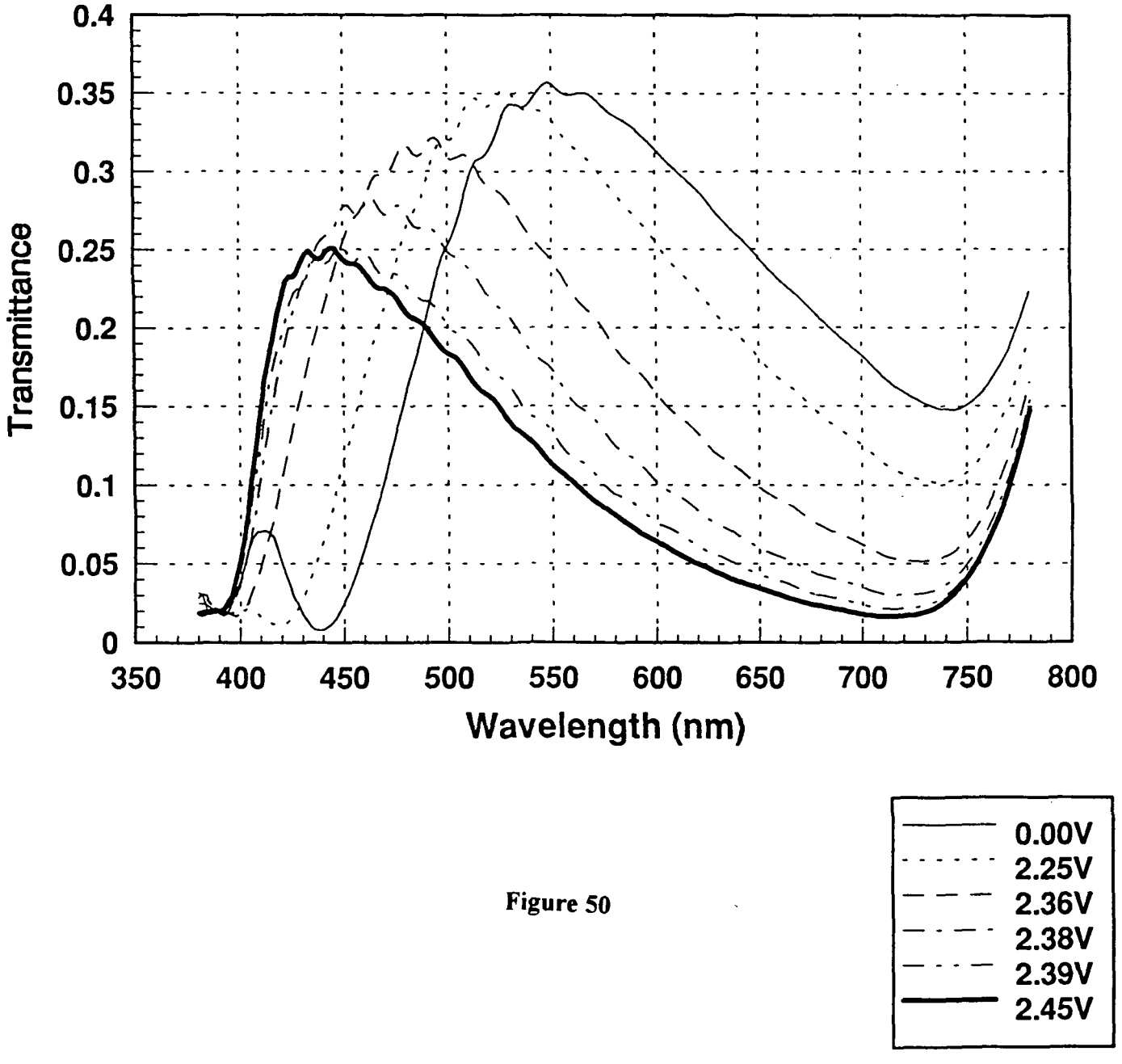


Figure 50

# Experimental Spectral Transmittance
# Standish STN Cell (1) (ZLI-4431)

## $\Theta$ = 30 degrees $\Phi$ = 45 degrees

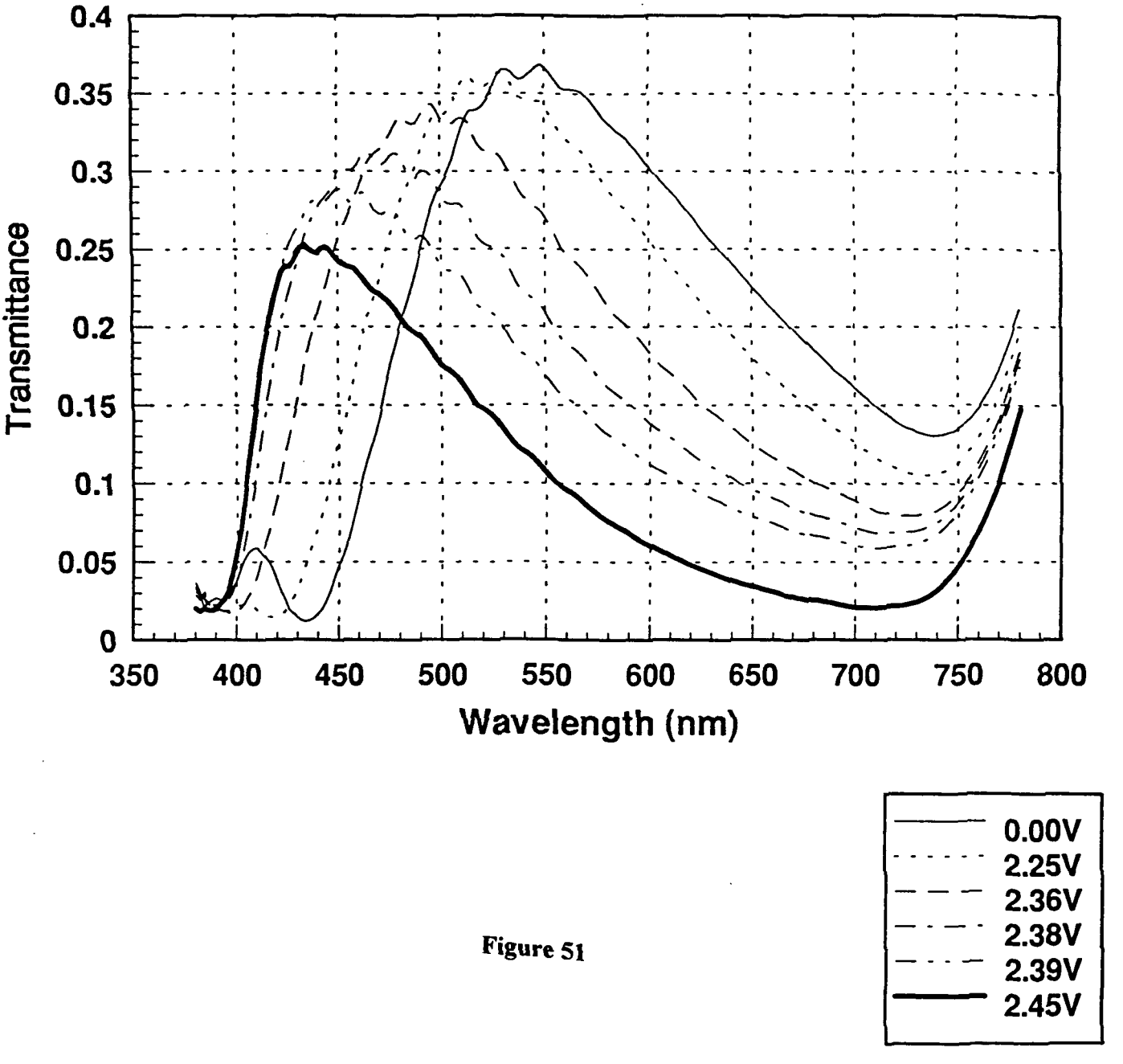


Figure 51

# Experimental Spectral Transmittance
# Standish STN Cell (1) (ZLI-4431)

## $\Theta = 30$ degrees $\Phi = 90$ degrees

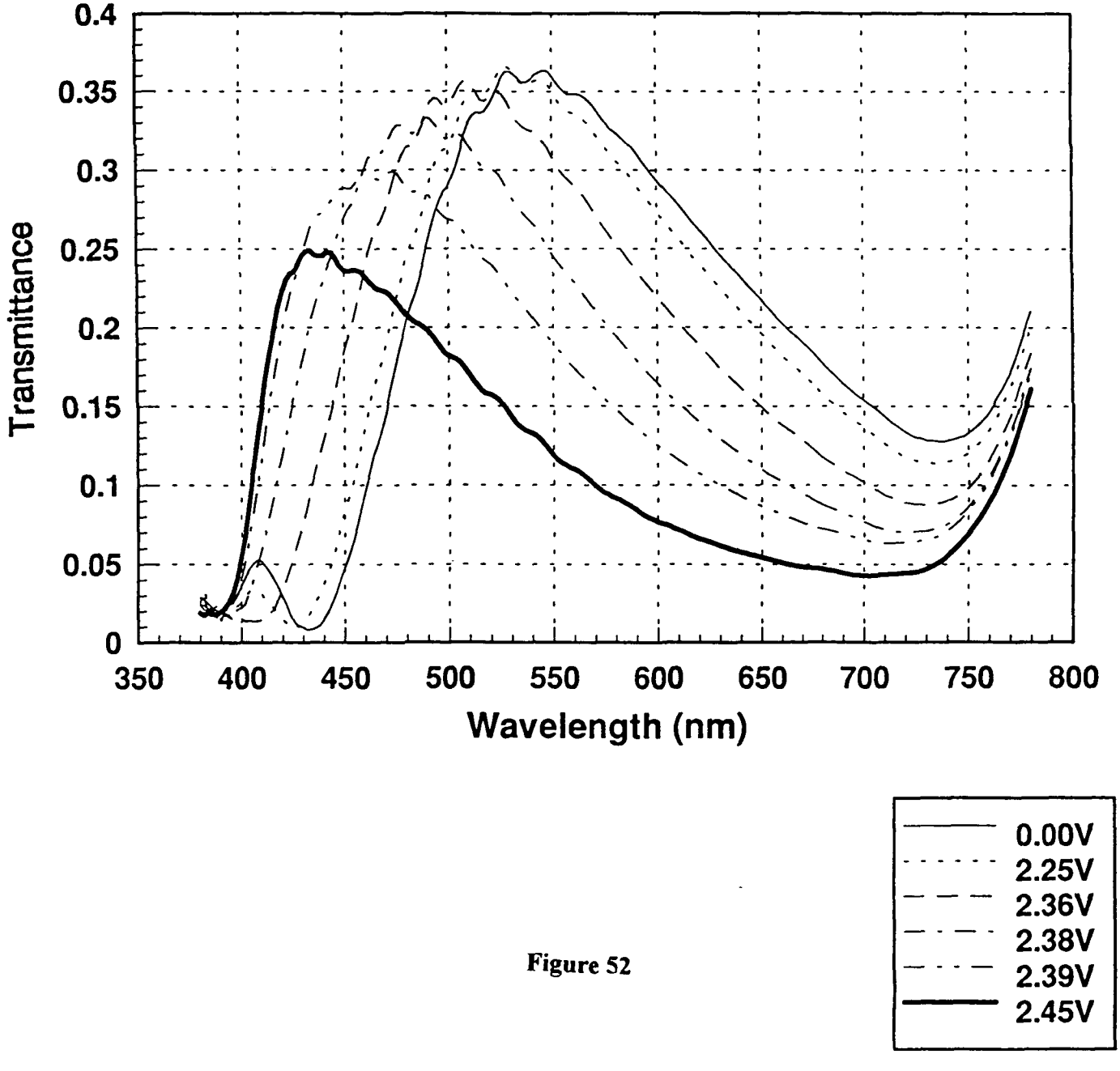


Figure 52

# Experimental Spectral Transmittance
# Standish STN Cell (1) (ZLI-4431)

## $\Theta$ = 30 degrees $\Phi$ = 135 degrees

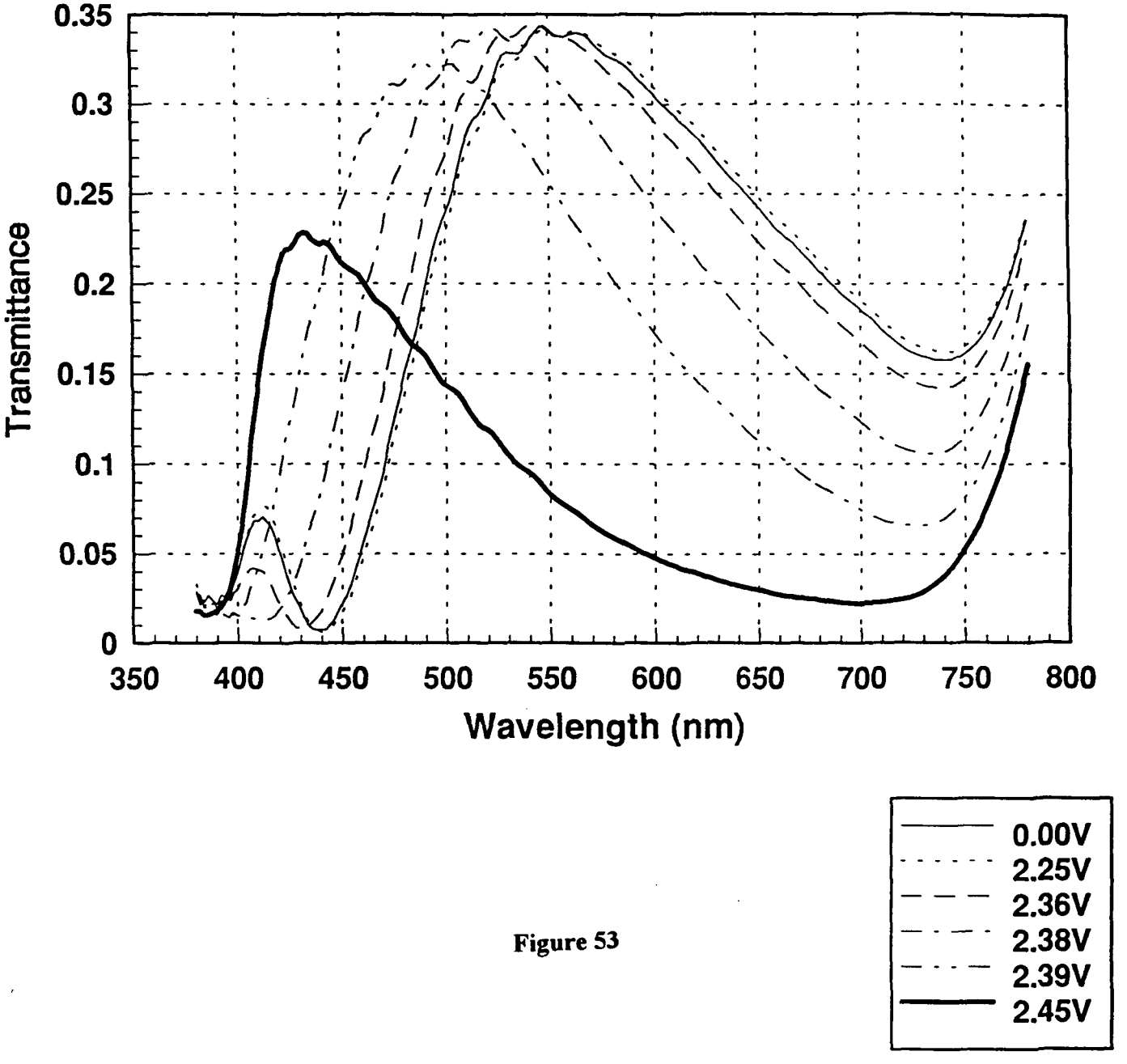


Figure 53

# Experimental Spectral Transmittance
# Standish STN Cell (1) (ZLI-4431)

## $\Theta = 30$ degrees $\Phi = 180$ degrees

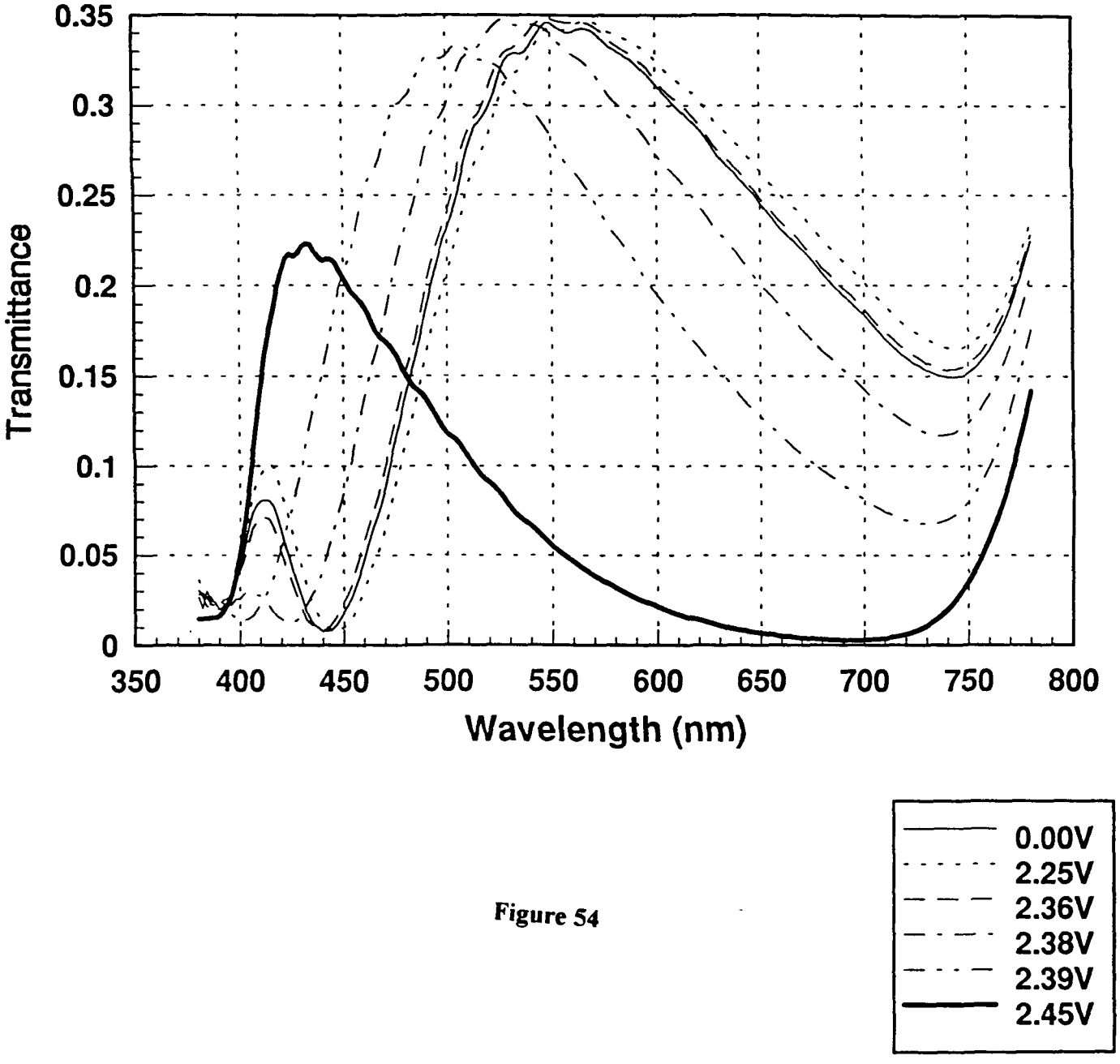


Figure 54

# Experimental Spectral Transmittance
# Standish STN Cell (1) (ZLI-4431)

## $\Theta = 30$ degrees $\Phi = 225$ degrees

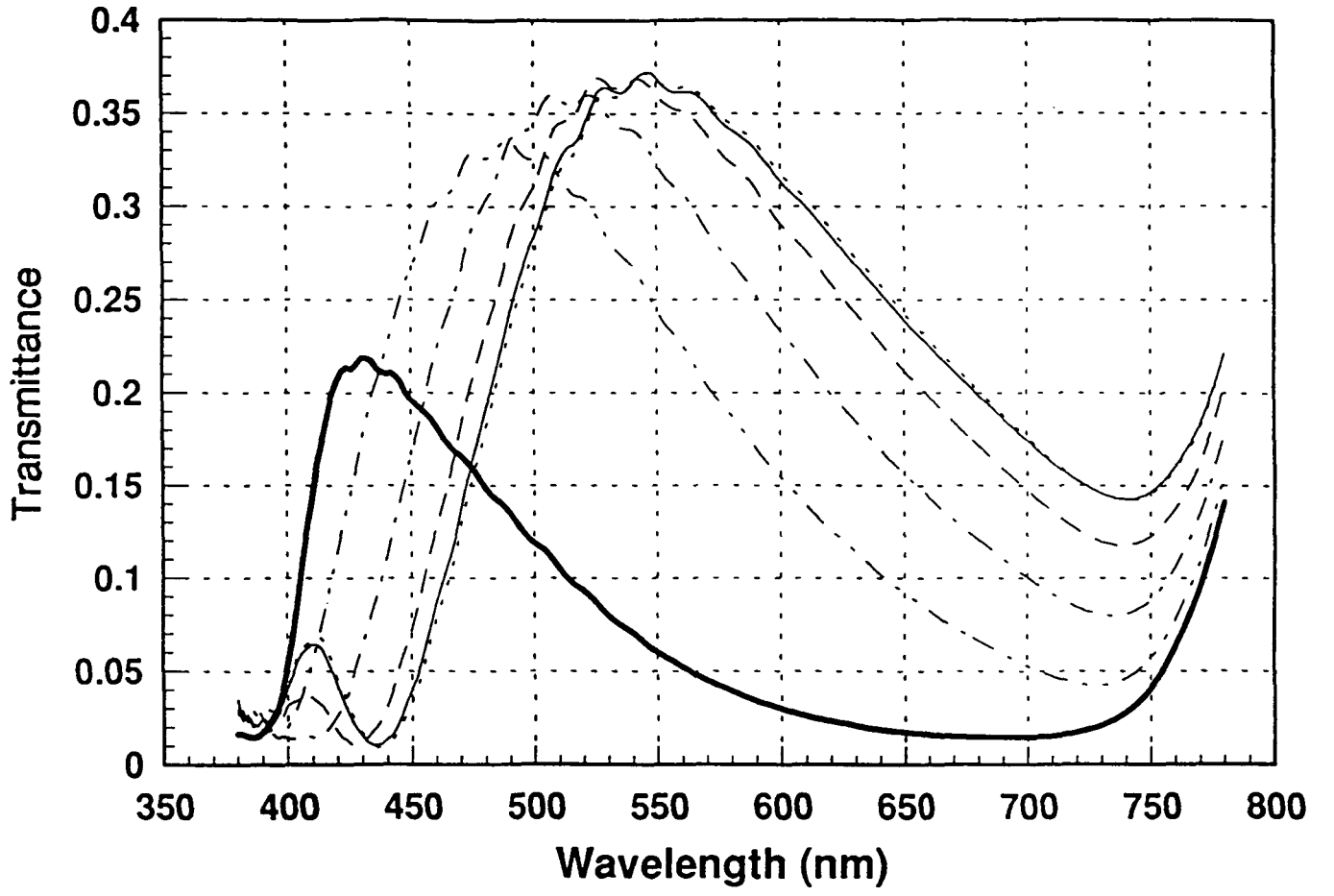


Figure 55

# Experimental Spectral Transmittance
# Standish STN Cell (1) (ZLI-4431)

## $\Theta = 30$ degrees $\Phi = 270$ degrees

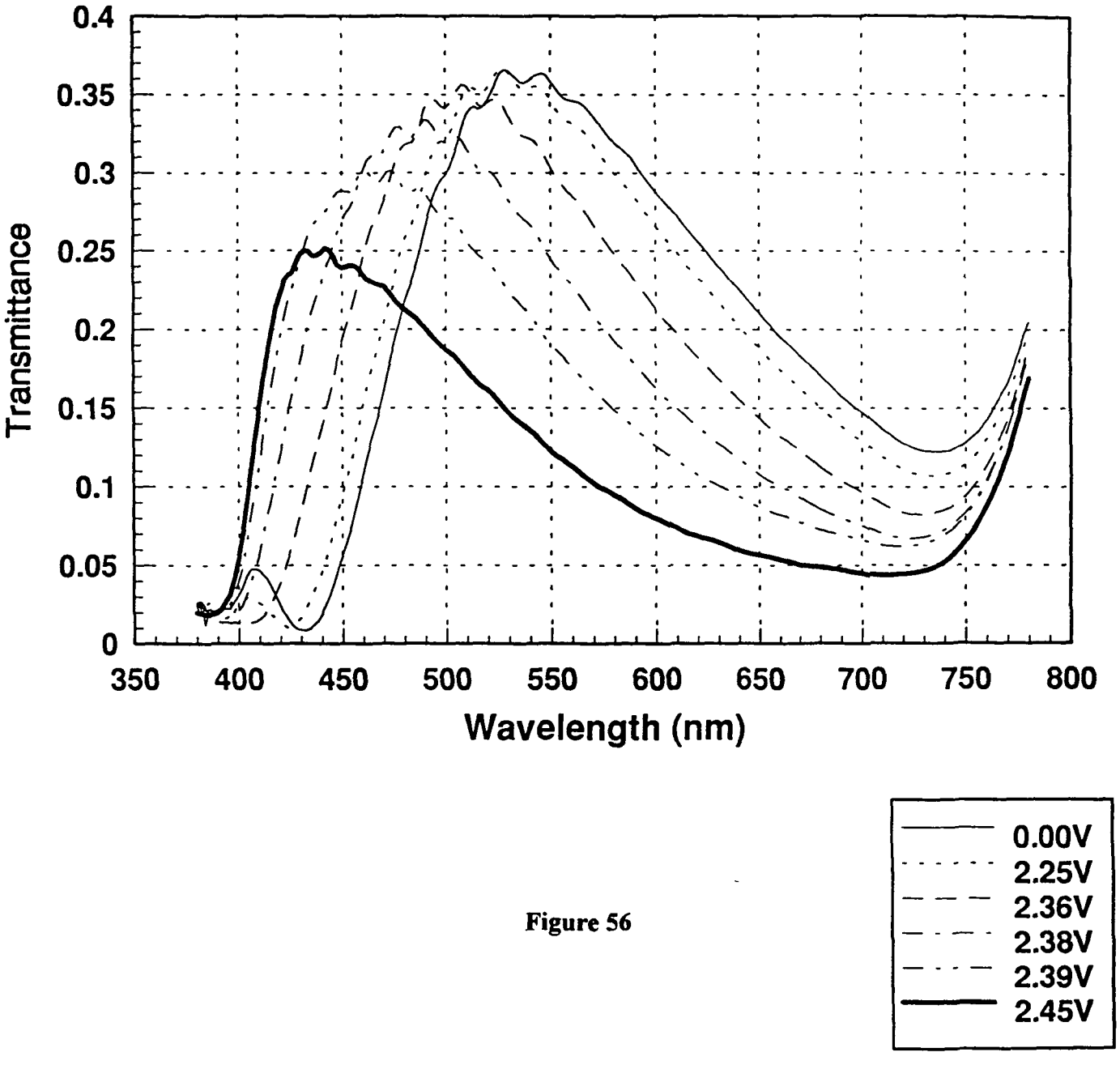


Figure 56

# Experimental Spectral Transmittance
# Standish STN Cell (1) (ZLI-4431)

## $\Theta = 30$ degrees $\Phi = 315$ degrees

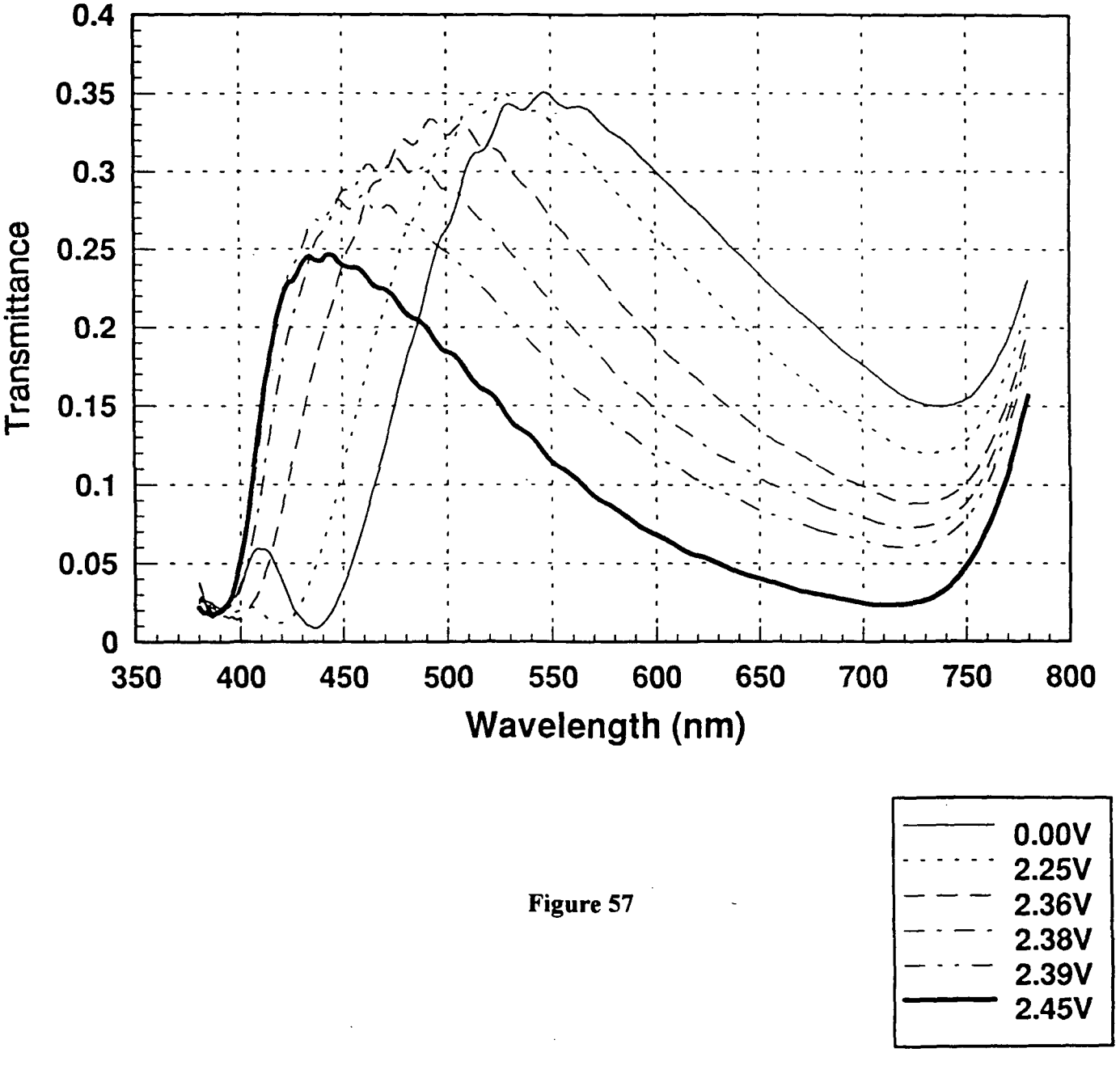


Figure 57

# Experimental Spectral Transmittance
# Standish STN Cell (1) (ZLI-4431)

## $\Theta = 50$ degrees $\Phi = 0$ degrees

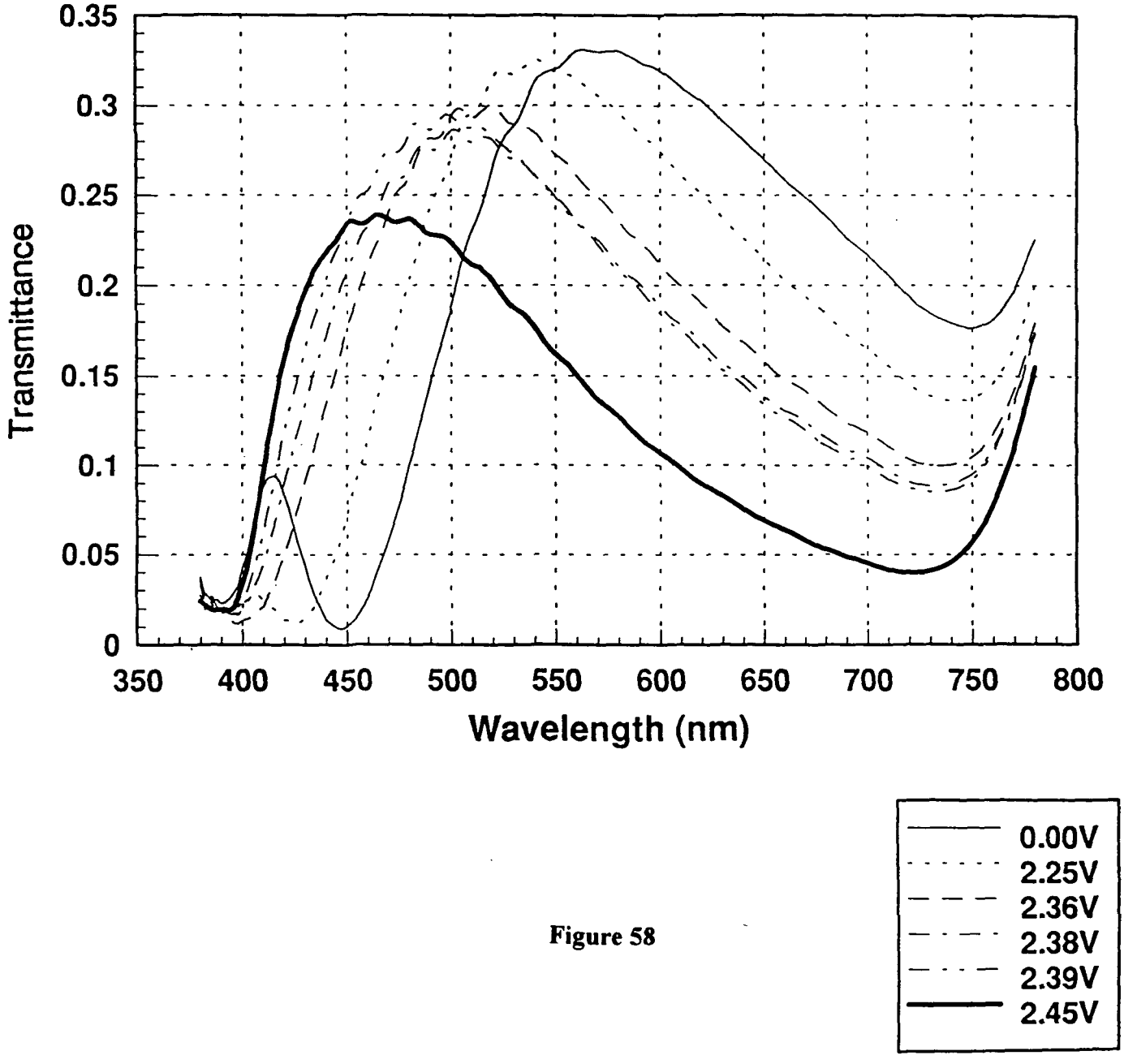


Figure 58

# Experimental Spectral Transmittance
# Standish STN Cell (1) (ZLI-4431)

## $\Theta = 50$ degrees $\Phi = 45$ degrees

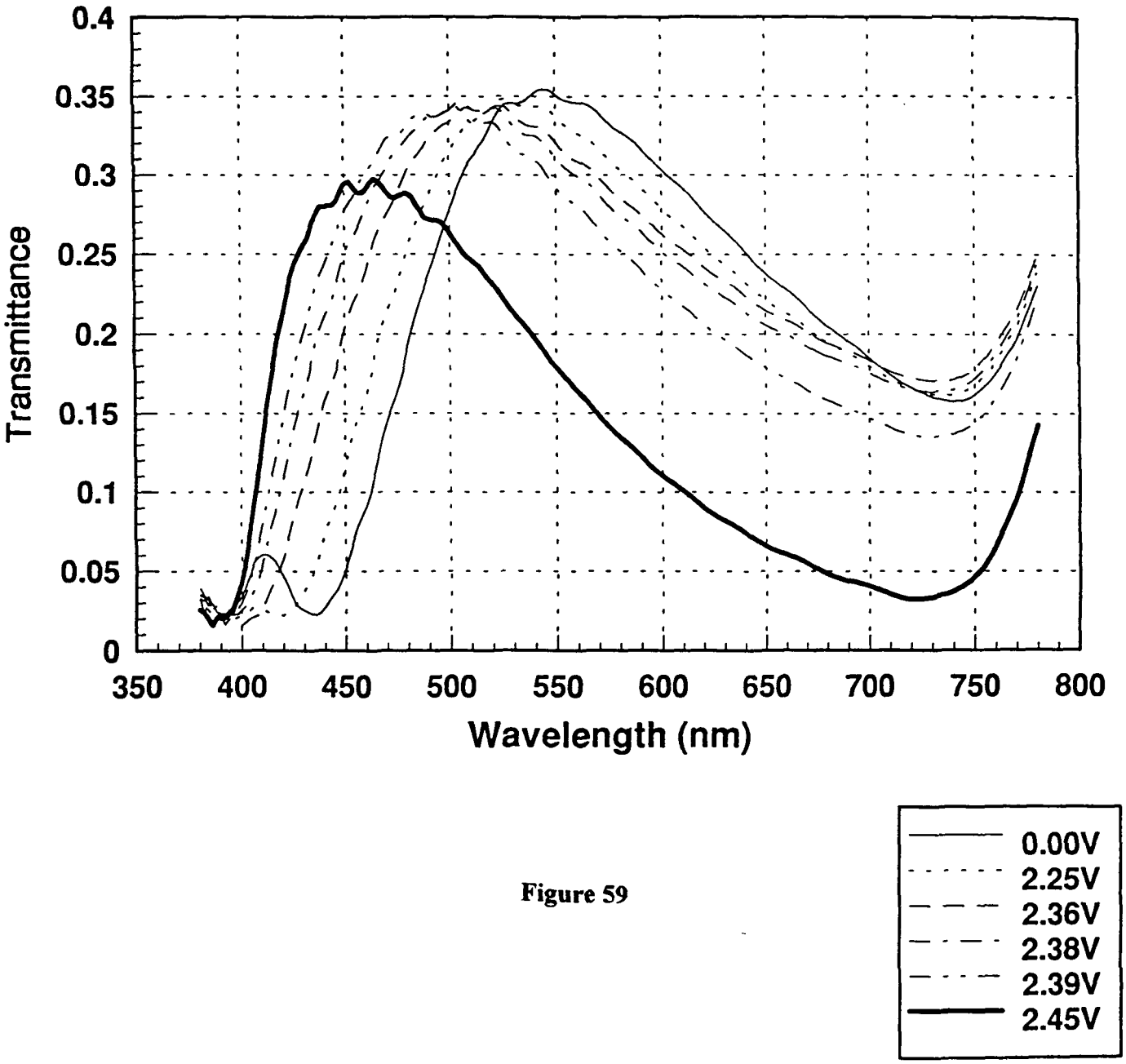


Figure 59

# Experimental Spectral Transmittance
# Standish STN Cell (1) (ZLI-4431)

## $\Theta = 50$ degrees $\Phi = 90$ degrees

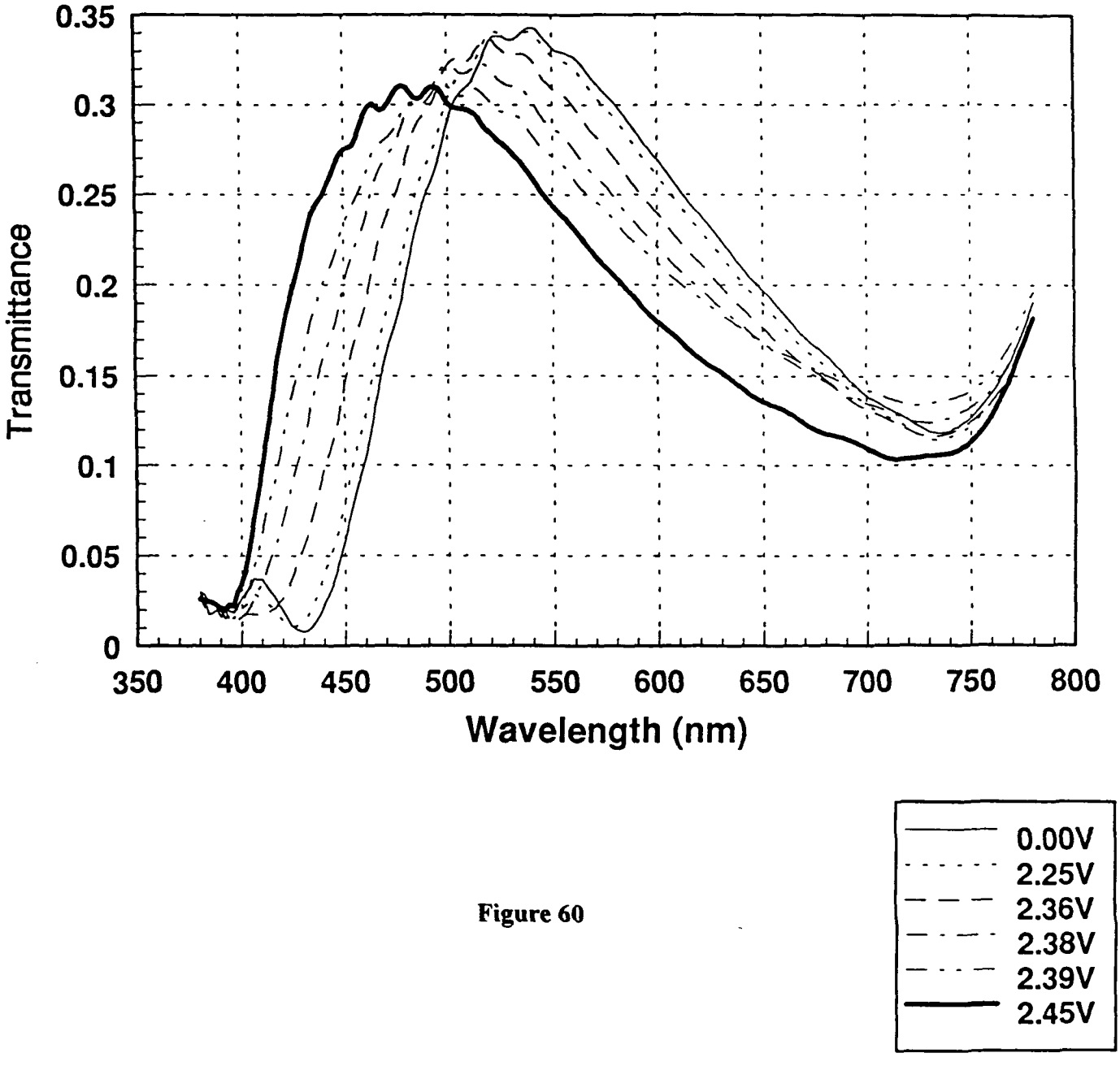


Figure 60

# Experimental Spectral Transmittance
# Standish STN Cell (1) (ZLI-4431)

## $\Theta = 50$ degrees $\Phi = 135$ degrees

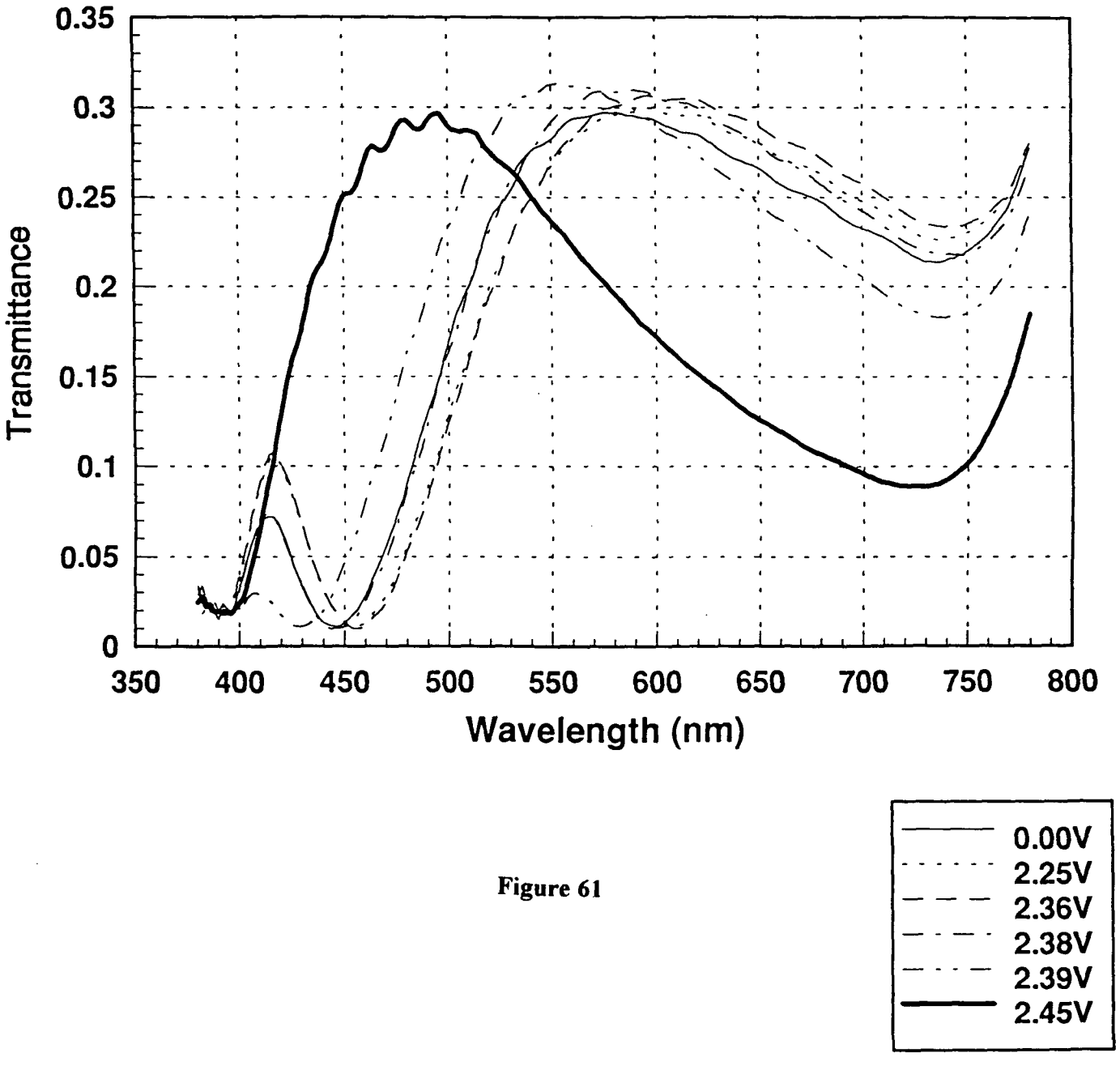


Figure 61

# Experimental Spectral Transmittance
# Standish STN Cell (1) (ZLI-4431)

## $\Theta = 50$ degrees $\Phi = 180$ degrees

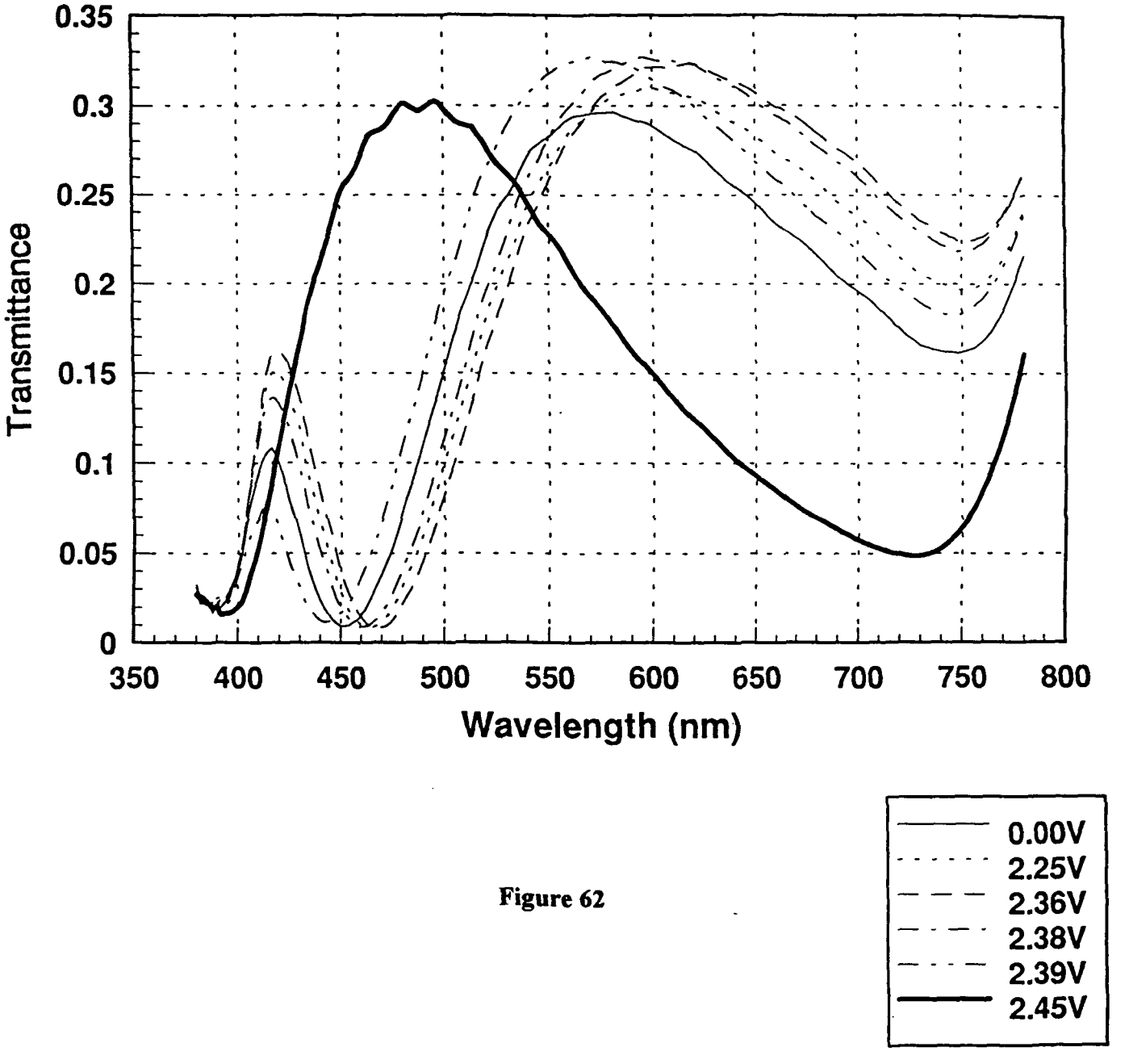


Figure 62

# Experimental Spectral Transmittance
# Standish STN Cell (1) (ZLI-4431)

## $\Theta = 50$ degrees $\Phi = 225$ degrees

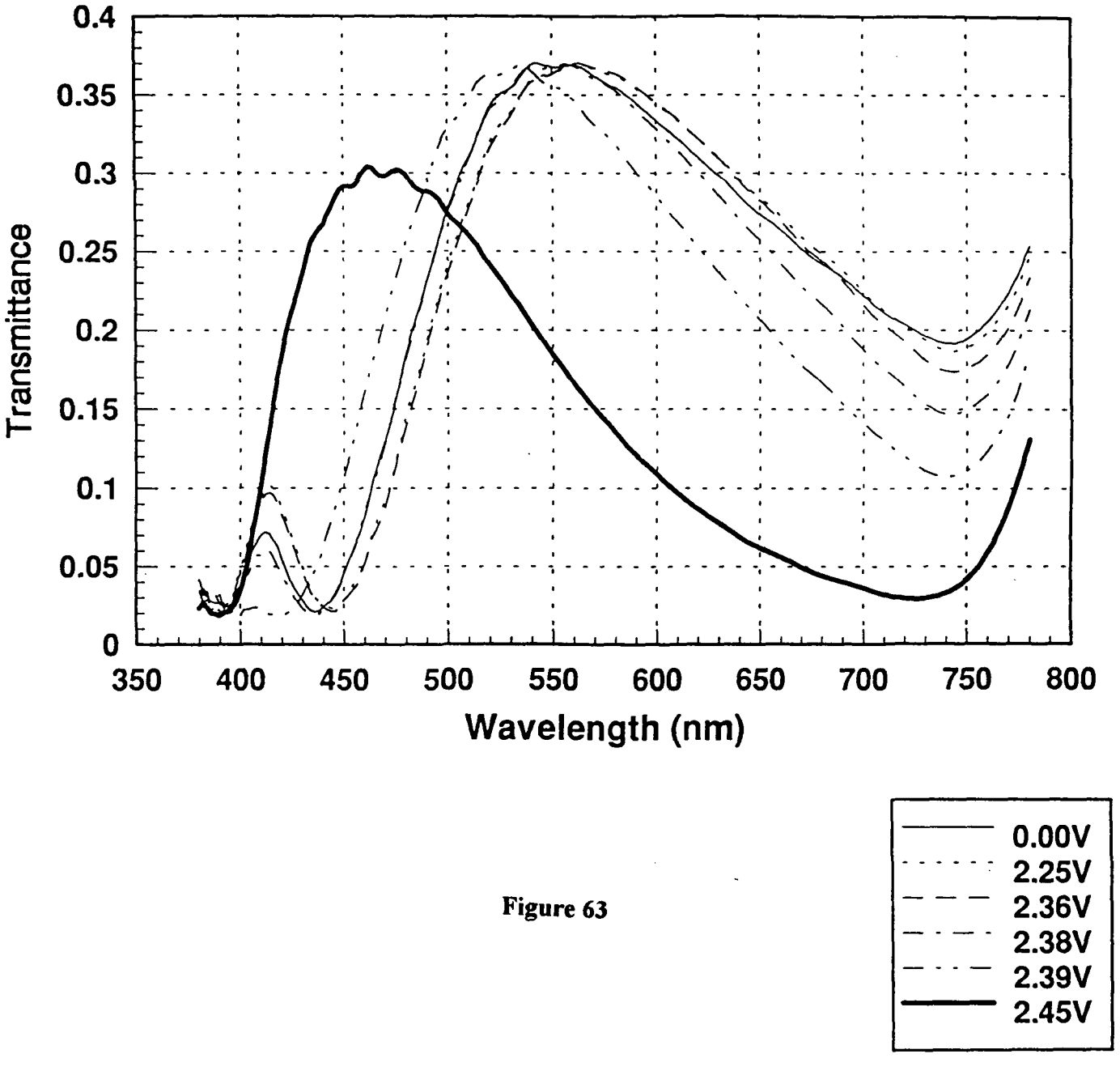


Figure 63

# Experimental Spectral Transmittance
# Standish STN Cell (1) (ZLI-4431)

## $\Theta = 50$ degrees $\Phi = 270$ degrees

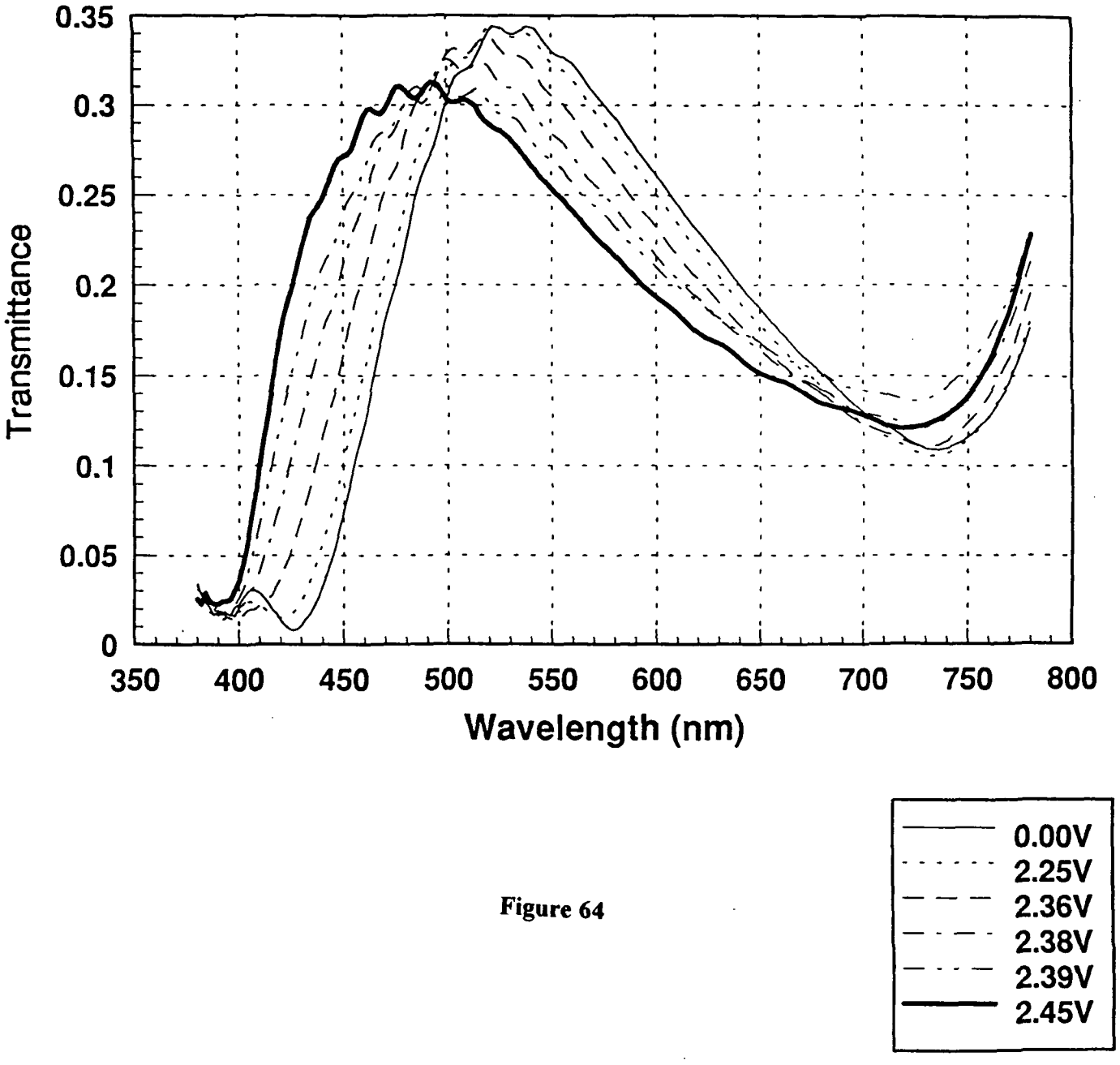


Figure 64

# Experimental Spectral Transmittance
# Standish STN Cell (1) (ZLI-4431)

## $\Theta = 50$ degrees $\Phi = 315$ degrees

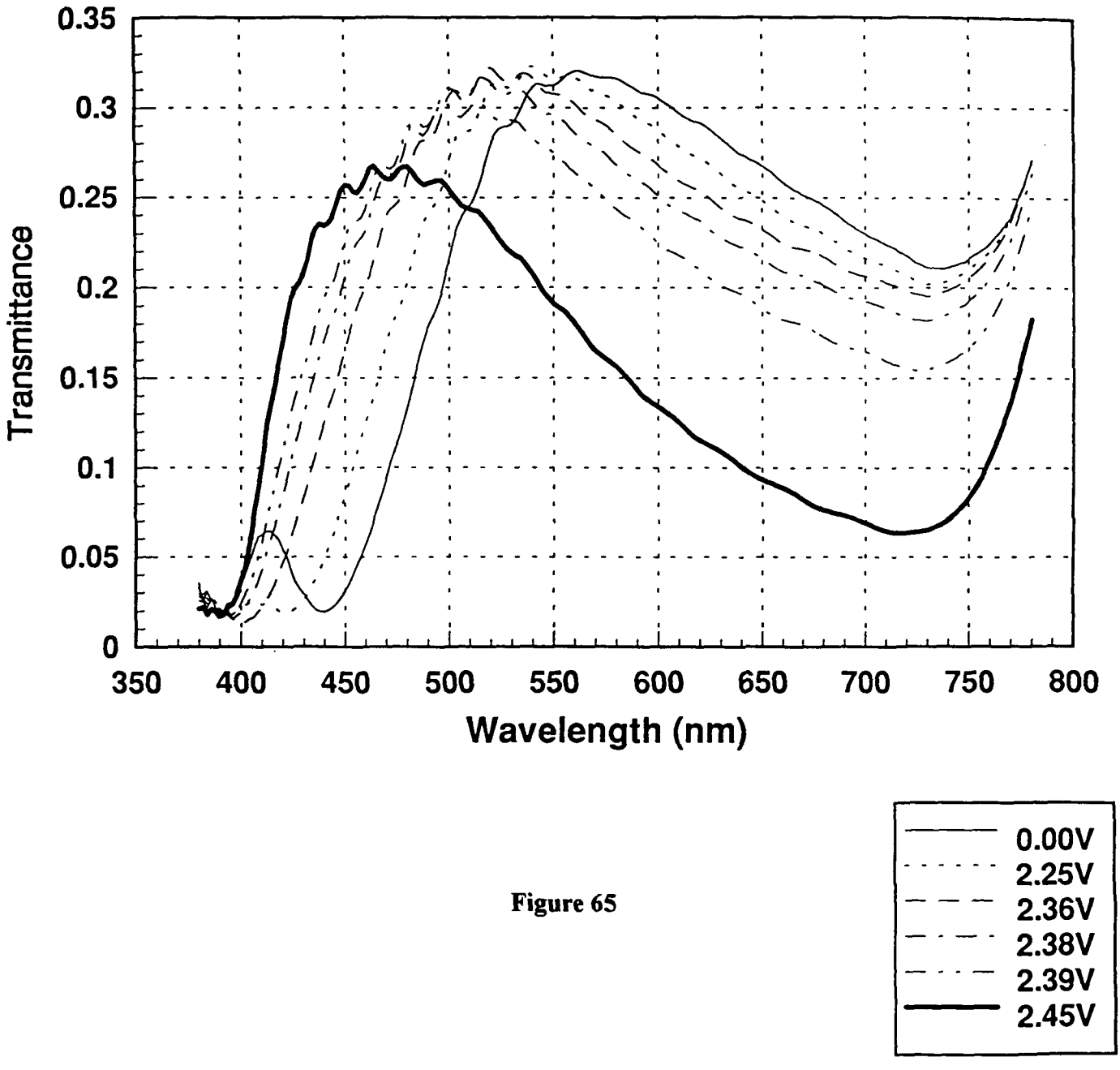


Figure 65

## Chromaticity Co-ordinates for on axis viewing ($\Theta = 0$ $\varphi = 0$) of Standish 240 deg. STN cell.

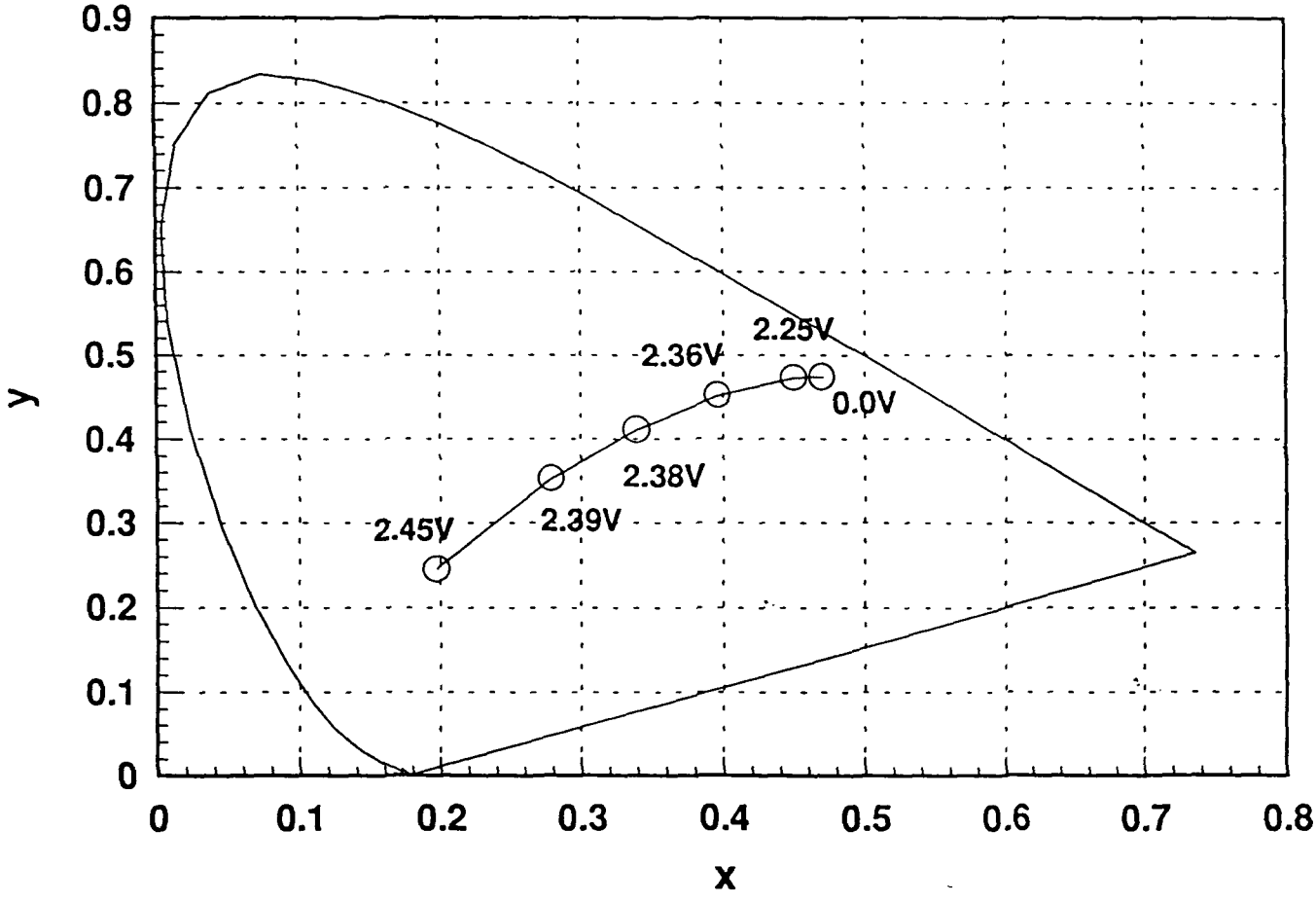


Figure 66

## Chromaticity Co-ordinates for $\Theta = 30\,\Phi = 0$ viewing angle of Standish 240 deg. STN cell.

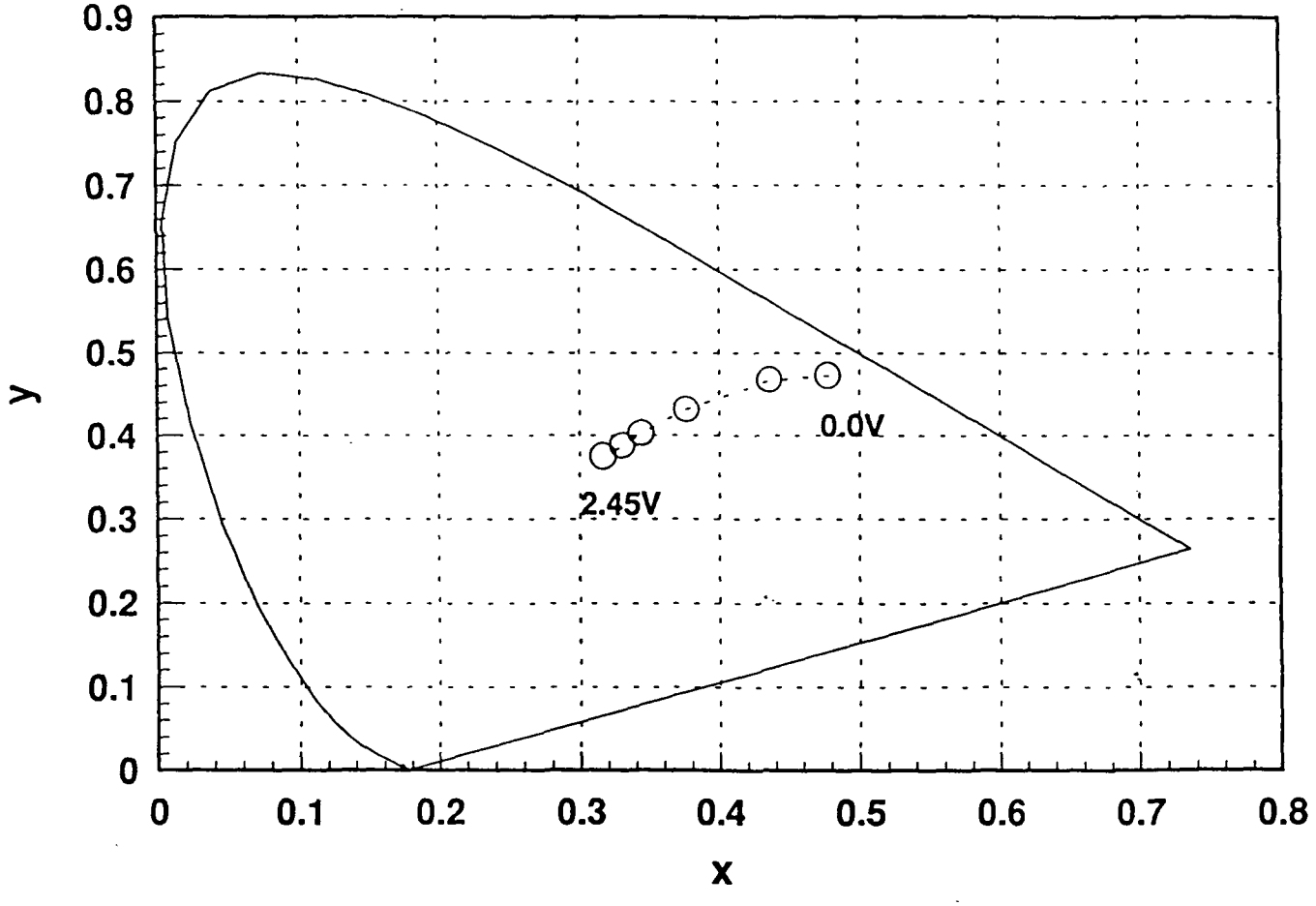


Figure 67

**Chromaticity Co-ordinates for $\Theta = 30$ $\Phi = 90$viewing angle of Standish 240 deg. STN cell.**

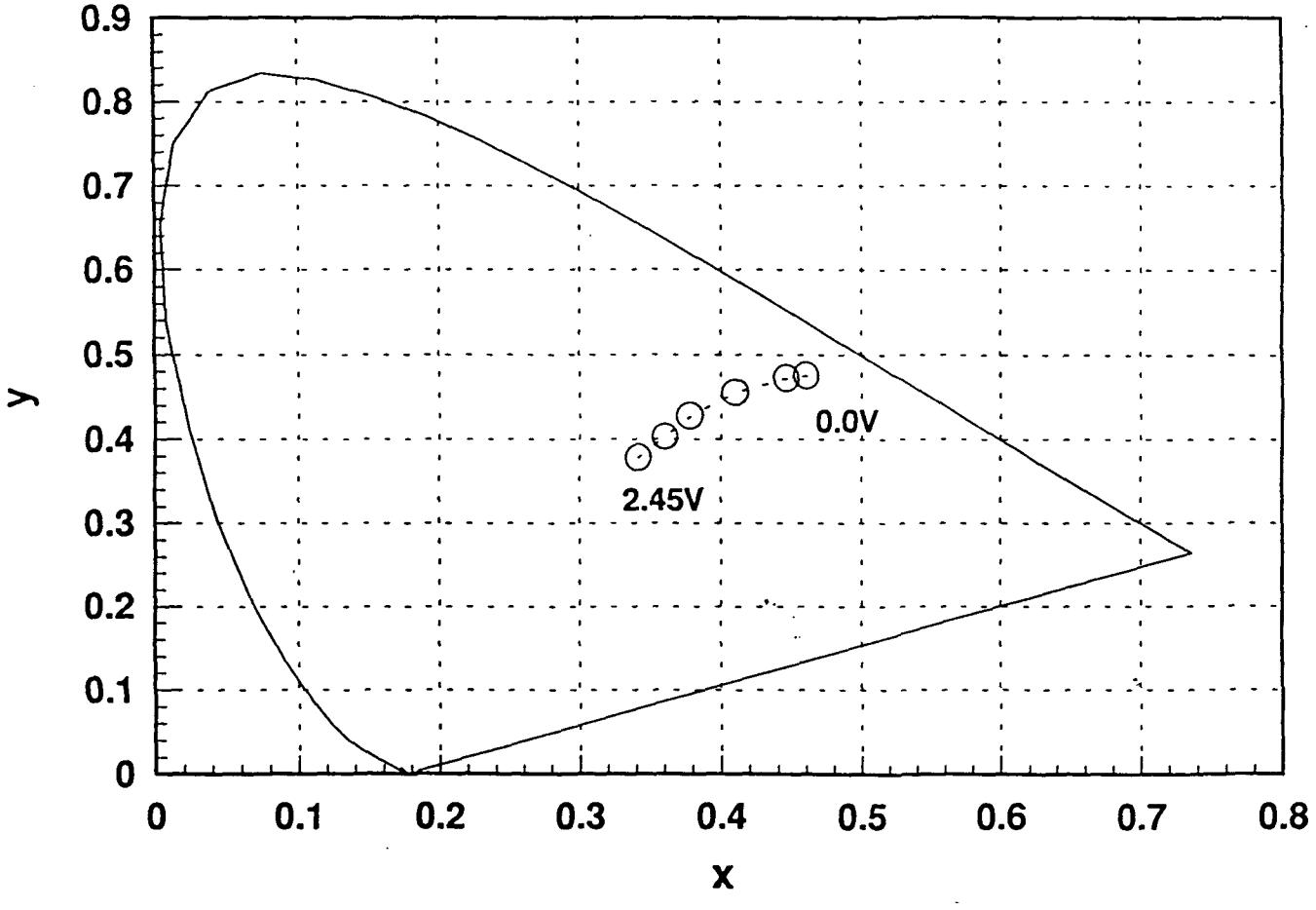


Figure 68

**Chromaticity Co-ordinates for $\Theta = 30$ $\Phi$=180viewing angle of Standish 240 deg STN cell.**

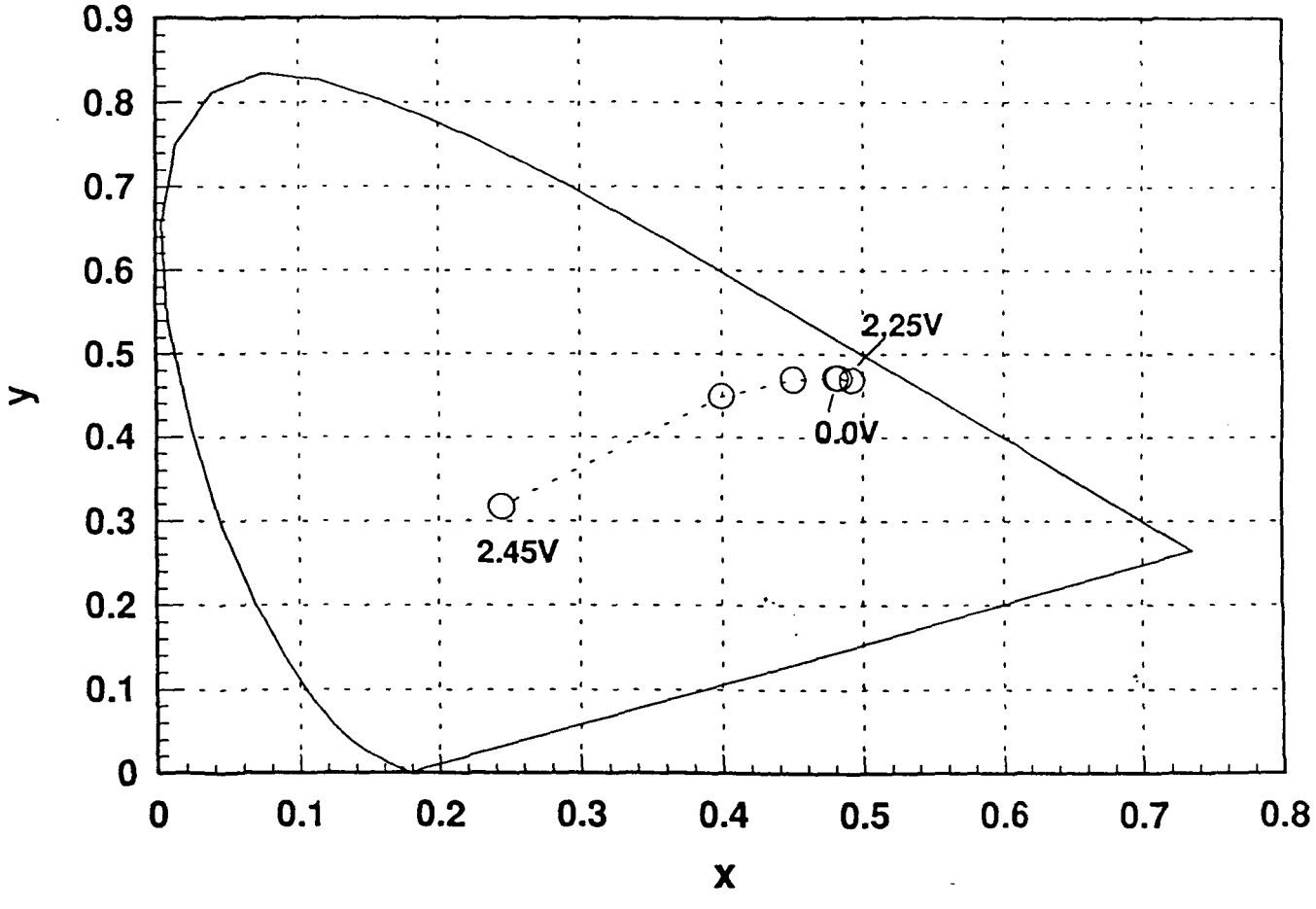


Figure 69

**Chromaticity Co-ordinates for $\Theta = 30$ $\Phi = 270$viewing angle of Standish 240 deg STN cell.**

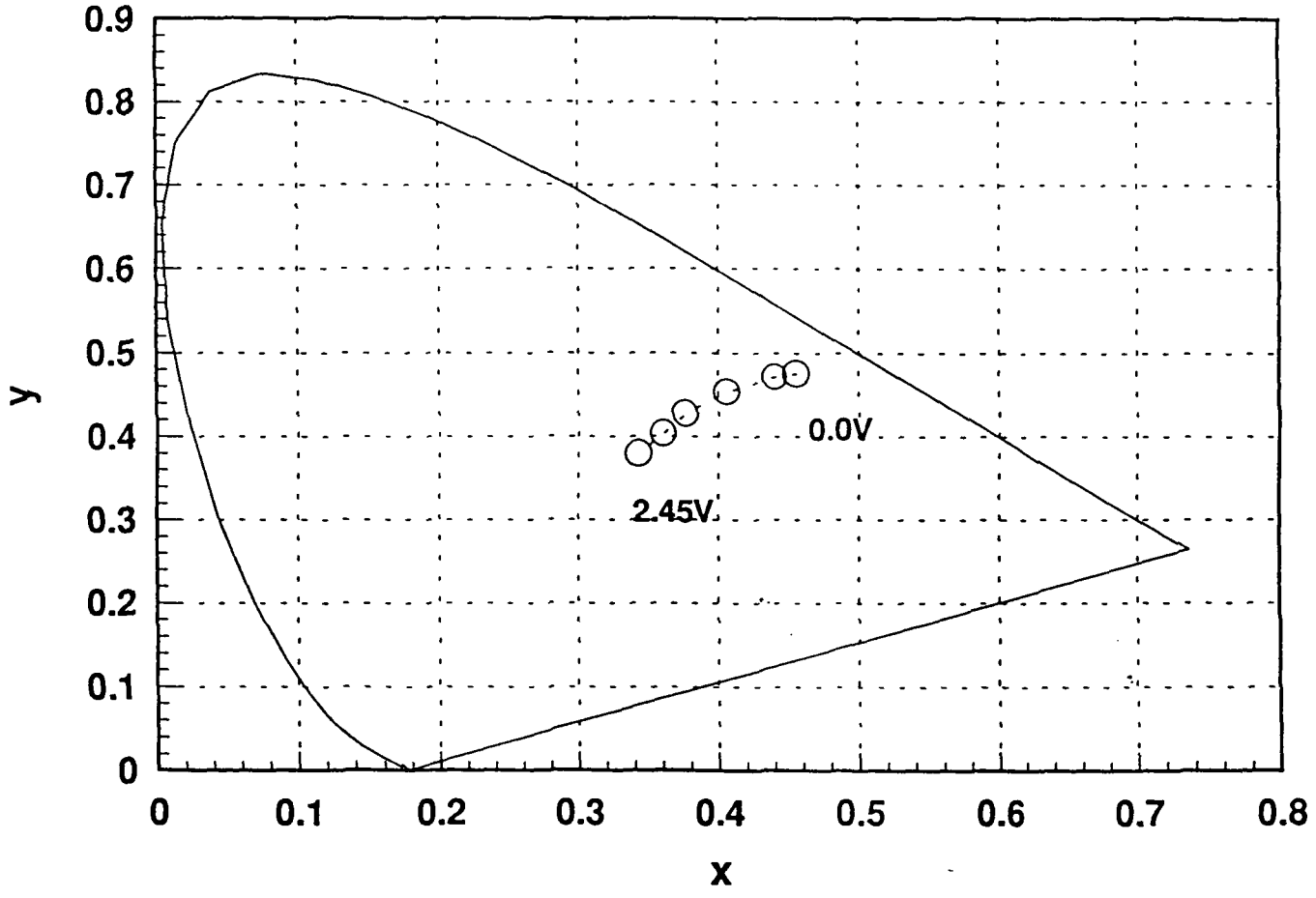


Figure 70

**Chromaticity Co-ordinates as a function of polar viewing angle from Standish STN 240 deg. cell with: V(rms) = 2.38V, Φ=0 deg., and Θ as shown on diagram in degrees (negative values indicate Φ = 180).**

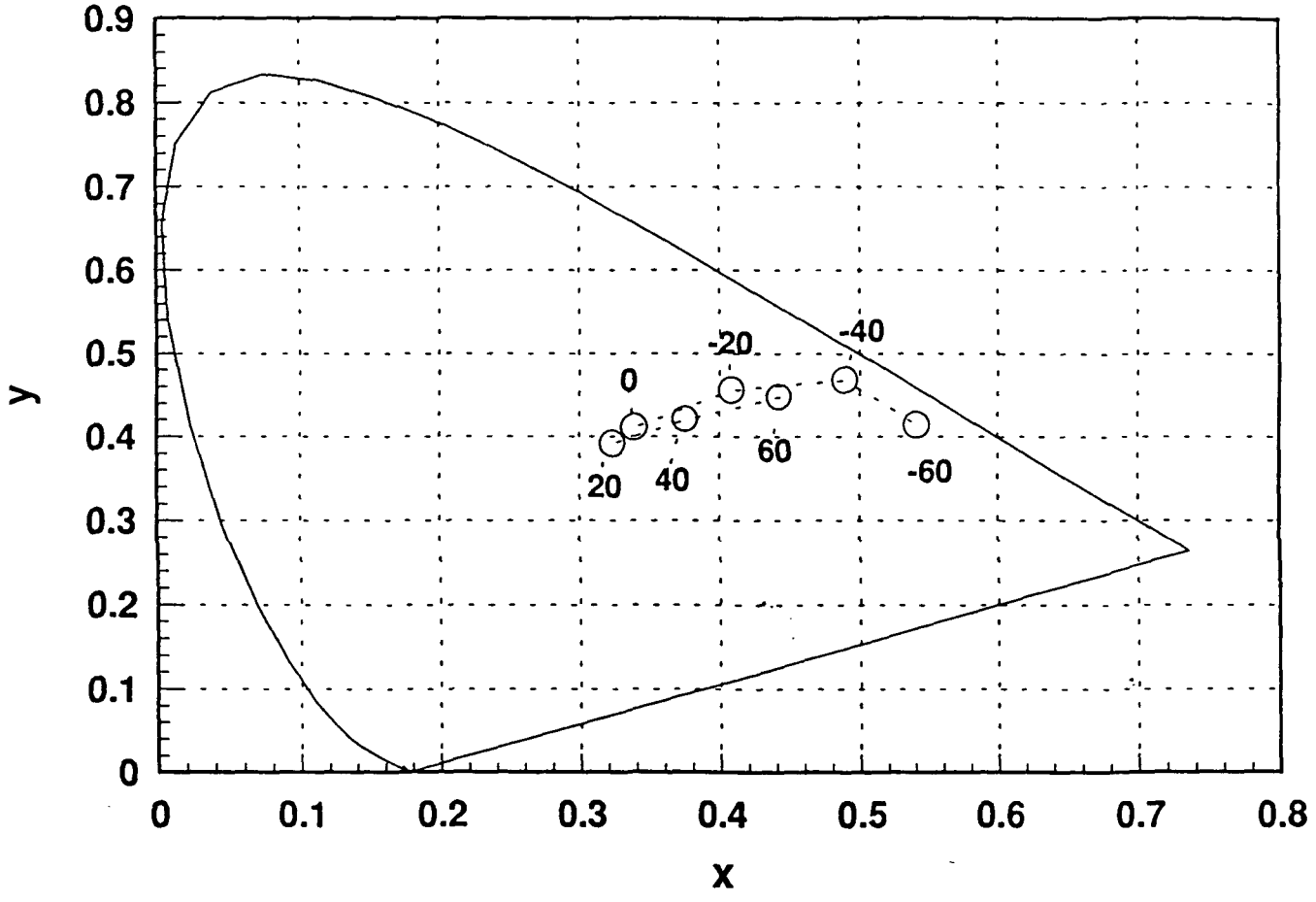


Figure 71

**Chromaticity Co-ordinates as a function of polar viewing angle from Standish STN 240 deg. cell with: V(rms) = 2.38V, $\Phi$ = 90 deg., and $\Theta$ as shown on diagram (negative values indicate $\Phi$ = -90 deg.).**

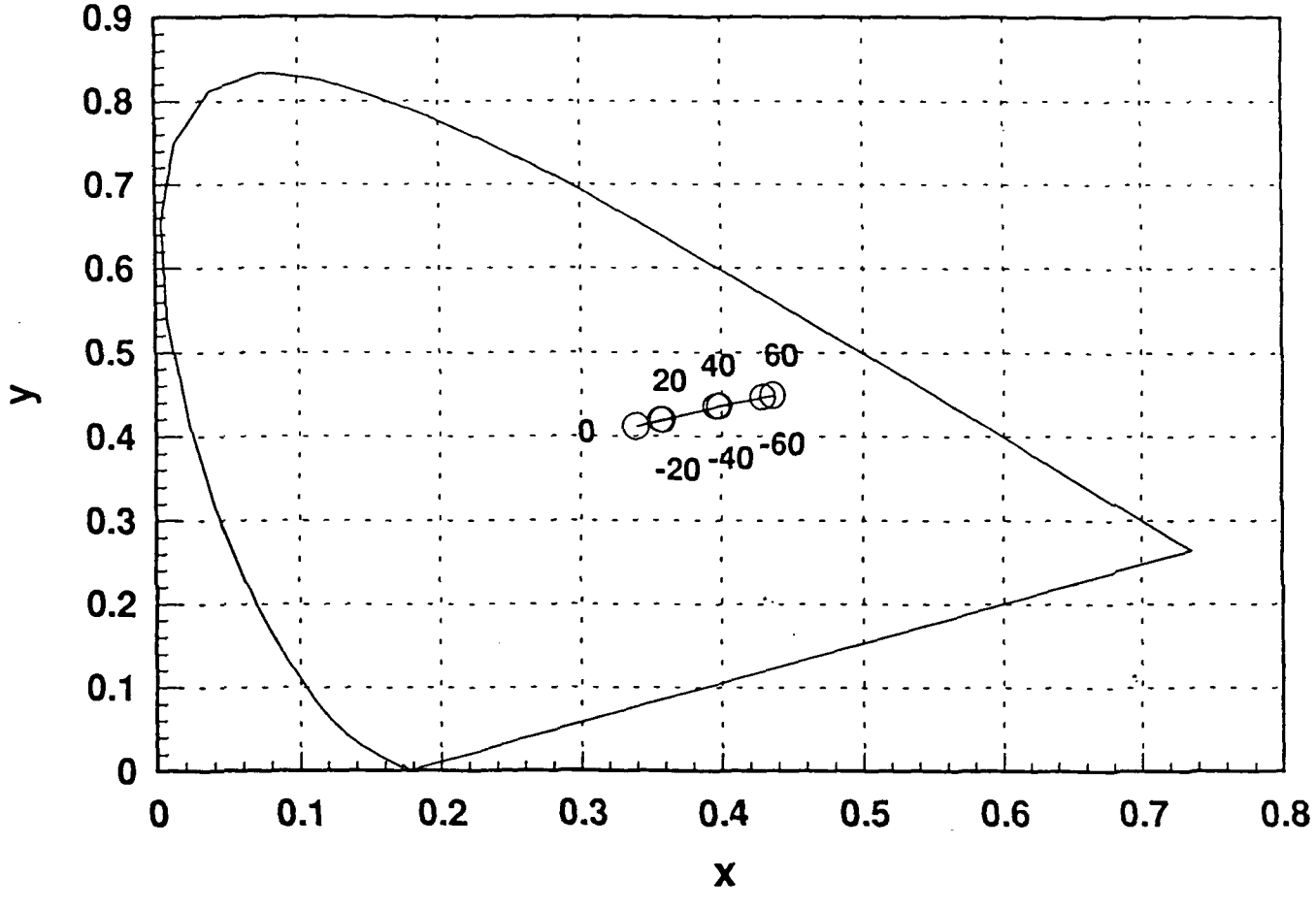


Figure 72

**Chromaticity Co-ordinates as a function of azimuthal viewing angle from Standish STN 240 deg. cell with: V(rms) = 2.38V, $\Theta$ = 30 deg., and $\phi$ as shown on diagram in degrees.**

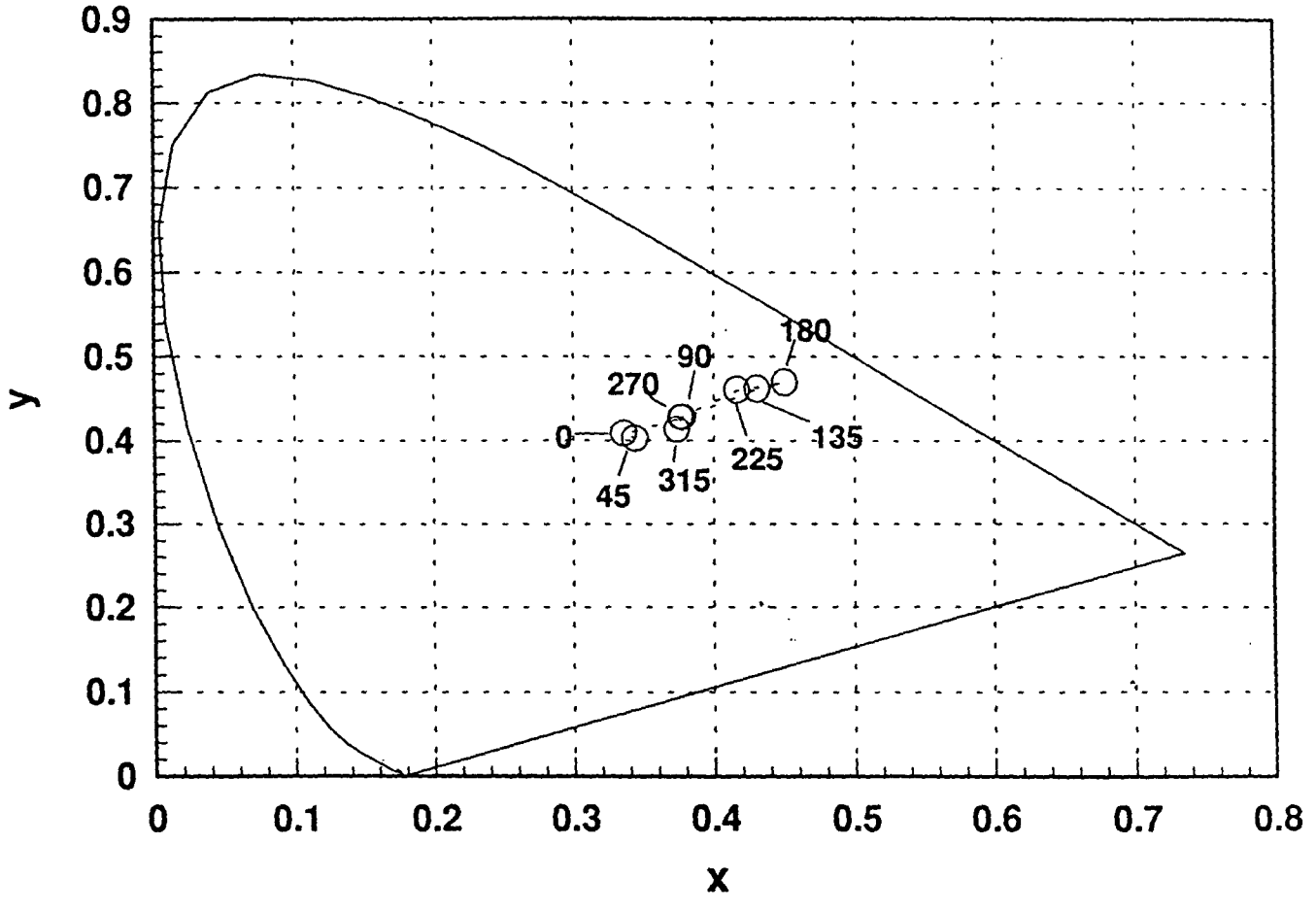


Figure 73

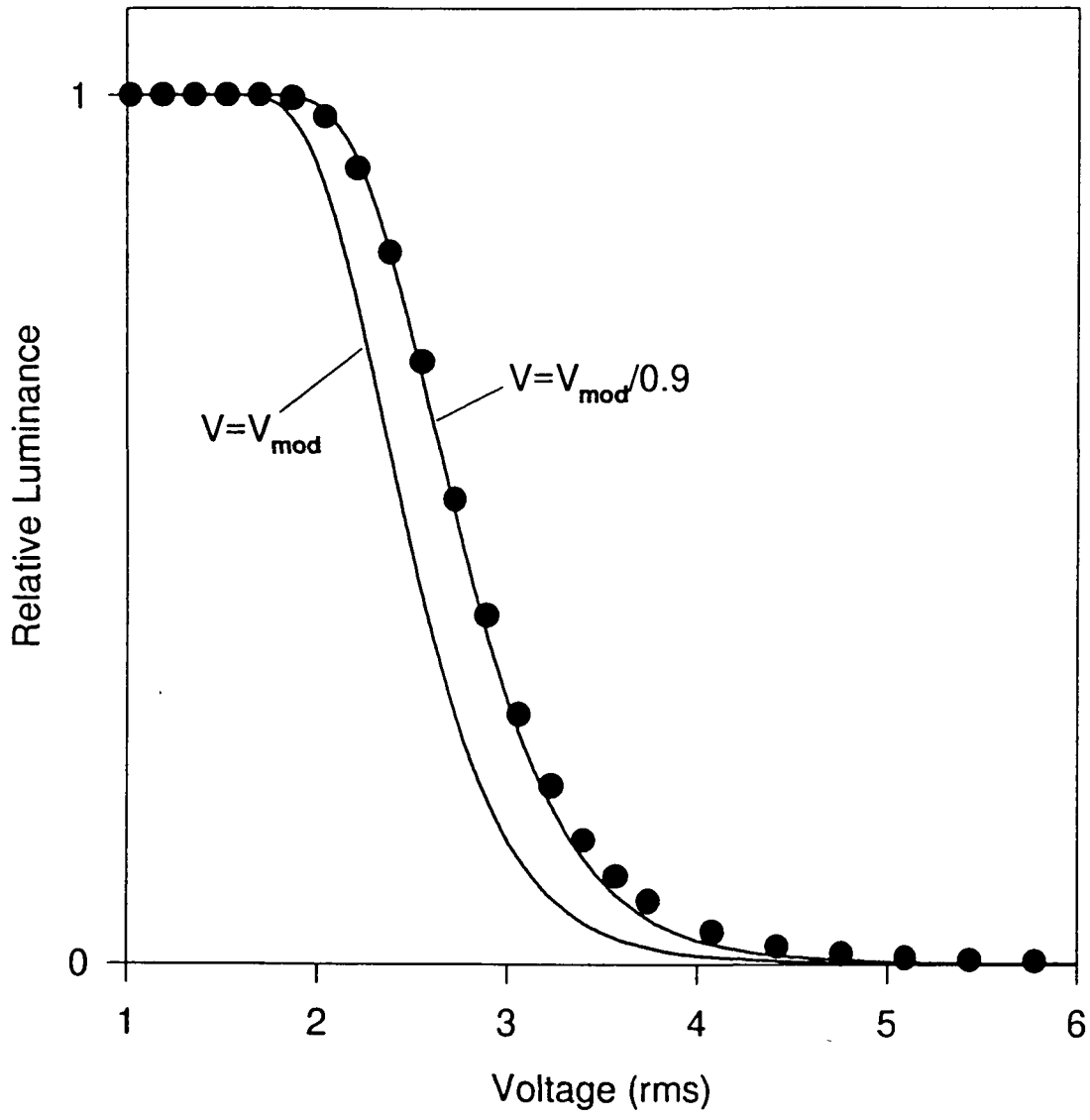
Luminance vs Voltage for TN cell #1
Experimental data (circles)
Model data (lines)
Relative Luminance
1
0
1
2
3
4
5
6
Voltage (rms)
V=V_mod
V=V_mod/0.9

Figure 74

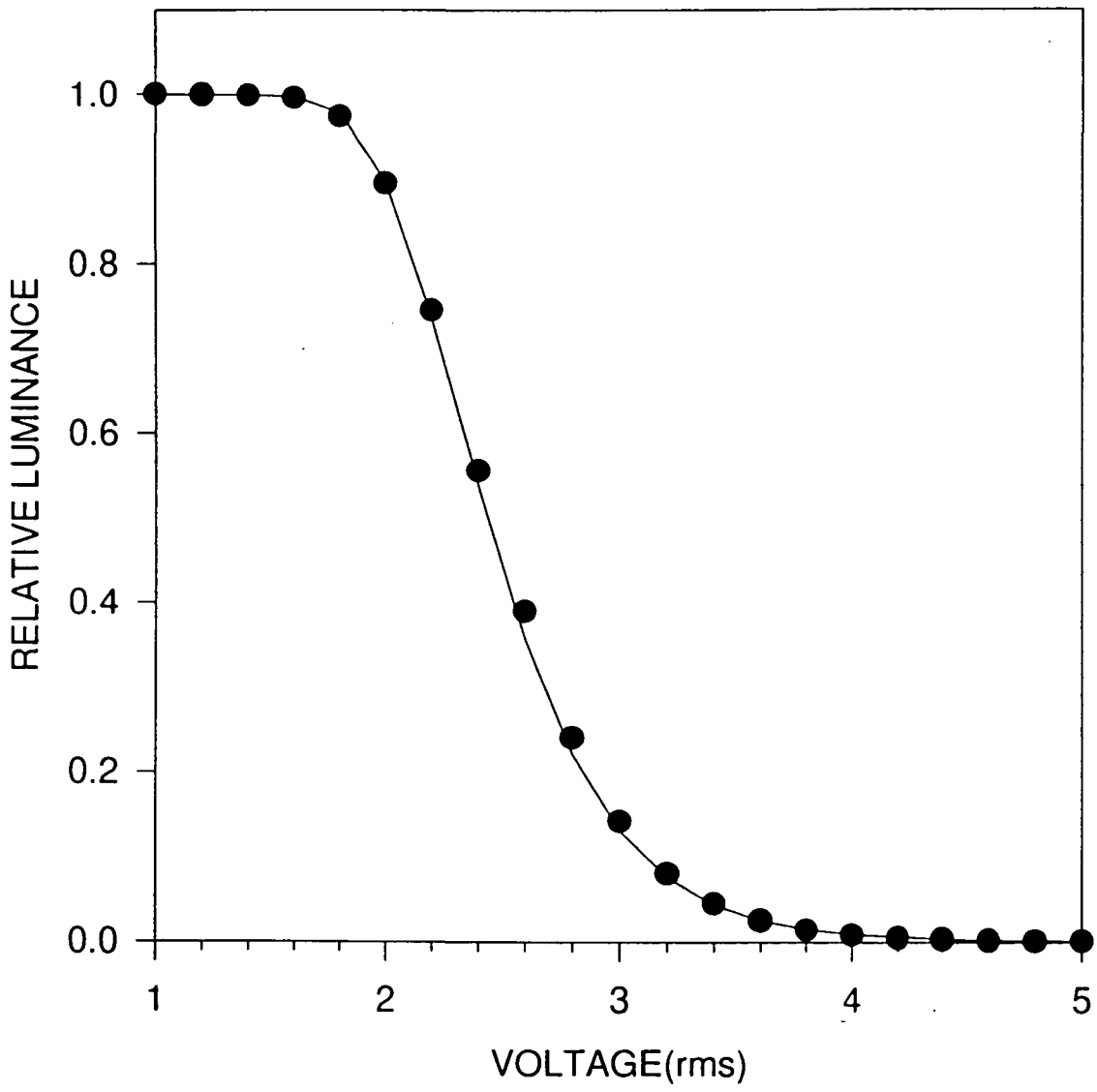
LUMINANCE vs VOLTAGE for IQT cell#1.
Comparison of Experiment (circles) to
Model (line)
RELATIVE LUMINANCE
1.0
0.8
0.6
0.4
0.2
0.0
1
2
3
4
5
VOLTAGE(rms)

**Figure 75**

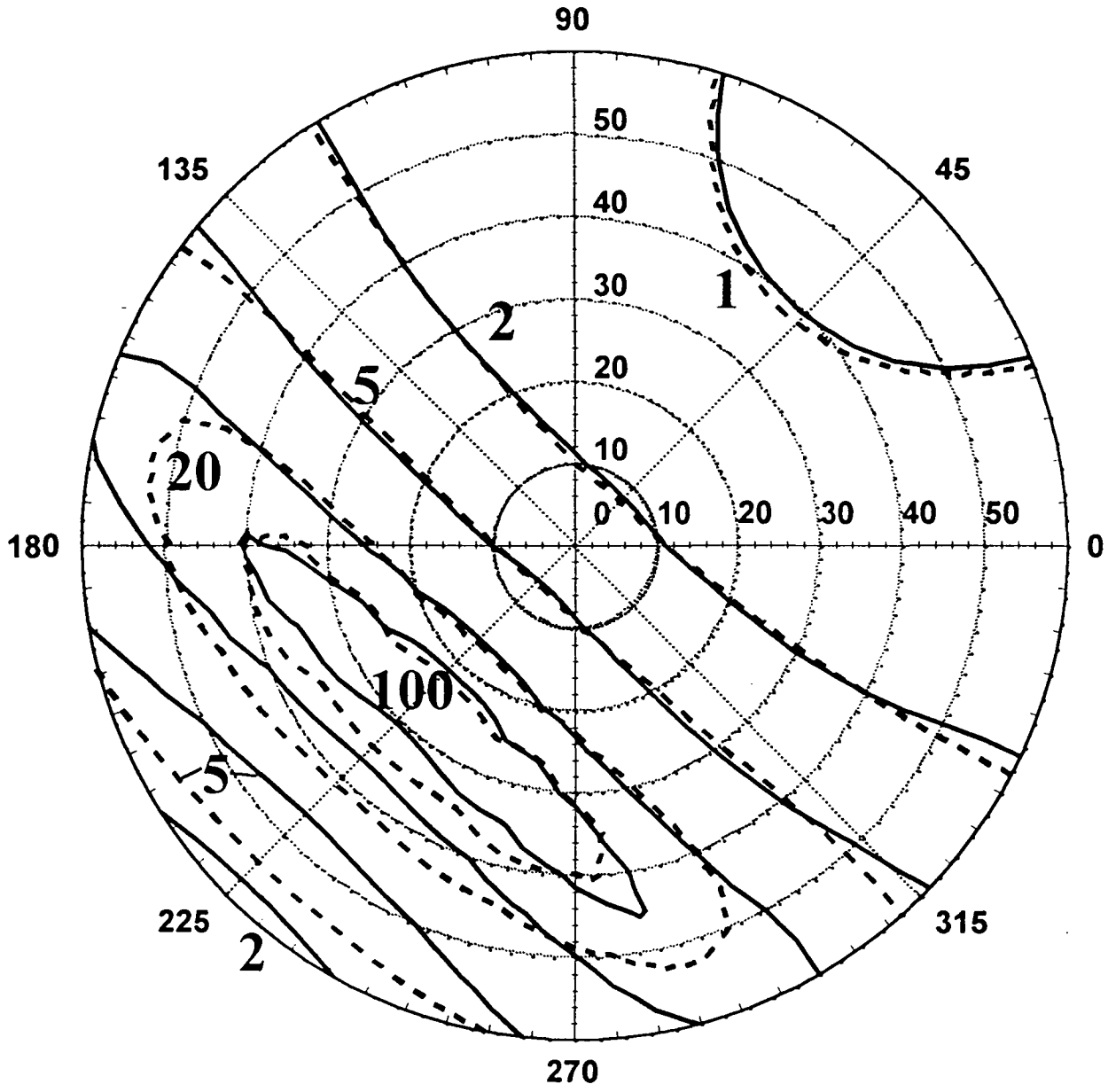


**Figure 76:** Iso-contrast plot comparing experiment (solid lines) to model (dotted), ignoring negative retardation associated with polarizers, at an on axis contrast ratio of 3.

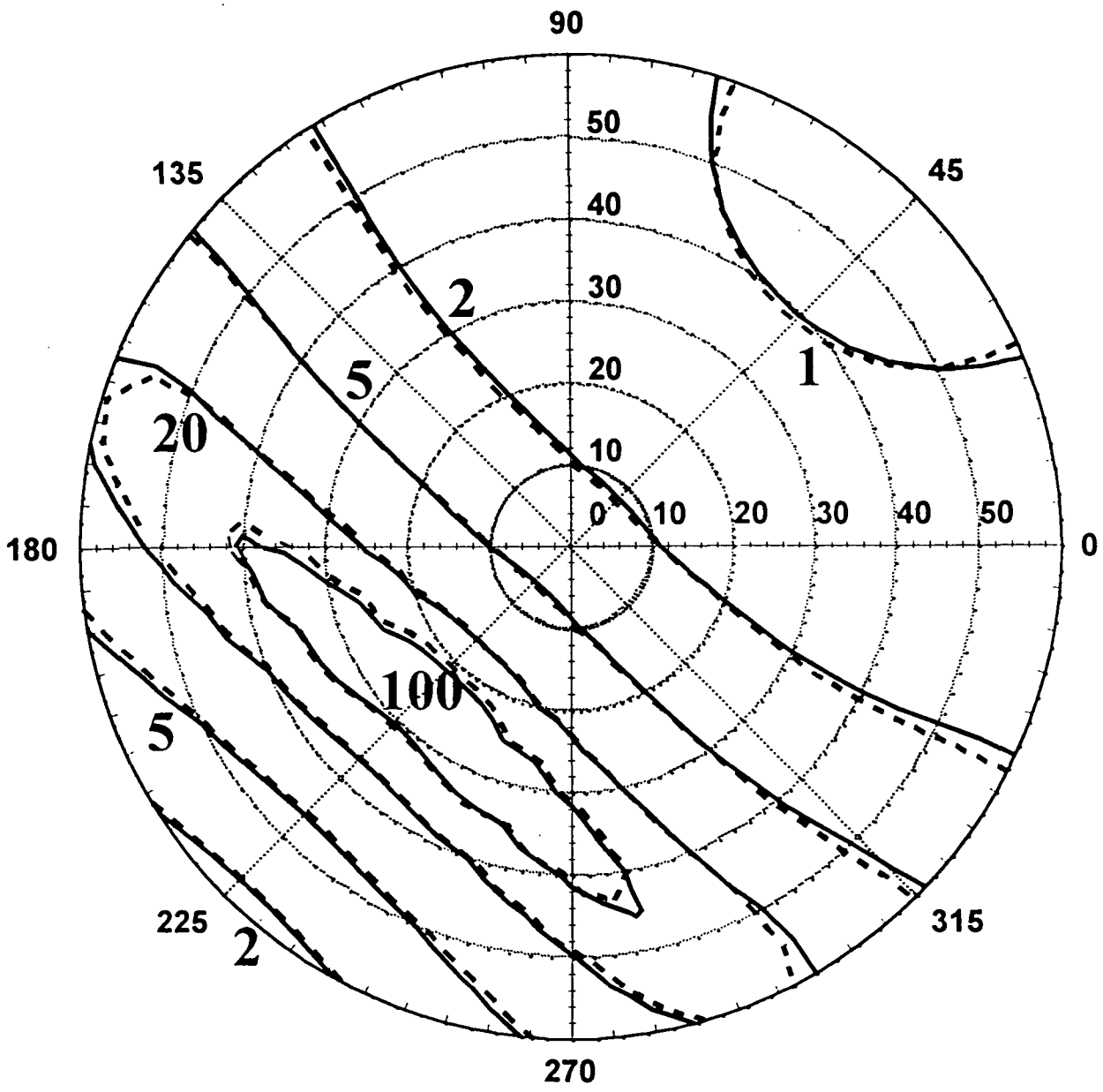


**Figure 77:** Iso-contrast plot comparing experiment (solid lines) to model (dotted), including negative retardation associated with polarizers, at an on axis contrast ratio of 3.

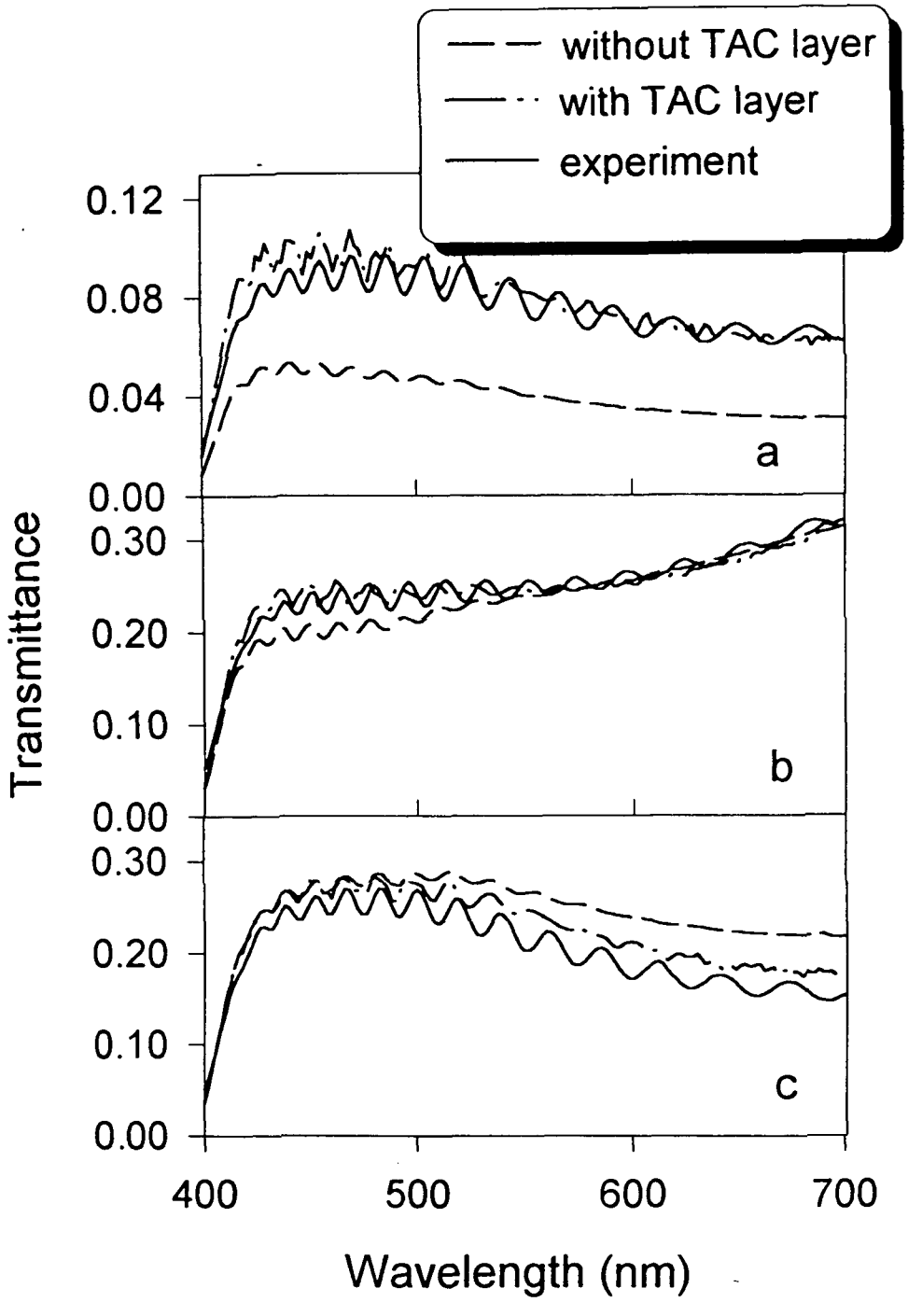


**Figure 78:** Comparison of experimental to modeled, both with and without a negative birefringent TAC layer, transmission spectra through a normally white TN cell. Plots differ in both viewing angle and excitation voltage. For plot **a)** polar viewing angle ($\Theta$) = 50° , azimuthal viewing angle ($\Phi$) = 225° and voltage set so that, compared to 0V, the on axis contrast ratio (OACR) = 3.8 **b)** $\Theta$ = 50° , $\Phi$ = 135° and OACR = 1.02 **c)** $\Theta$ = 50° , $\Phi$ = 45° and OACR = 105.

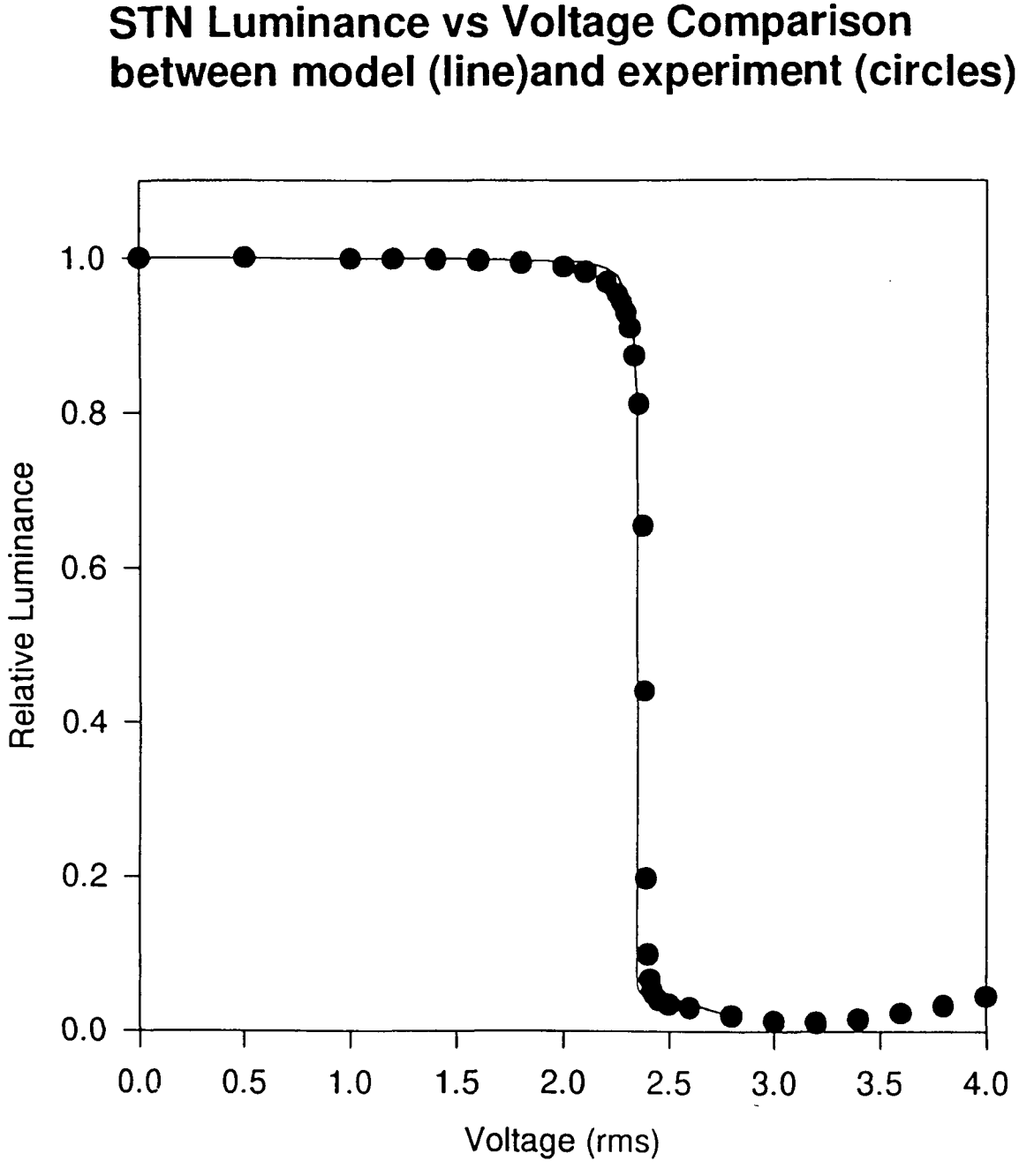
STN Luminance vs Voltage Comparison
between model (line)and experiment (circles)
Relative Luminance
1.0
0.8
0.6
0.4
0.2
0.0
0.0
0.5
1.0
1.5
2.0
2.5
3.0
3.5
4.0
Voltage (rms)

**Figure 79**

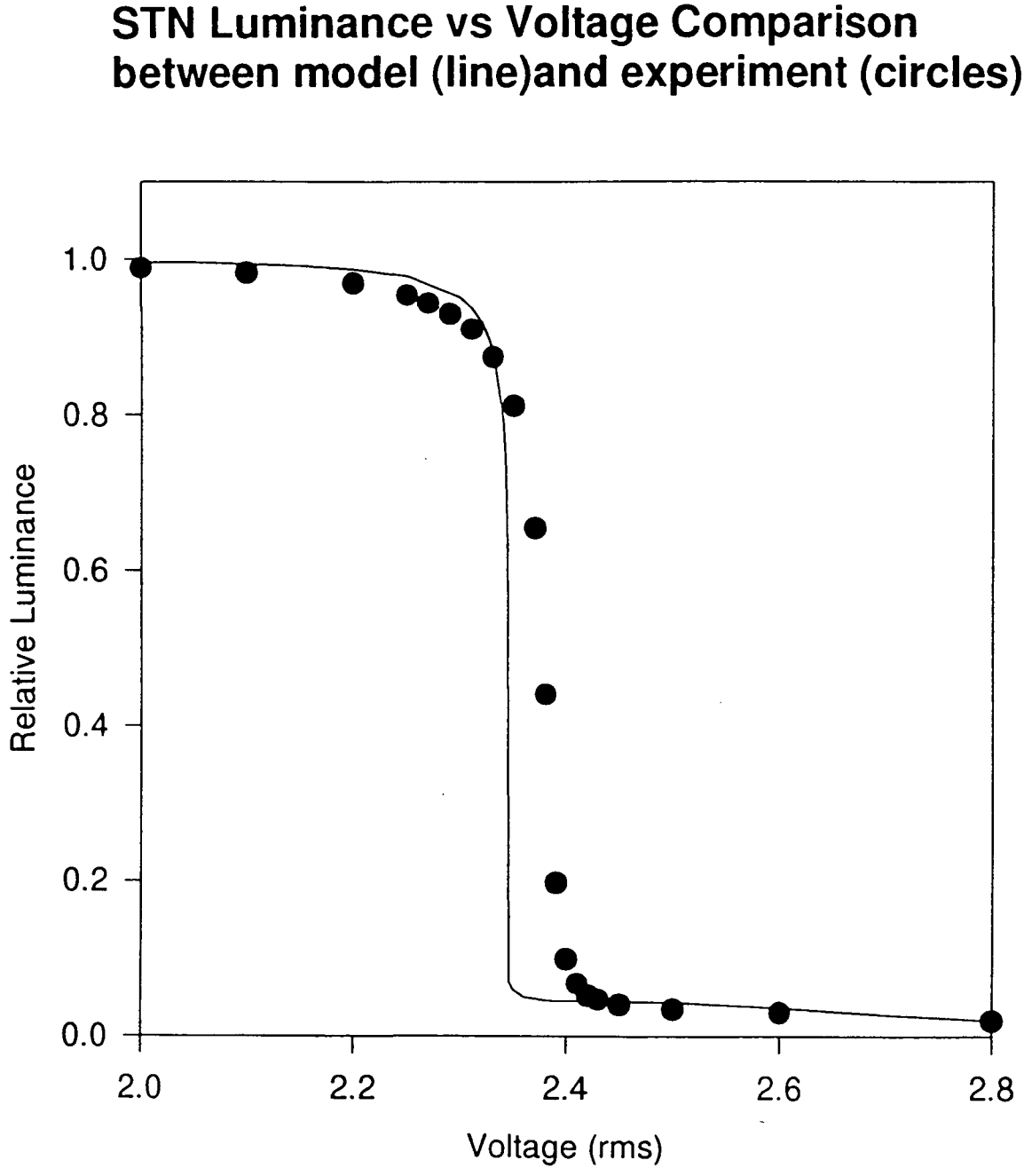
STN Luminance vs Voltage Comparison
between model (line)and experiment (circles)
Relative Luminance
1.0
0.8
0.6
0.4
0.2
0.0
2.0
2.2
2.4
2.6
2.8
Voltage (rms)

**Figure 80**

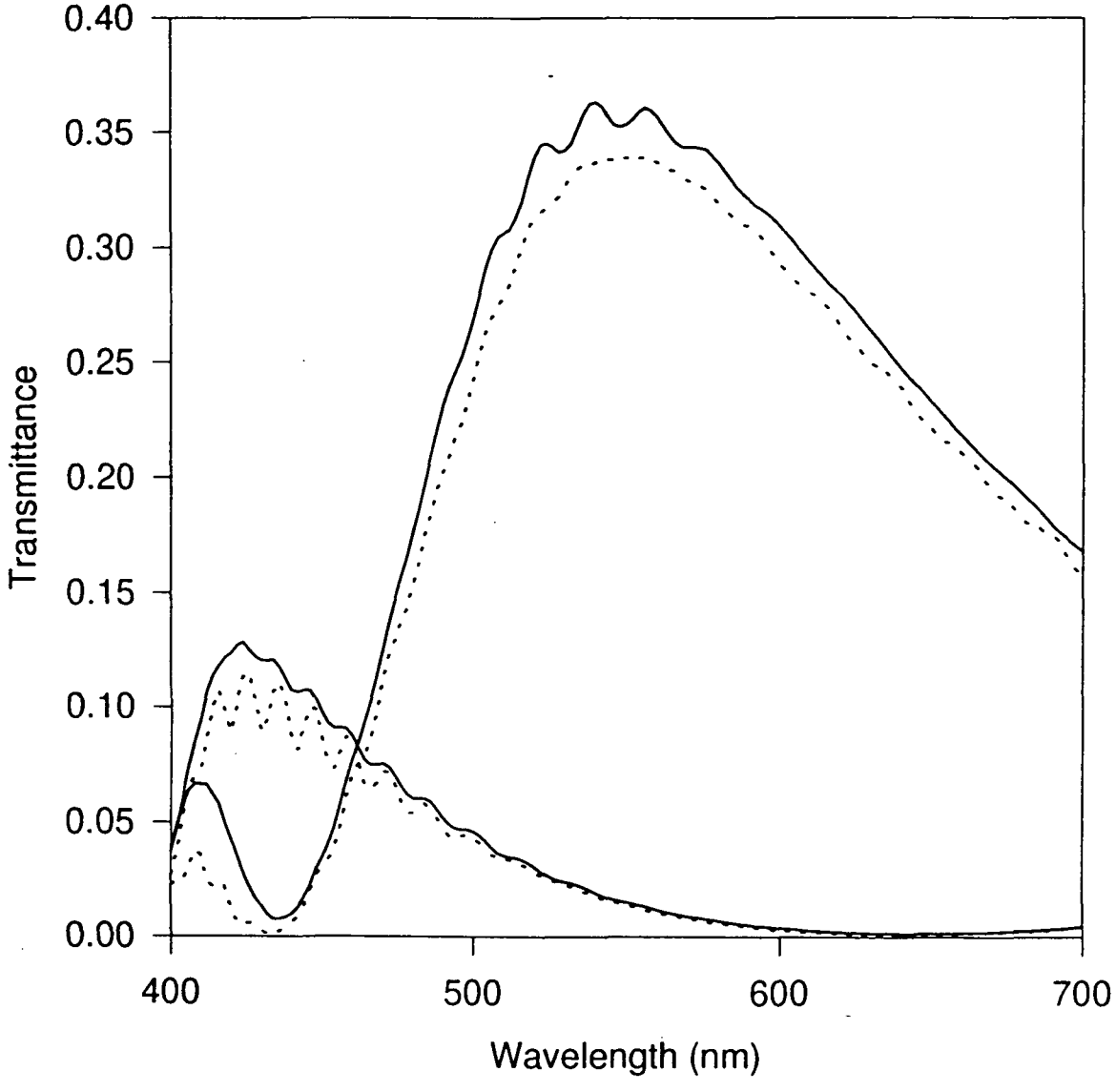
Comparison of Experimental (solid) to
Model (dotted) STN Transmission
at θ = 0 ϕ = 0
0.40
0.35
0.30
0.25
0.20
0.15
0.10
0.05
0.00
Transmittance
400
500
600
700
Wavelength (nm)

**Figure 81**

## Comparison of Experimental (solid) to Model (dotted) STN Transmission at $\theta = 30$ $\phi = 45$

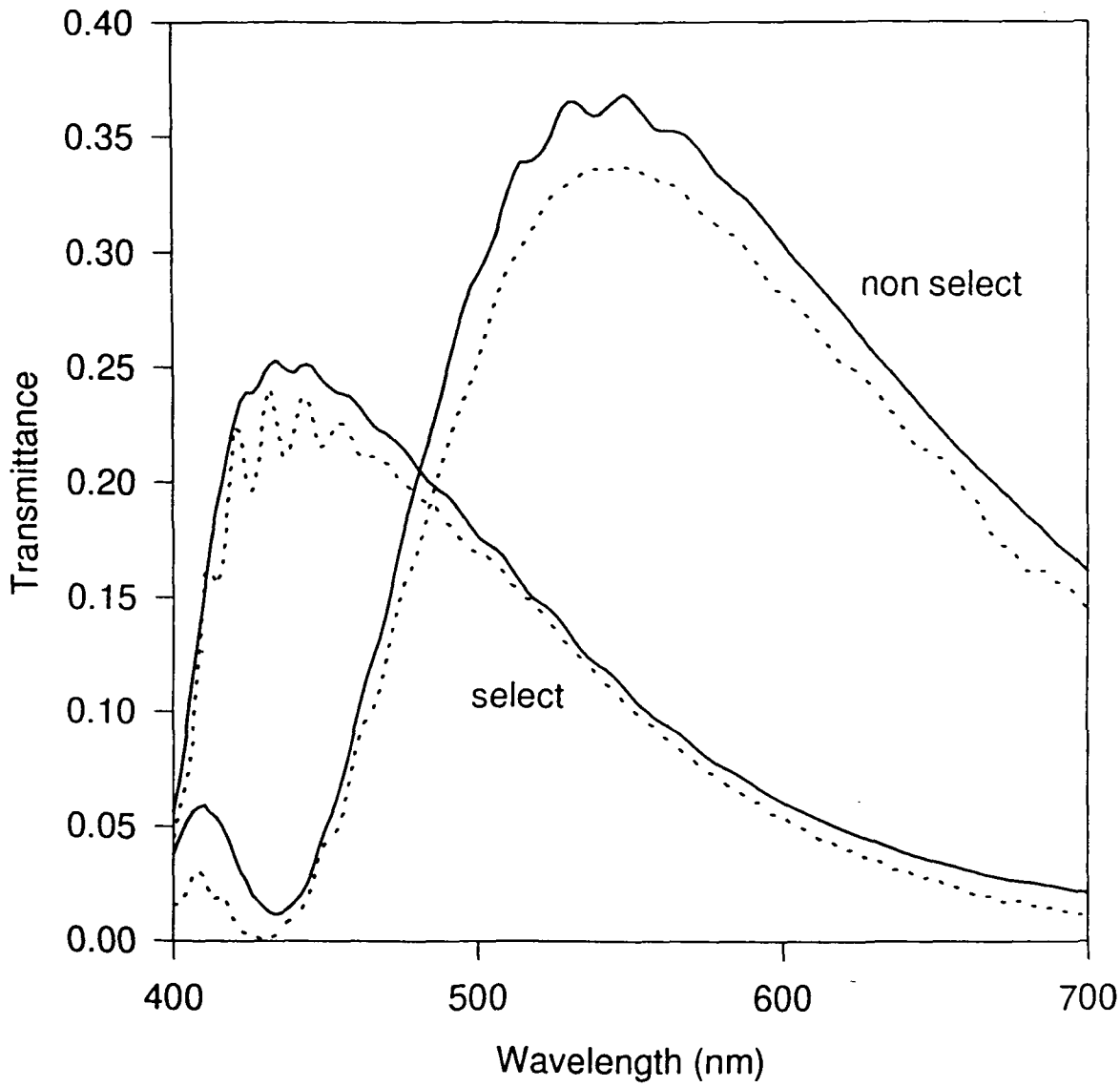


**Figure 82**

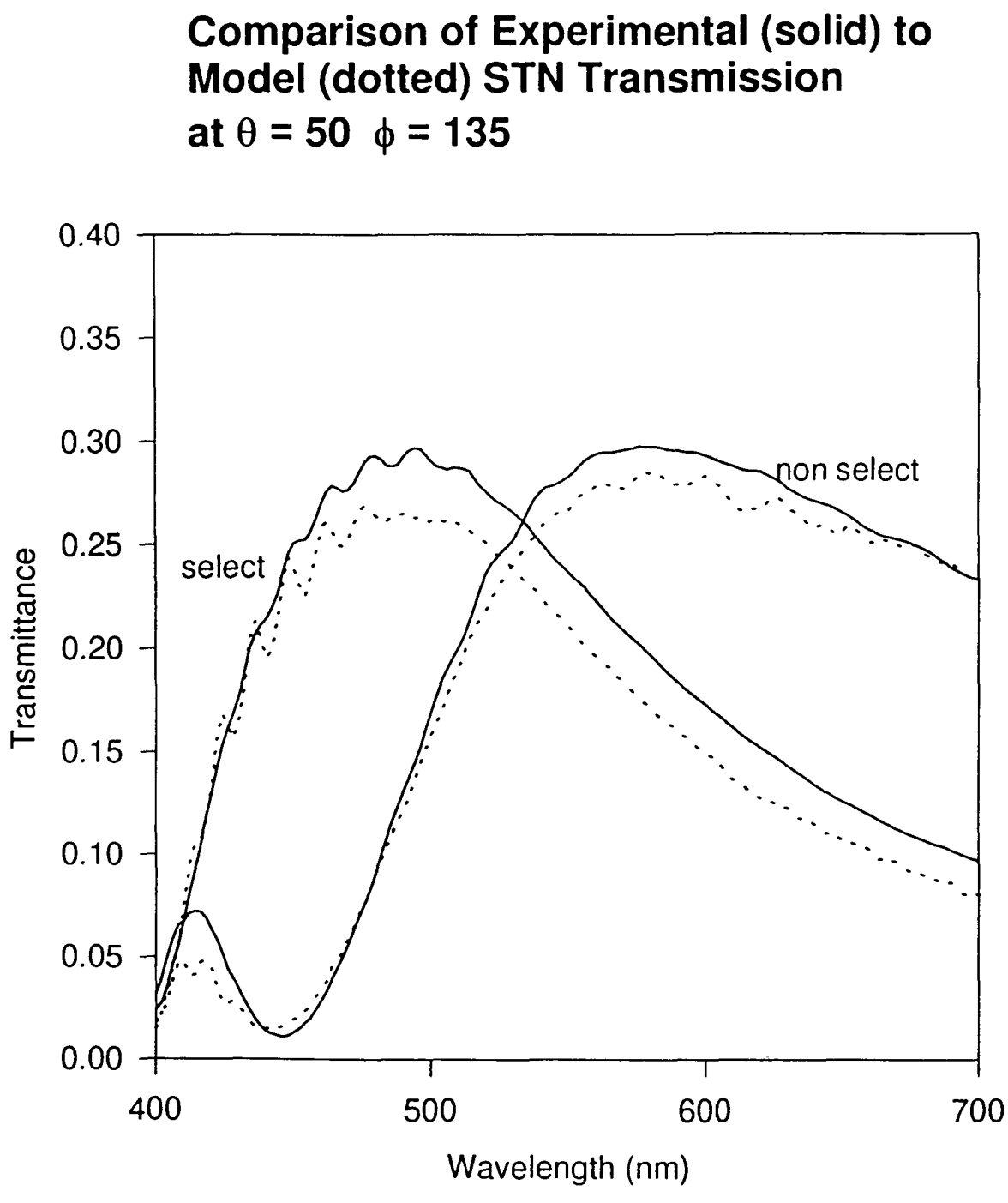
Comparison of Experimental (solid) to Model (dotted) STN Transmission at θ = 50 ϕ = 135
0.40
0.35
0.30
0.25
0.20
0.15
0.10
0.05
0.00
Transmittance
select
non select
400
500
600
700
Wavelength (nm)

**Figure 83**

**Chromaticity Co-ordinates for on axis viewing ($\Theta = 0$ $\varphi = 0$) of Standish 240 deg. STN cell (circles--experimental, line--model).**

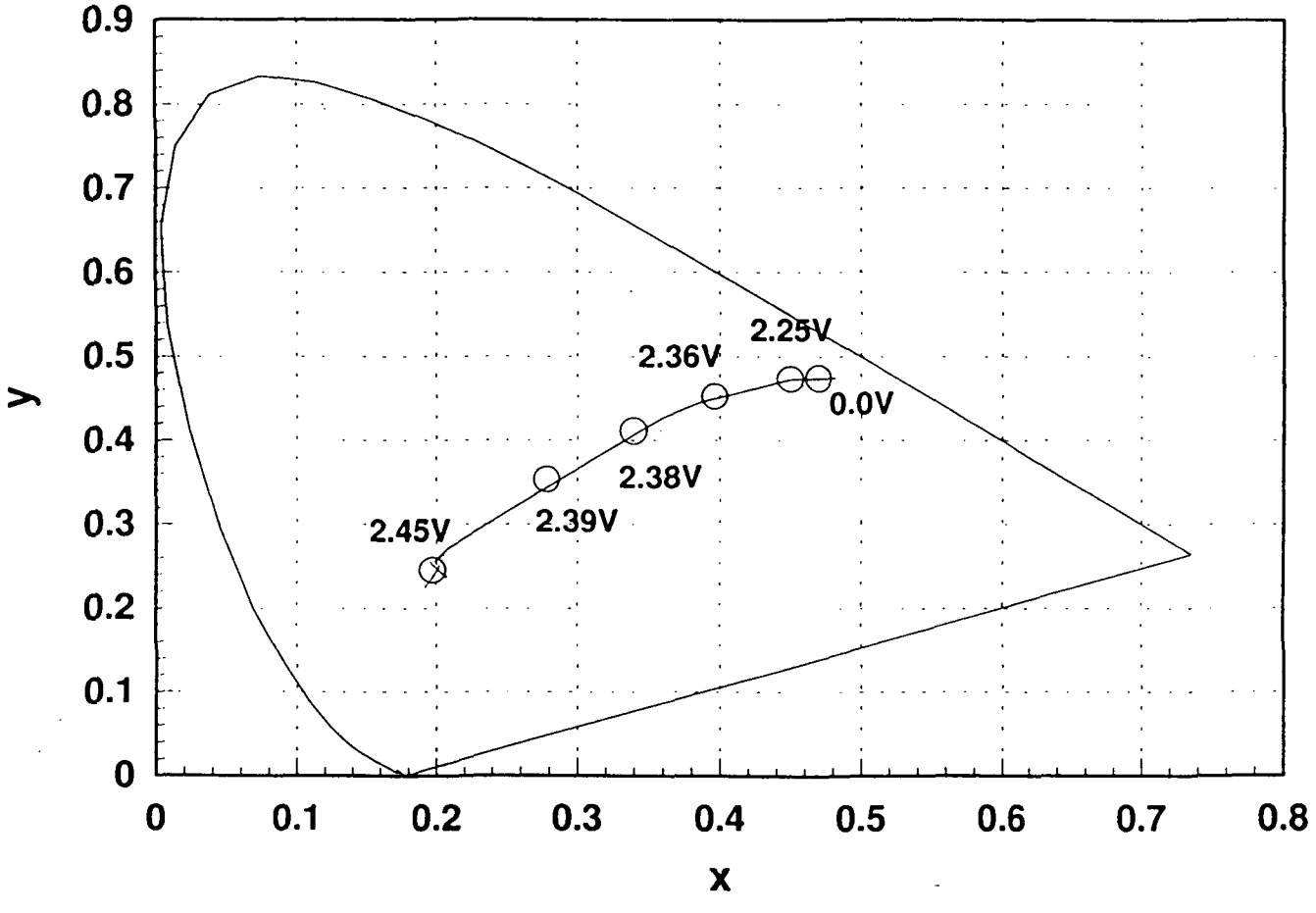


Figure 84

**Chromaticity Co-ordinates for $\Theta = 30$ $\Phi = 0$ viewing angle of Standish 240 deg. STN cell (circles--experimental, line--model).**

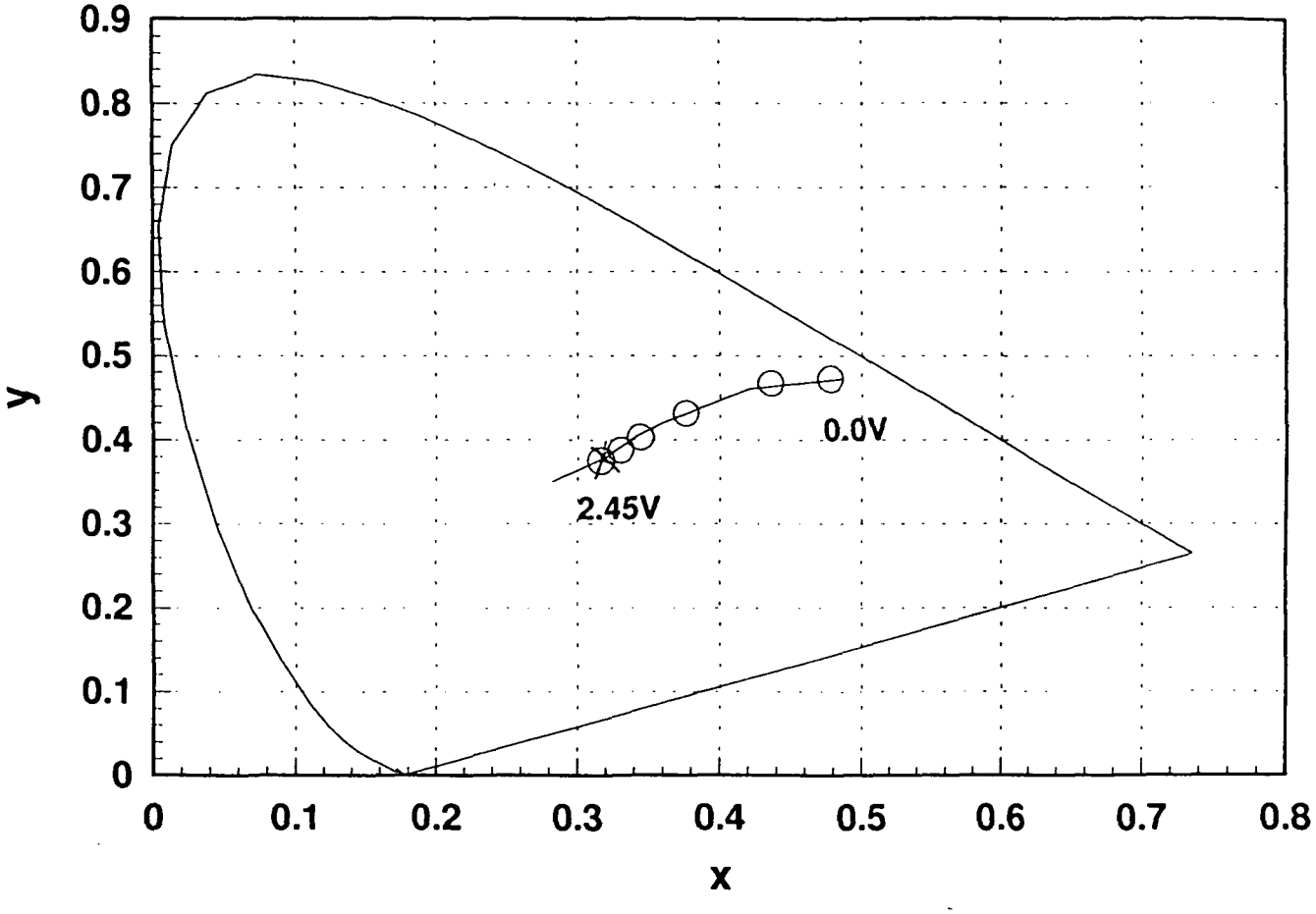


Figure 85

**Chromaticity Co-ordinates for $\Theta = 30\ \Phi = 90$ viewing angle of Standish 240 deg. STN cell (circles--experimental, line--model).**

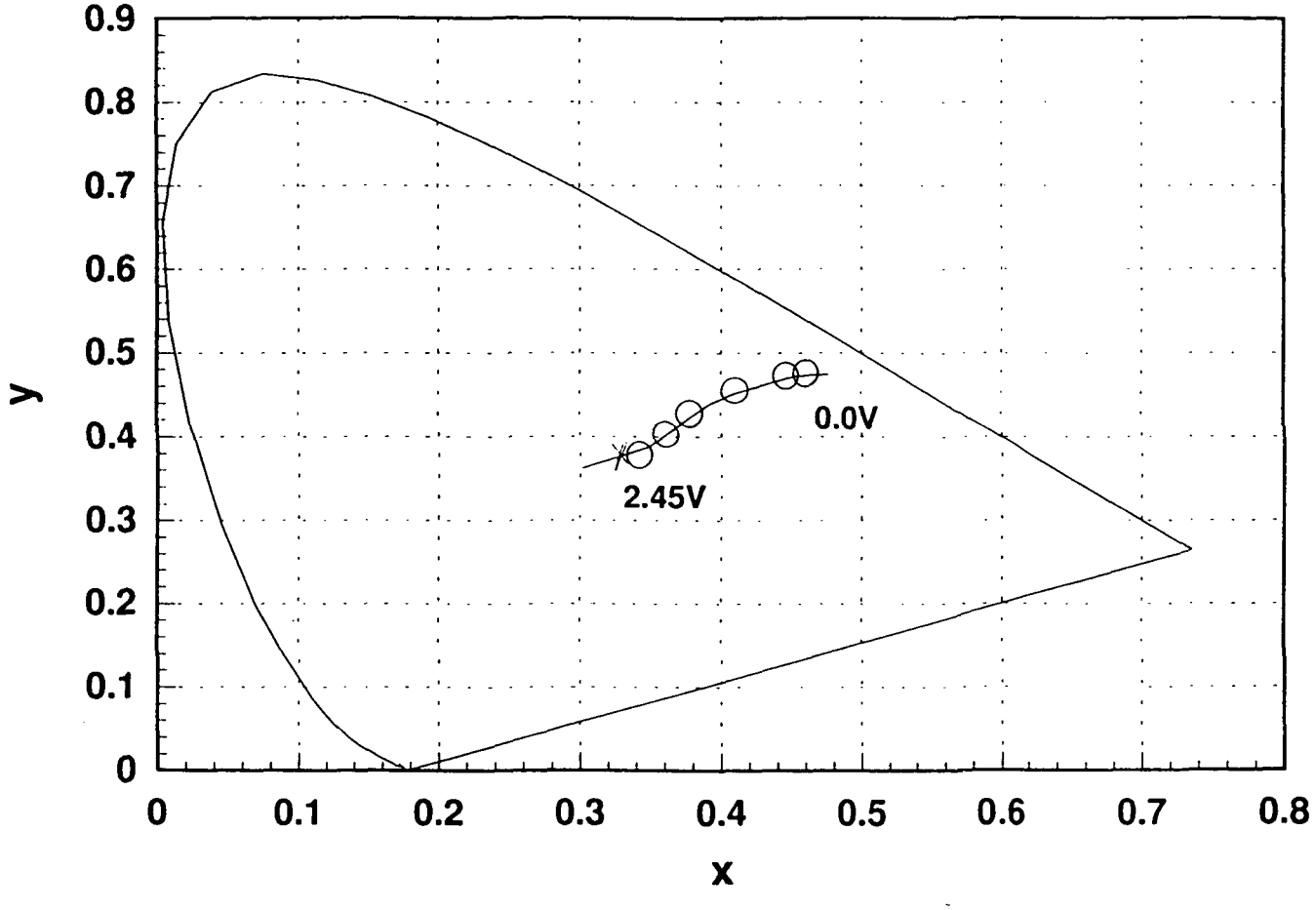


Figure 86

**Chromaticity Co-ordinates for $\Theta = 30$ $\Phi=180$ viewing angle of Standish 240 deg STN cell (circles--experimental, line--model).**

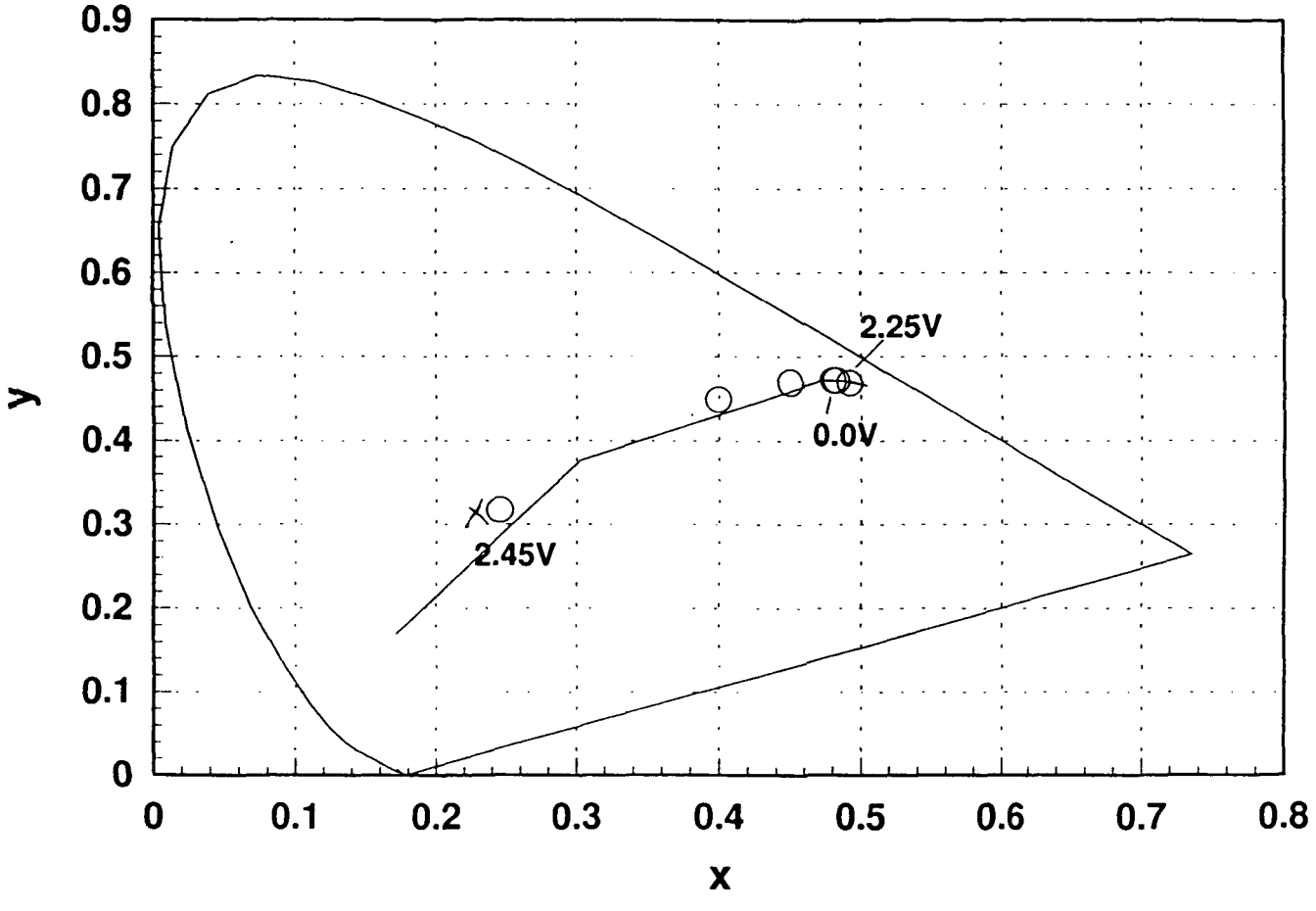


Figure 87

**Chromaticity Co-ordinates for $\Theta = 30$ $\Phi = 270$ viewing angle of Standish 240 deg STN cell (circles--experimental, line--model).**

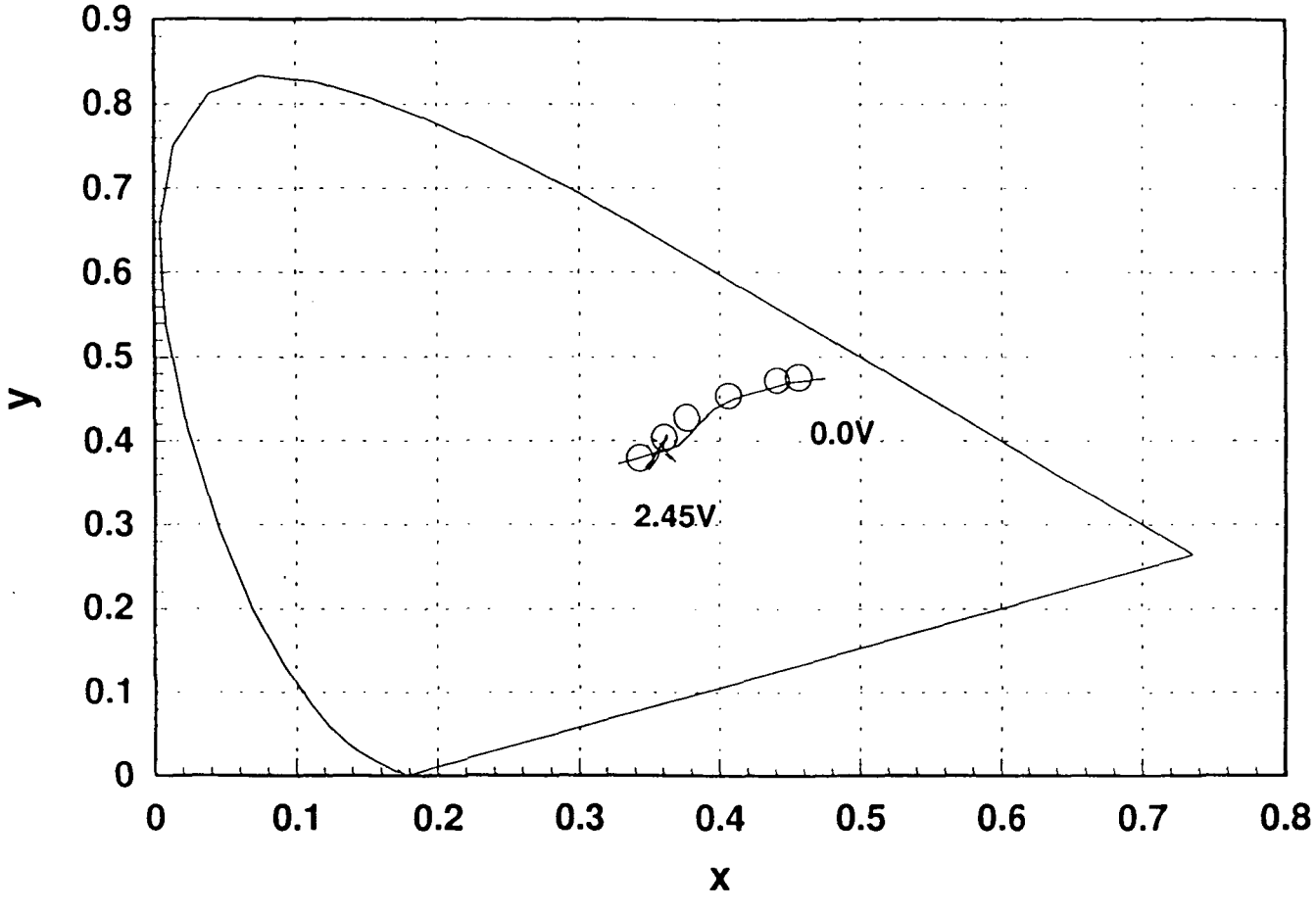


Figure 88

# IMPROVED REPRESENTATION OF POLARIZERS FOR LIQUID CRYSTAL DISPLAY MODELING

Richard Herke[1], Syed Jamal[1,2], Jack Kelly[1,2]

[1] Liquid Crystal Institute, Kent State University, Kent OH 44242

[2] Department of Physics, Kent State University, Kent OH 44242

**Abstract**

Dichroic sheet polarizers required for most liquid crystal displays are generally modeled as simple uniaxial films. This leads, however, to significant errors in display modeling at high viewing angles both in luminance and spectral transmission. The primary source of these errors appears to be a negative out of plane birefringence (on the order of 50nm for sample polarizers) of the protective outer layers of the polarizer. A straightforward methodology for measuring the relevant optical properties for modeling purposes via transmission measurements through crossed polarizers and optical microscopy is described.

**Keywords**--polarizers, modeling, LCD, viewing angle.

**Address correspondence to:**

**Richard Herke**

**Liquid Crystal Institute, Kent State University, Kent OH 44242**

**(216) 672-4875, fax (216) 672-2796, e-mail: herke@scorpio.kent.edu**

## 1. Introduction

Computer modeling of liquid crystal displays is becoming increasingly important in the display design process, as it allows for the quick characterization and possible optimization of proposed displays without the expense and time needed to construct a multitude of test cells. The 4x4 matrix method of Berreman[1,2] based on Maxwell's equations and assuming only that the optical properties vary in one direction has the potential of essentially exactly modeling display systems, and is the method chosen for example for the ViDEOS [3] display modeling program. However, the actual fidelity of any modeling program is dependent on the precision with which the optical properties of the various display components are known, and in practice there is often a significant difference between modeled and experimental display measurements. This is particularly true at high viewing angles which is where liquid crystal displays are in most need of improvement[4] and modeling could be most beneficial. In our laboratory we have thus been involved in identifying the key areas responsible for and resolving the discrepancies between model and reality. We have determined that besides the liquid crystal layer itself which has been the subject of much investigation [5] the factor most responsible for poor modeling results has been an ignorance of the optical structure of real polarizers.

## 2. Polarizer Background

In modeling, the polarizer is typically treated as a uniaxial film with complex indices [6]. The absorbing direction, along the optic axis, is oriented parallel to the plane of the sheet. To account for the high absorption the index in this direction contains an imaginary component much larger than that perpendicular to the optic axis. Such a model in fact does reproduce rather well the *qualitative* viewing characteristics of a polarizer. For example Figures 1 and 2 compare the

measured and modeled viewing angle characteristics of crossed polarizers. In these contour plots the radius represents the polar viewing angle with the origin being for on axis viewing and the perimeter corresponding to 60° off axis, and the azimuthal angle corresponds to the azimuthal viewing angle with 0° being approximately along the transmission direction of the front polarizer. The numerical value of each contour is the luminance of the sample compared to the luminance from the backlighting illuminant A light source at the sample position.

We took the data of Figure 1 using two crossed high performance (polarization efficiency of 99.95%) G1220DU Nitto Denko polarizers, attached across an isotropic medium. The slightly larger transmission in the first and third quadrants is due to the angle between the polarizers being slightly larger than perpendicular at approximately 91°. The test cell sat on a computer controlled goniometer stage that automatically varied viewing angle in 5° increments in both polar and azimuthal angles. A diffuse illuminant A light source backlit the cell and luminance data was collected using a Photo Research 704 spectroradiometer. Figure 2 shows the data for the same configuration, calculated using a fast 4 x 4 Berreman matrix method at each viewing angle. In the model the real parts of the indices were supplied by the manufacturer and assumed constant with respect to wavelength while the imaginary components were determined from on axis measurements of the transmitted spectra taken through parallel and crossed polarizers. Yet while the qualitative shape of Figures 1 and 2 are nearly identical, the model underestimates the amount of transmission for viewing angles greater than 30° by a factor of two or more. Furthermore if we adjust the index components to bring the high viewing angles into agreement then the lower viewing angles suffer from even a greater discrepancy. Clearly a more detailed picture of an actual polarizer is needed.

Figure 3 shows the macroscopic structure of a dichroic sheet polarizer typically used on liquid crystal displays. These polarizers are commonly manufactured by first running a polyvinyl alcohol (PVA) film through an aqueous solution containing (among other ions such as boron which help stabilize the film) iodine. The iodine absorbs into and is concentrated at the surfaces of the film. In the case of our polarizers, cross sectional energy dispersive x-ray studies [7] revealed that the absorbed iodine was concentrated within roughly 2.5μm to 3.5μm of the PVA surfaces. These layers, in fact, can easily be seen and thicknesses roughly estimated by cutting a thin sample of the polarizer along the absorbing direction and viewing edgewise under a polarizing microscope. Inside the PVA the Iodine forms long chains, possibly held in the center of helices formed by the PVA molecules [8]. These chains presumably allow conduction along their backbone, and when the PVA film is then stretched the iodine chains are oriented and produce the polarizing effect. Afterward a triacetyl cellulose (TAC) layer is laminated on each side in order to protect the polarizer, and a thin layer of pressure sensitive adhesive (PSA) is placed on one side for attachment to the display.

## 3. Optical properties of other polarizer components

A logical first step in improving polarizer modeling would be to incorporate the double layer structure at each surface. This was tried but found to have little affect for these high performance polarizers. However, for less efficient polarizers the birefringence of the PVA between the polarizing layers may produce a noticeable change in the polarization state. Attention was therefore drawn to the other layers of the polarizer, the TAC and PSA, which as a rule have been simply ignored or, perhaps more charitably, assumed to be isotropic. To test the assumption we used Senarmont ellipsometry [9] with both He-Ne (632.8nm) and Ar-ion

(514.5nm) laser light sources to measure the birefringence of a sample of TAC film supplied by the manufacturer. This revealed a small in plane retardation through the film of about 10nm. Presumably the principal axes of the TAC film are aligned with the polarizer or this retardation would greatly increase the amount of light passing through the crossed polarizers at normal incidence. Out of plane we found the TAC film to be negatively birefringent, i.e., index lower out of plane than in plane, with a retardation over the thickness of the film of 81nm for the He-Ne wavelength and 67nm for the Ar-ion. Inserting a negative birefringent film in the model does indeed improve the match in the case of the crossed polarizers, but these retardations actually produce too large of an effect causing the model to go from predicting too little transmission at high viewing angles to too much. A negative birefringence of 55nm on the other hand produces excellent agreement between model and experiment as Figure 4 demonstrates. Possible explanations for this discrepancy include variations from batch to batch of TAC film, modifications due to the laminating process, or contributions of the PSA film. In any case the measurements on the crossed polarizers give a precise method, for the purposes of further modeling, of measuring *in situ* the negative birefringence associated with the polarizers. That the disagreement is due to an out of plane retardation is confirmed by this change in one parameter producing agreement over the entire viewing cone.

## 4. Studies on liquid crystal display test cell

When TAC films with a 55nm negative birefringence are inserted into the model of a typical display it does indeed produce significant improvement. To compare with the model, data was taken on a normally white twisted nematic (TN) liquid crystal test cell using the goniometer system mentioned above. The test cell consisted of two ITO (thickness ~ 25nm) coated

borosilicate glass plates with a gap spacing of 5.2μm filled with the fluorinated liquid crystal ZLI-4792. To align the liquid crystal the ITO layers were further coated with a rubbed polyimide layer (thickness ~20nm). The polarizers were attached to the glass plates with their transmission axes crossed to each other and parallel to the respective polyimide rubbing directions. The model treats the glass plates as semi-infinite (to remove multiple reflections in the glass) dielectric slabs with essentially constant indices of refraction found from refractometry measurements. The polyimide is also treated as a dielectric slab while the ITO layer has a complex index of refraction that varies with wavelength, found using ellipsometry [10,11]. The liquid crystal is approximated by a series of 20 or more slabs (increasing this number beyond 20 results in luminance changes of << 1%) with each slab having a constant director orientation found from a minimization of the Oseen-Frank free energy over the entire layer [12]. The director orientation sets each slab's refractive indices with the Cauchy equation, as supplied by the manufacturer, determining the wavelength dependence. Figures 5a and 5b are isocontrast plots comparing data taken on the liquid crystal display test cell to model data with and without incorporating the TAC film retardation respectively. The rubbing direction of the front plate polyimide layer is along the 0° axis of the Figures. The contrast ratios for the experiment are between an applied excitation voltage of 0V and a 100Hz square wave of $V_{rms}$=2.93V while for the model the voltage has been adjusted to $V_{rms}$= 2.77V to yield the correct contrast ratio for *on axis viewing*. The agreement over the entire viewing cone increases with the high viewing angle-high contrast regions showing marked improvement.

The improvement in model characteristics goes beyond isocontrast plots. The inclusion of the TAC birefringence improves actual shapes of the transmittance spectra through the liquid

crystal cell. Figure 6 displays transmittance spectra, both model with and without the TAC layers and experimental data, for high viewing angles and a variety of switching voltages. The oscillations in the curves are due to multiple reflections in the liquid crystal between the ITO layers. Again we chose the model voltages to minimize the errors for on axis viewing. The most marked improvement is in the high contrast regions (e.g., quadrant 3 of Figure 5) of which Figure 6a is an example. However, improvement is seen in the shape of the spectra for each case. Presumably if the TAC layer retardation was measured as a function of frequency the improvement would be even better.

## 5. Summary

Thus in the modeling of liquid crystal displays it is important to incorporate a realistic model of polarizer performance. At the very least this includes not only a uniaxial absorbing film of a few microns thickness but the optical properties, for example, negative birefringence of the protective TAC layers as well. In lower contrast polarizers, often used on super twist nematic cells, the double layer nature of the polarizer, that is, two iodine containing polarizing layers separated by a birefringent PVA layer may also need to be taken into account. A few simple measurements and the Berreman model allow for the determination of these constants. Normal incidence transmission through a polarizer will yield the imaginary value of $n_o$ while the transmission through crossed polarizers can give that of $n_e$. An off axis measurement through crossed polarizers can then yield up the negative birefringence of the TAC layer. If needed for lower efficiency polarizers the thickness and separation of the dual polarizing layers can be estimated by viewing a thin slice edgewise through a polarizing microscope.

**Acknowledgments**

The authors wish to thank Louis D. Silverstein of VCD Sciences Inc. and Giorgio Trapani of Polaroid Corp. for useful discussions, and Paul Melby for assistance with measurements and figure presentation.

This work was supported by NASA under grant NCC 2-803 and the NSF under ALCOM grant DMR89-20147.

## FIGURE CAPTIONS

**Figure 1:** Contour plot of experimentally measured percent transmission through crossed polarizers. Radius and azimuthal angles of plot correspond to polar and azimuthal viewing angle respectively.

**Figure 2:** Contour plot of modeled percent transmission through crossed polarizers.

**Figure 3:** Layer structure of dichroic sheet polarizer typically used on liquid crystal displays. Consists of a layer of pressure sensitive adhesive (PSA), two protective triacetyl cellulose (TAC) layers, and a layer of stretched polyvinyl alcohol (PVA) with absorbed iodine at its surfaces.

**Figure 4:** Contour plot comparing experimental (black lines) to modeled (gray lines) percent transmission through crossed polarizers. The difference in the modeled data from figure 2 is the inclusion of a TAC film on each polarizer with a negative out of plane birefringence of 55nm.

**Figure 5:** Contour plot comparing experimental (black) to modeled (gray) contrast ratios of a normally white twisted nematic cell. Model data calculated **a)** using polarizers without a negatively birefringent TAC layer and **b)** using TAC layer with an out of plane negative birefringence of 55nm.

**Figure 6:** Comparison of experimental to modeled, both with and without a 55nm negatively birefringent TAC layer, transmission spectra through a normally white TN cell. Plots differ in both viewing angle and excitation voltage. For plot **a)** polar viewing angle ($\Theta$) = 50°, azimuthal viewing angle ($\Phi$) = 225° and voltage set so that, compared to 0V, the on axis contrast ratio (OACR) = 105 **b)** $\Theta$ = 50°, $\Phi$ = 135° and OACR = 1.02 **c)** $\Theta$ = 50°, $\Phi$ = 45° and OACR = 3.8.

1 D. W. Berreman, "Optics in Stratified and Anisotropic Media: 4 x 4-Matrix Formulation," J Opt. Soc. Am. **62,** 502-510 (1972).

2 K. Eidner, et al., "Optics in Stratified Media--The Use of Optical Eigenmodes of Uniaxial Crystals in the 4 x 4 Matrix Formalism," Mol. Cryst. Liq. Cryst. **172,** 191-200 (1989).

3 J. Larimer, et al., "A Video Display Engineering and Optimization System: ViDEOS," SID 94 Digest, **25,** 197-200 (1994).

4 T. Sugiyama, et al., "Analytical Simulation of Electro-Optical Performance of amorphous and Multidomain TN-LCDs," SID 94 Digest, **25,** 919-922 (1994).

5 B. Bahadur (ed), "Liquid Crystals: applications and uses," **vol. 1-3,** (World Scientific, Singapore: 1991).

6 G. Haas, et al., "Polarizer model for liquid-crystal devices," J. opt. Soc. Am. A, **5,** 1571-1575 (1988).

7 Performed by Surface Science Laboratories of Mountain View CA.

8 M. M. Zwick, "Poly(Vinyl Alcohol)-Iodine Complexes," J. Appl. Poly. Sci., **9,** 2393-2424 (1965).

9 K. Y. Han, P. Vetter, T. Uchida, "Determination of Molecular Inclination in Rubbed Polymer for Liquid Crystal Alignment by Measuring Retardation," Jpn. J. Appl. Phy. **32, part 2,** L1242-L1244 (1993).

10 R. M. A. Azzam, N. M. Bashara, "Ellipsometry and polarized light," (North-Holland Publishing Company, Amsterdam: 1977).

11 J. A. Woolam, W. A. McHagan, "Spectroscopic Ellipsometry Analysis of ITO and Other coatings on Glass: Microscopic Evaluation Over Large Areas," SID 93 Digest, **24,** 558-560 (1993).

12 D. W. Berreman, "Numerical Modelling of twisted nematic devices," Philos. Trans. R. S. London, **309,** 203-216 (1983).

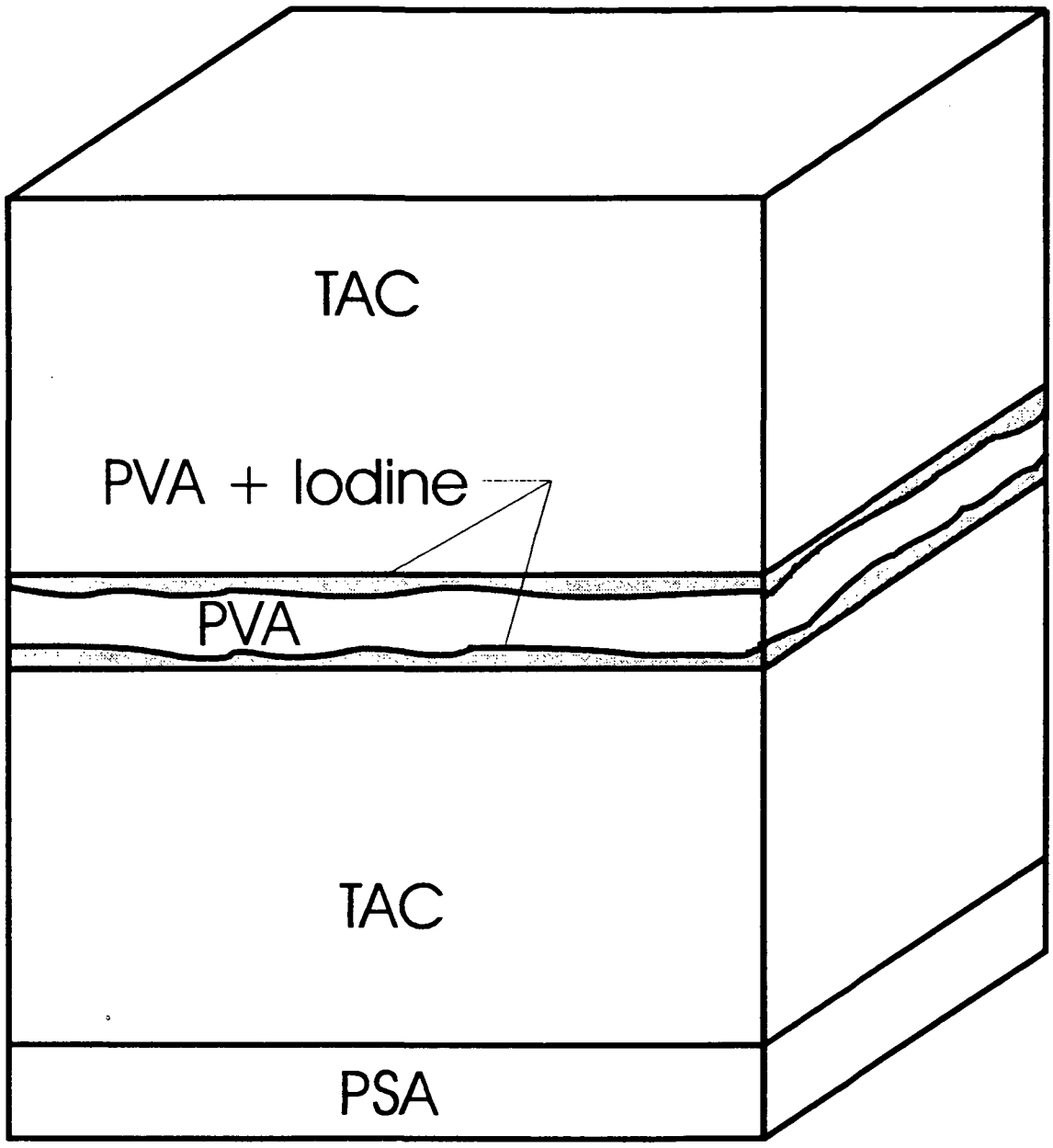

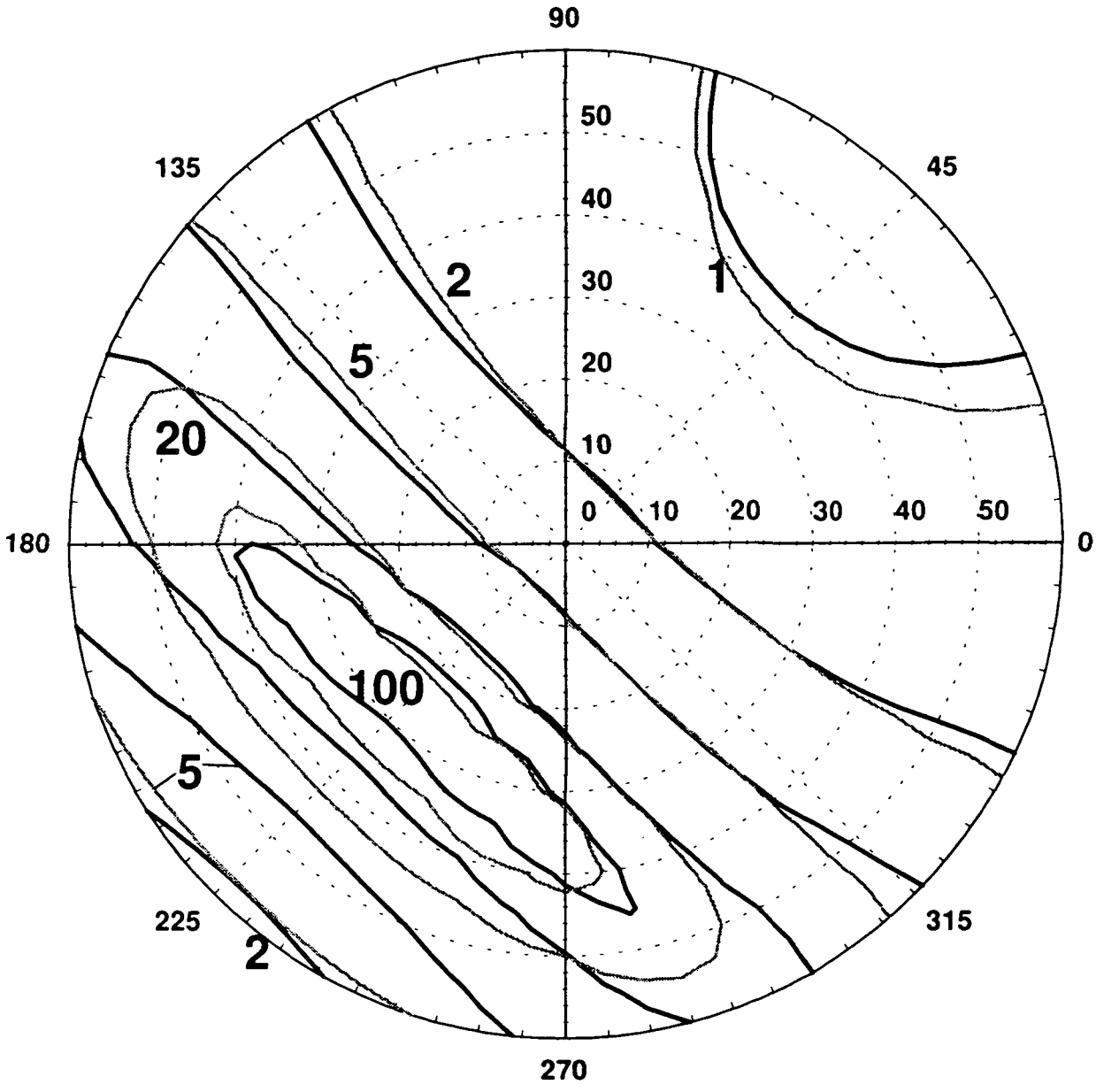

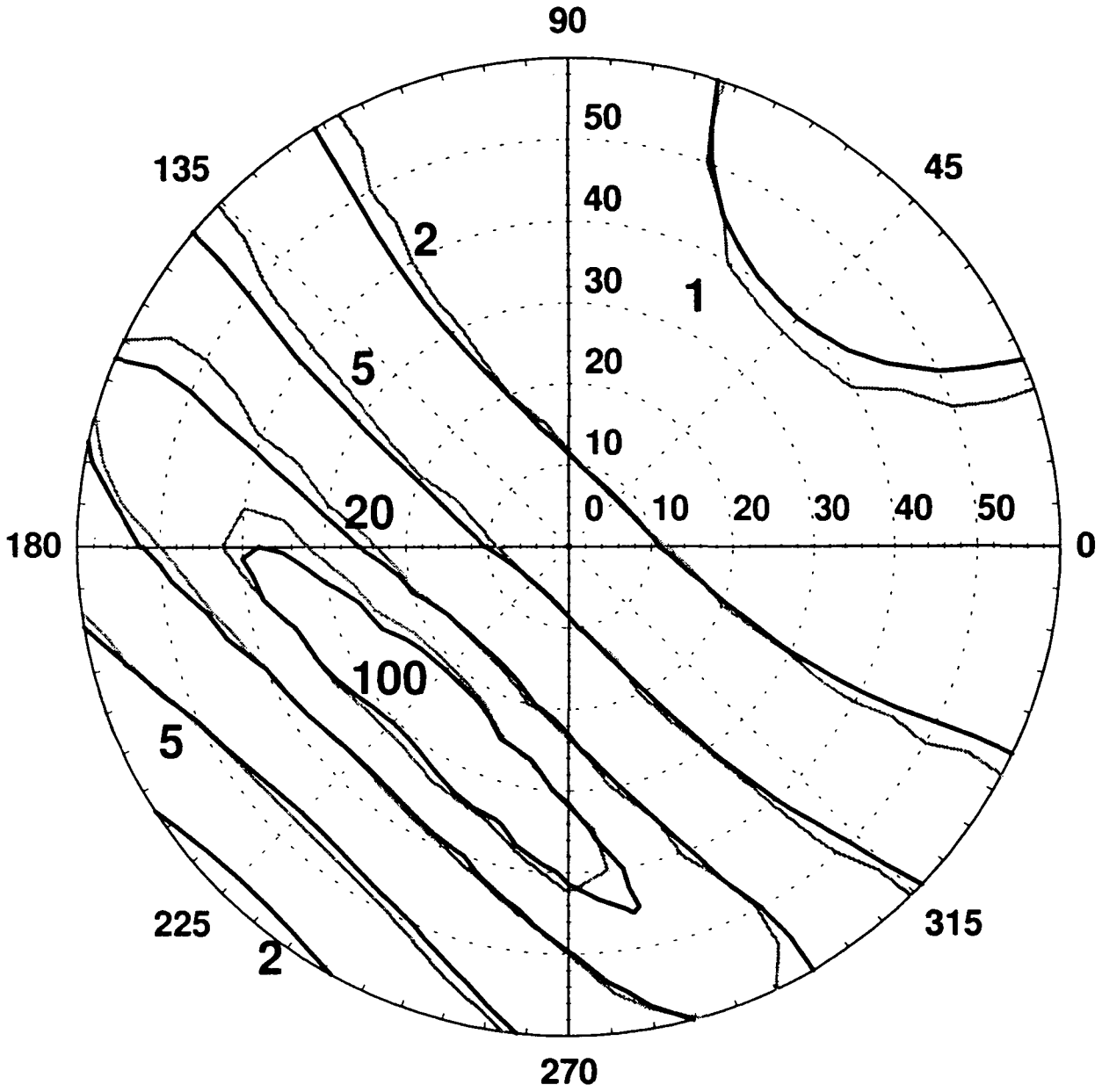
90
135
45
180
0
225
315
270
50
40
30
20
10
0
10
20
30
40
50
1
2
5
20
100
5
2

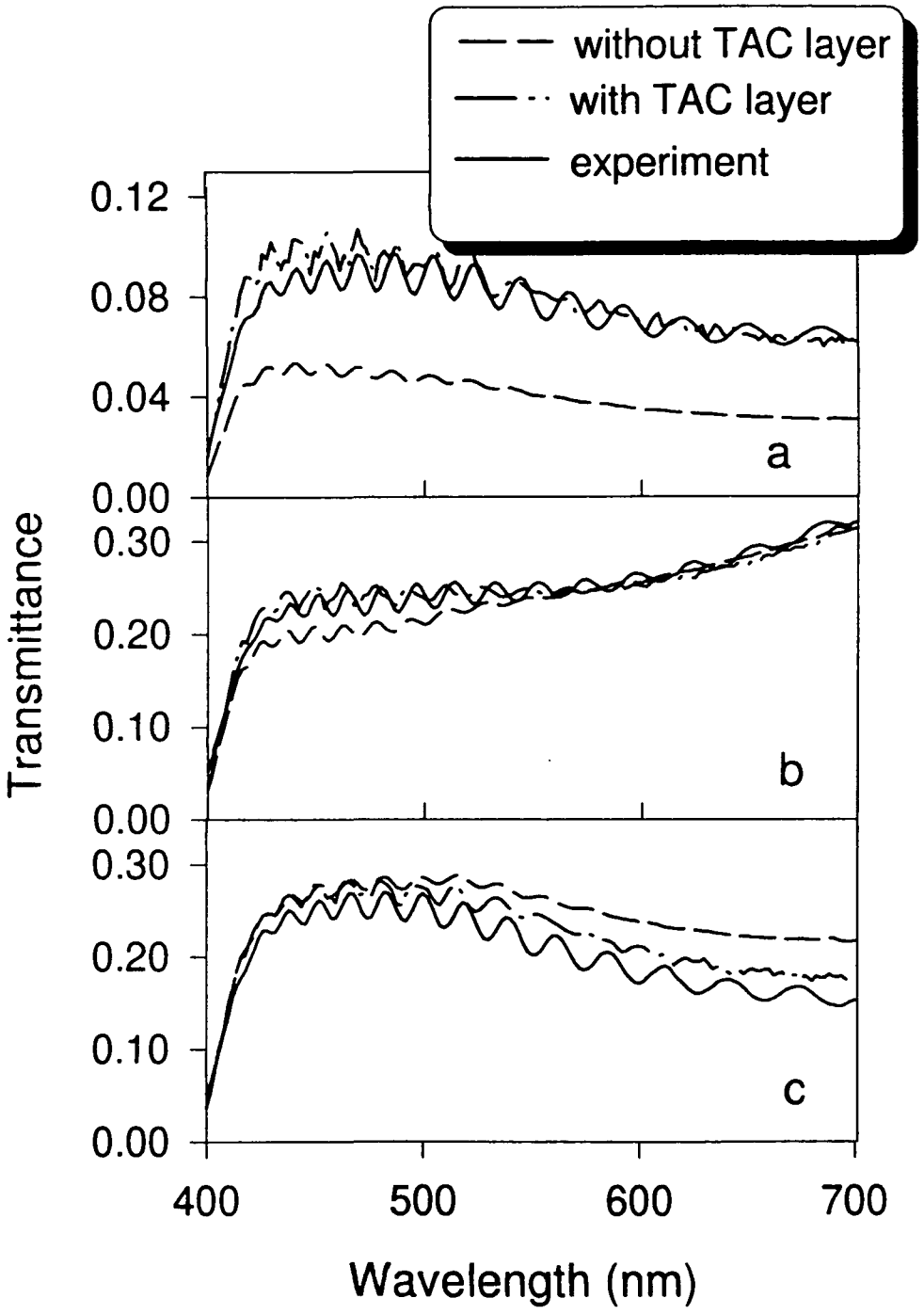
without TAC layer
with TAC layer
experiment
0.12
0.08
0.04
0.00
a
0.30
0.20
0.10
0.00
b
0.30
0.20
0.10
0.00
c
Transmittance
400
500
600
700
Wavelength (nm)

# LCD MODELING AS A DISPLAY CHARACTERIZATION TOOL

*Richard Herke, Syed H. Jamal, Jack R. Kelly*
**Liquid Crystal Institute, Kent State University, Kent OH**

**Abstract**

**We describe a user friendly TN and STN LCD modeling program based on the Berreman 4x4 matrix method. An accurate model of this type is not only useful for design work but can also serve as a versatile LCD characterization tool. The optical parameters necessary to produce an accurate model at the pixel level are discussed briefly, and examples are given of the models use in the determination of surface pretilt, cell thickness, and film retardation.**

## Introduction

The computer modeling of liquid crystal displays (LCD's) is an area of great interest for its potential to increase the efficiency of display design. However, in order to be effective the modeling program must faithfully simulate real LCD behavior. The primary obstacle to a faithful simulation is not in the basic theory. The 4x4 matrix approach of Berreman [1,2] is simply a rewriting of Maxwell's equations for a geometry where the optics changes in only one direction, and it is therefore essentially exact. The primary obstacle to faithful simulation is in the model depiction of the various optical components making up a LCD.

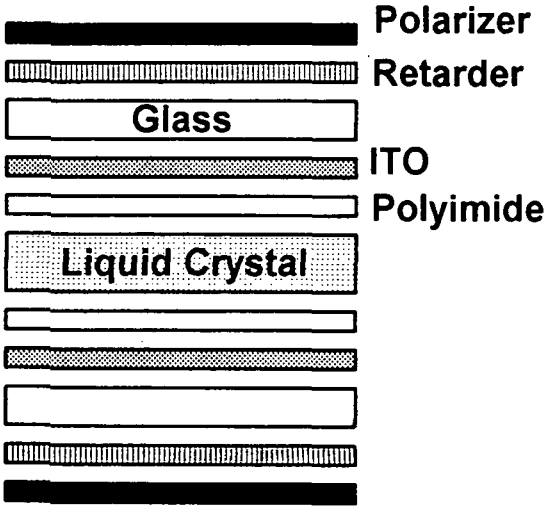


Figure 1: Structure of model liquid crystal cell pixel.

In order to develop adequate representations of typical LCD components we have been optically characterizing these components and comparing model output employing the optical characterization data to experimental measurements from TN and STN liquid crystal cells employing the components. This has yielded a better understanding of what are the important optical properties of each LCD component and the realization that the model itself can act as a versatile characterization tool.

## Model Description

The modeling program used in this work was "Twist Cell Optics", a package developed at the Liquid Crystal Institute. It is based on the Berreman 4x4 matrix approach[1], and uses an eigenfunction representation for the exact propagator matrix[2]. For ease of use and convenience the program runs under MS-windows on an IBM compatible. The graphical user interface was developed using MS Visual Basic while for speed compiled Fortran code performs the necessary heavy duty calculations. The model supplies luminance, chromaticity and spectral transmission data at any single viewing angle or luminance and chromaticity data over a user adjustable viewing cone. The light source is user adjustable and calculations are made for wavelengths between 400nm and 700nm with a resolution of down to 2nm. For rough calculations the package also comes with an 'optimizer' module which utilizes only 3 wavelengths and 17 strategically placed viewing angles to quickly generate an approximate conoscopic view.

Figure 1 shows the structure of a general modeled display pixel. Table 1 gives a brief summary of the properties of each layer which we have found necessary to include in the model in

Table 1: Optical Parameters of Model Pixel Layers

| Layer | Parameters | Comments |
|---|---|---|
| Liquid Crystal | $K_{11}$, $K_{22}$, $K_{33}$, $\varepsilon_{\parallel}$, $\varepsilon_{\perp}$, p, $V_{rms}$ | Director: from elastic (K) and dielectric ($\varepsilon$) constants with pitch (p) and applied voltage (V) (polyimide $\theta_s$, $\theta_r$ also needed) |
| | $n_e(\lambda), n_o(\lambda), d_{LC}$ | indices typically follow Cauchy relation |
| Polyimide | $d_{PI}$, $n_{PI}$, $\theta_s$, $\theta_r$ | critical parameters surface pretilt $\theta_s$, rub directions $\theta_r$ |
| ITO | $d_{ITO}$, $N_{ITO}=n_{ITO}(\lambda)+i\kappa_{ITO}$ | $n_{ITO}(\lambda)$ typically linear e.g. $n_{ITO}(\lambda)$~2.47-1.17$\lambda$ ($0.4\mu m<\lambda<0.7\mu m$) $\lvert\kappa_{ITO}\rvert$ typically small e.g. < 0.1 (*almost* ignorable) [4] |
| Glass | $n_G$ | Modeled as semi-infinite to avoid multiple reflections. |
| Retardation Film | $n_x$, $n_y$, $n_z$, $d_R$ | Lack of $\lambda$ dependence may cause some coloration errors |
| Polarizers | $N_{\parallel}=n_{\parallel}+i\kappa_{\parallel}(\lambda)$ $N_{\perp}=n_{\perp}+i\kappa_{\perp}(\lambda)$ $d_P$, $\theta_P$ | $d_P$ non-critical (a few $\mu m$). $\kappa$'s set to match on axis transmissions. Retardation of protective coating must be included in with Retardation Film[5]. Transmission directions ($\theta_P$) are of course critical. |
| Color Filters | Not Implemented: may be approximated by adjusting light source | |

order to produce an accurate match to experiment. In the table d refers to the thickness of each layer while n and $\kappa$ represent the indices of refraction and extinction coefficients, some of which it is important to have, as noted, as functions of wavelength.

Each layer is assumed homogenous except that of the liquid crystal whose director orientation varies through the layer. This variation is accounted for, as is standard practice, by breaking the layer into a series of sub-layers in which the director is assumed to be a constant. The orientation in each sub-layer is found from a dynamic minimization of the Oseen-Frank free energy[3] coupled to the electric field and assuming strong (i.e. infinite) anchoring at the layer boundaries. Once the director orientation of each sub-layer is known the optical calculation can proceed using the Berreman method. Since the model uses the eigenfunction representation of the propagator matrix typically only around 20 sub-layers are needed to reduce discrepancies to <<1%.

An example of the accuracy achievable by the model is shown in figure 2a (figure 2b depicts the viewing angle coordinate system employed). The iso-contrast plot of 2a compares the contrast ratio as a function of viewing angle found with a normally white TN cell and the model at a voltage where the on axis, $\theta = 0°$, contrast ratio is 3.

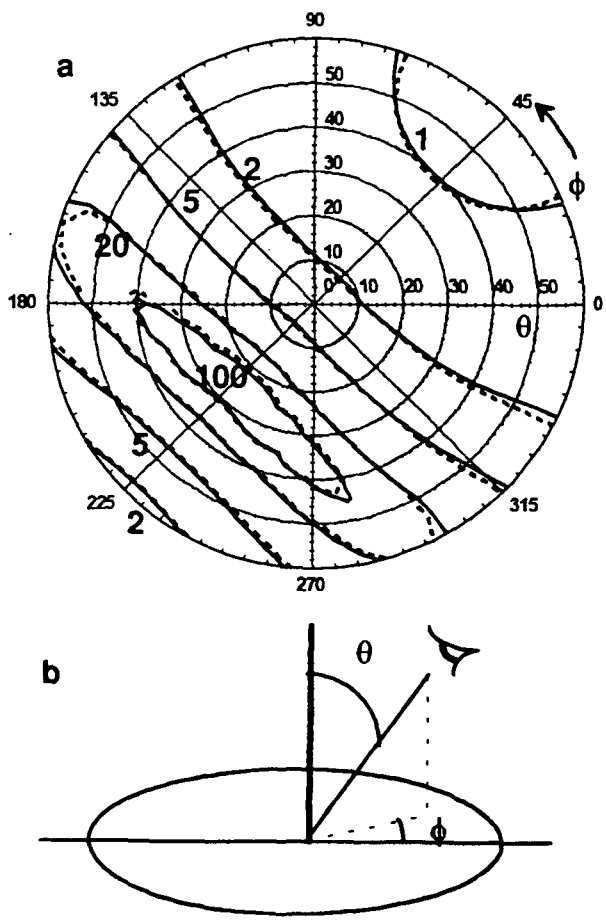


Figure 2: a) Iso-contrast plot comparing model (dashed lines) and experiment (solid lines).
b) schematic of viewing angle coordinates.

## Characterization Tool

In any optical characterization procedure one compares the results of optical measurements to the predictions of optical theory. Since the model is in essence a rewriting of optical theory in a form convenient to LCD's, this makes it potentially useful as a characterization tool. In particular it is well suited to situations where 'standard' test configurations are difficult to achieve, for example, when the polarizers have already been attached to the cell. As with any characterization procedure to accurately determine a particular parameter most of the other cell parameters must already be known.

## Surface Pretilt

Figure 3 shows an example of using the model to determine surface pretilt. The experimental test cell was a 240° STN with polarizers attached to operate in the yellow mode. Since both the nematic director and the polarizer transmission axes are symmetric with respect to rotations of $\pi$ radians, if the two lie in the same plane the transmitted luminance will also have this symmetry. In other words at 0 applied volts if there is no surface pretilt the luminance of a TN or STN cell at a polar viewing angle $\theta$ and azimuthal angle $\phi$ will be the same as at $\theta$ and $\phi+\pi$. Conversely any anisotropy will be due to the surface pretilt angle $\theta_s$.

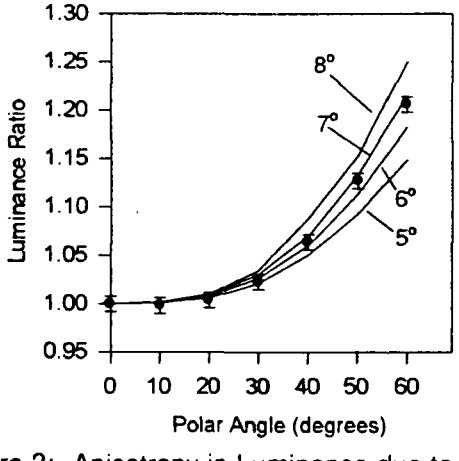


Figure 3: Anisotropy in Luminance due to surface pretilt. Lines are model with indicated pretilts. Data Points are for 240° STN cell.

The data points in figure 3 represent the ratio of the two luminances at the polar angle indicated but separated azimuthally by $\pi$ radians, along a line $\phi$ = constant, while the lines are model generated. An added benefit of the model is that its optimizer module allows one to quickly locate an angle $\phi$ along which the anisotropy and/or signal is expected to be large. The inferred surface pretilt of slightly less than 7° agrees well with the 6° to 8° quoted by the cell manufacturer.

## Cell Thickness.

Due to multiple reflections between the ITO coatings on the glass plates, interference fringes are visible in the transmission spectrum. The locations of these Fringes of Equal Chromatic Order (FECO) can be used to very precisely determine thickness assuming the refraction indices of the liquid crystal are well known. If a photospectrometer is not available a similar interference effect occurs for one wavelength as a function of polar viewing angle.

Figure 4 illustrates the use of the FECO interferometry technique to determine the

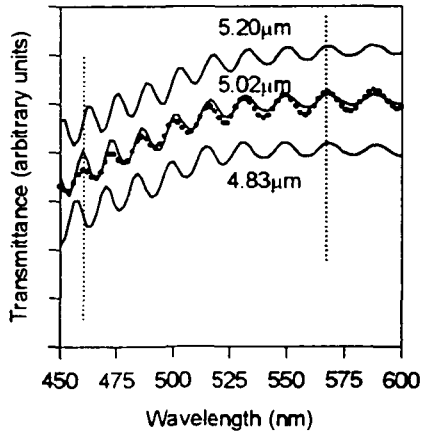


Figure 4: Transmission spectra of NWTNs of different cell gaps. Dots are experimental data whereas lines are model (4.83μm and 5.20μm have been vertically shifted for clarity.)

thickness of a normally white TN cell of 5.0μm nominal thickness. A transmission spectrum has been generated for the three thicknesses nearest 5.0μm which match the experimental interference

maximum at 568nm. However only that of 5.02μm continues to match with the experimental maxima as the wavelength is decreased to 462nm. A thickness of 5.20μm incorporates roughly an extra 1/4 of a fringe between these two wavelengths while 4.83μm falls behind by 1/4 a fringe.

Retardation Measurement

Retardation films are becoming increasingly important in the LCD industry. At present there is a great deal of interest in the use of negative retardation films to widen TN viewing angles. Once such a film is attached to a polarizer, however, most standard methods of birefringence measurement become difficult. Still, an effect which may be exploited in the measurement of this out of plane birefringence is the increase in transmission it causes at high polar viewing angles.

As a simple example take the tri-acetyl cellulose (TAC) protective layer laminated on most sheet polarizers. If it were isotropic the transmission through two crossed polarizers at $\theta$=60° and $\phi$=45° would be that shown by the bottom line in Figure 5. Senarmont ellipsometry, however, shows that these type films exhibit a small negative retardation of a few tens of nanometers. While this ellipsometric technique can no longer be used to determine the retardation of the film laminated on the polarizer, the increase in transmission is clearly visible as shown by the measured spectrum (circles) in Figure 5. The lines are model generated spectra assuming the indicated retardation in each TAC layer. Thus the TAC layer appears to have an out of plane retardation of approximately 50nm in the blue rising to 60nm in the red.

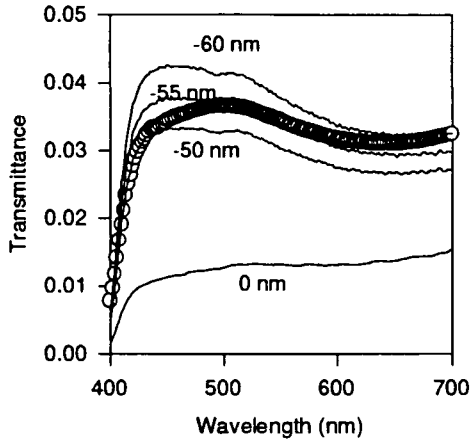


Figure 5: Transmission through crossed polarizers at $\theta$=60° $\phi$=45°. Circles are experimental while lines are model generated assuming indicated protective layer retardation.

Conclusion

There are many examples [6-9] of optical characterization procedures. Some are certainly more accurate than those examples shown here, but what a user friendly computer model brings to this field is the flexibility to quickly generate theoretical predictions for actual display geometries rather than optimal test set ups. Display modeling thus can not only provide accurate predictions of proposed LCD's but also help characterize and troubleshoot existing displays and processes.

References

1 D.W. Berreman, J Opt. Soc. Am. **62,** 502-510 (1972).

2 K. Eidner, et al., Mol. Cryst. Liq. Cryst. **172,** 191-200 (1989).

3 D.W. Berreman, Philos. Trans. R. S. London, **309,** 203-216 (1983).

4 J. A. Woolam, W.A. McHagan, SID 93 Digest, **24,** 558-560.

5 R. Herke, et al., J. of the SID, (in press).

6 R.M.A. Azzam, N.M. Bashara, "Ellipsometry and polarized light," (North Holland Publishing Company, Amsterdam: 1977).

7 K.Y. Han et al., Jpn. J. Appl. Phys. **32 part 2,** L1242-1244 (1993).

8 T.J. Scheffer, J. Nehring, J. Appl. Phys. **48,** 1783-1792 (1977).

9 H.L. Ong, SID 94 Digest, **25,** 787-790 (1994).